



National Aeronautics and
Space Administration

NASA CR-159429

DESIGN AND FABRICATION OF THE MINI-BRAYTON RECUPERATOR (MBR)

Final Report

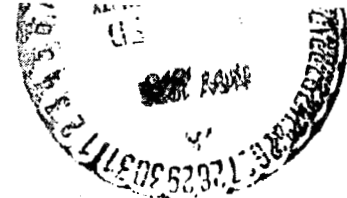
April 1978

(NASA-CR-159429) DESIGN AND FABRICATION OF
THE MINI-BRAYTON RECUPERATOR (MBR) Final
Report, Mar. 1974 - Jul. 1978 (AiResearch
Mfg. Co., Torrance, Calif.) 99 p
HC A05/MF A01

N79-11476

CSCL 10B G3/44 36956

Unclass



AIRESEARCH MANUFACTURING COMPANY OF CALIFORNIA
A DIVISION OF THE GARRETT CORPORATION
2525 W. 190th Street
Torrance, California 90509

Prepared for
NATIONAL AERONAUTICS AND SPACE ADMINISTRATION

Lewis Research Center
Cleveland, Ohio 44135
Contract NAS 3-18029

1. Report No. NASA CR159429	2. Government Accession No.	3. Recipient's Catalog No.	
4. Title and Subtitle FINAL REPORT: DESIGN AND FABRICATION OF THE MINI-BRAYTON RECUPERATOR (MBR)		5. Report Date April 1978	
		6. Performing Organization Code	
7. Author(s) J.J. Killackey, R. Graves, and G. Mosinskis		8. Performing Organization Report No. 78-14972	
		10. Work Unit No.	
9. Performing Organization Name and Address AiResearch Manufacturing Company of California A Division of The Garrett Corporation 2525 W. 190th Street Torrance, California 90509		11. Contract or Grant No. NAS3-18029	
		13. Type of Report and Period Covered Contractor Report March 1974 - July 1978	
12. Sponsoring Agency Name and Address National Aeronautics and Space Administration Washington, D.C. 20546		14. Sponsoring Agency Code	
15. Supplementary Notes Project Manager: Paul T. Kerwin Power Generation and Storage NASA-Lewis Research Center			
16. Abstract <u>Abstract</u> Development of a recuperator for a 2.0-kW closed Brayton space power system is described. The plate-fin heat exchanger is fabricated entirely from Hastelloy X and is designed for 10 years continuous operation at 1000°K (1300°F) with a Xenon-helium working fluid. Special design provisions assure uniform flow distribution, crucial for meeting 0.975 temperature effectiveness. Low-cycle fatigue resulting from repeated startup and shutdown cycles was identified as the most critical structural design problem. It is predicted that the unit has a minimum fatigue life of 220 cycles. This is in excess of the BIPS requirement of 100 cycles. Heat transfer performance and thermal cycle testing with air using a prototype unit verified that all design objectives can be met.			
17. Key Words (Suggested by Author(s)) Recuperator Closed Brayton cycle Plate-fin heat exchanger Low-cycle fatigue Space power systems		18. Distribution Statement Unclassified - Unlimited.	
19. Security Classif. (of this report) Unclassified	20. Security Classif. (of this page) Unclassified	21. No. of Pages 95	22. Price*

* For sale by the National Technical Information Service, Springfield, Virginia 22151

FOREWORD

The program described in this report was conducted by the AiResearch Manufacturing Company of California, a division of The Garrett Corporation, under contract NAS3-18029. Program activity started in March 1974 and was completed in July 1978. The work was performed under the direction of Mr. Paul T. Kerwin, Project Manager, Power Generation and Storage, NASA-Lewis Research Center. The AiResearch Program Manager was James J. Killackey.

The valuable contributions of the members of the AiResearch technical staff are acknowledged: Robert E. Preston and Peter Lecko, development engineering; Landon Stratton and George Mosinskis, thermal design; W. H. Feng, Richard F. Graves, and Harry A. Warren, structural design; and Kenneth K. Yap, mechanical design.

Values for the physical quantities are given in both SI and U.S. Customary Units. Measurements and calculations were made in U.S. Customary Units.

CONTENTS

	<u>Page</u>
SUMMARY	1
INTRODUCTION	1
HISTORY AND BACKGROUND	5
Solar Brayton-Cycle Recuperator	5
Brayton Heat Exchanger Unit (BHXU)	5
Alternate Design BHXU	8
Heat Exchanger and Duct Assembly (HXDA)	8
Brayton Heat Exchanger Technology	10
HEAT EXCHANGER DESIGN	12
Design Features	12
Thermal Design	17
Structural Design	28
Failure Mode, Effect and Criticality Analysis (FMEA)	31
PROTOTYPE HEAT EXCHANGER	34
Fabrication	34
Performance Test	41
Thermal Cycle Test	45
Conclusions	53
MINI-BRAYTON RECUPERATOR	53
Acceptance Test	55
CYCLIC LIFE ANALYSIS	59
Startup Transient	62
Preliminary BIPS Analysis	62
Improved BIPS Analysis	64
APPENDIX--LOW-COST, HIGH-TEMPERATURE BRAZE ALLOY DEVELOPMENT	66
REFERENCES	70

REPLACING PAGE BLANK NOT REAMAS

LIST OF ILLUSTRATIONS

<u>Figure</u>		<u>Page</u>
1	MBR As-Built Configuration	3
2	Solar Brayton-Cycle Recuperator	7
3	Brayton-Cycle Heat Exchanger Unit	7
4	Alternate Design BHXU	9
5	Brayton-Cycle Heat Exchanger, Recuperator Submodule	11
6	Recuperator Outline	13
7	MBR Preliminary Design	14
8	Core Construction	16
9	Splitter-Core Joint Design	18
10	End Section Design	21
11	Flow Distribution with an 11 Percent Pressure Drop	23
	Imbalance	
12	Flow Distribution Provisions	24
13	Manifold Pressure Gradients	25
14	Three-Dimensional Finite Element Model	30
15	Thermal Distortions of MBR Manifold at Mid-Stack Height	30
	Section	
16	Maximum Principal Thermal Stress Contours	32
17	Thermally Induced Loads in the Splitter/Core Braze Joint	33
	Due to System Startup Transient	
18	Passage Assembly	35
19	Core Assembly After Machining of the Header Bar Surface	36
	and Manifold Splitter Groove	
20	Manifold Splitter Plates	36
21	Core Assembly Following Braze to Attach Seal Plates and	37
	Splitter	
22	Manifold Attachment Flange	38
23	Core Assembly Following Braze to Attach the Manifold	39
	Side Flanges	
24	Mini-Brayton Recuperator, Prototype Assembly	40
25	Performance Test Setup	42
26	Pressure Drop with XeHe for the Prototype Mini-Brayton	43
	Recuperator	
27	Performance Test Setup	46
28	Thermal Performance with Air	47
29	Predicted Thermal Performance with XeHe	48
30	Thermal Cycle Test Conditions	50
31	Blisters in Seal Plate Observed After 200 Cycles	52
32	Location of Fatigue Cracks	54
33	MBR Core Assembly	56
34	Closeup View of Corner Braze Joint Area	56
35	Completed Recuperator	57
36	MBR As-Built	58
37	High-Pressure (Cold) Side Pressure Drop	60
38	Low-Pressure (Hot) Side Pressure Drop	61

LIST OF ILLUSTRATIONS (Continued)

<u>Figure</u>		<u>Page</u>
39	Comparison of Transient Temperature Profiles	63
40	Run 600 MBR Inlet Conditions and Calculated Outlet	65
41	Location of MBR Section Analyzed	66
42	2-D Finite Element Model with Boundary Conditions	67
43	Temperature Map at 30 Seconds	69
44	Distorted Geometry at 30 Seconds	70
45	2-D Von Mises Stress Map at 30 Seconds	71
46	Temperature Map at 170 Seconds	72
47	Distorted Geometry at 170 Seconds	73
48	2-D Von Mises Stress Map at 170 Seconds	74
49	Temperature Map at Steady State	75
50	Distorted Geometry at Steady State	76
51	2-D Von Mises Stress Map at Steady State	77
52	Location of Most Highly Stressed Element	78
53	Variation of Von Mises Stress, Temperature, Yield Strength, and 1 Percent Creep Stresses with Time for Element 493	79
54	Life Fraction Analysis	80
55	Hastelloy X -3 Sigma Larson-Miller Curves for 1, 2, 5 Percent Creep and Rupture.....	81
56	Hastelloy X Nominal Curves for 1, 2, 5 Percent Creep and Rupture	82
57	Plate-Fin Creep-Rupture Behavior (from Reference 12)	86
58	MBR Submodule in Stacking Fixture--210/30 Combination	87
	Braze Alloy	

LIST OF TABLES

<u>Table</u>		<u>Page</u>
I	Mini-Brayton Recuperator Specifications	2
II	Brayton-Cycle Heat Exchanger Development	6
III	Thermal Design Requirements	19
IV	Prototype Heat Exchanger Design Characteristics	19
V	Recuperator Performance for High-Pressure Side	22
VI	Predicted Performance	27
VII	Structural Design Criteria	29

ORIGINAL PAGE IS
OF POOR QUALITY

Specifications for the counterflow plate-fin recuperator are presented in Table 1, and the as-built unit is shown in fig. 1. Special provisions are incorporated to (1) obtain uniform flow distribution, which is crucial for meeting the exceptionally high temperature effectiveness, and (2) achieve enhanced structural reliability.

Low-cycle fatigue was identified as the most critical and life-limiting structural design problem. Previous cyclic life estimates were refined. Results indicate that the recuperator has a minimum fatigue life of 200 cycles. This is in excess of the BIPS requirements of 100 cycles.

Fabrication and development testing of a prototype heat exchanger were completed. For the heat transfer performance test, a special procedure was developed to accurately account for heat leak effects. These are especially significant at a high temperature effectiveness. Test data obtained with air indicate that heat transfer performance with xenon-helium will slightly exceed requirements. The pressure drop exceeds the required value by less than 10 percent and will be offset by the available excess heat transfer capability.

The prototype unit was subjected to 200 rapid startup and shutdown test cycles designed to validate the cyclic life prediction and to shake down the structural design. After this exposure, the external helium leakage was less than 2.3×10^{-10} scc/sec, which is below the specification limit. Some internal bypass leakage was detected after 100 thermal cycles, but the resulting effect on system performance is negligible.

A second unit, scheduled for installation in a power system, was proof pressure tested, tested for isothermal pressure drop (flow calibration), helium leak checked, and cleaned to spacecraft cleanliness standards prior to delivery.

INTRODUCTION

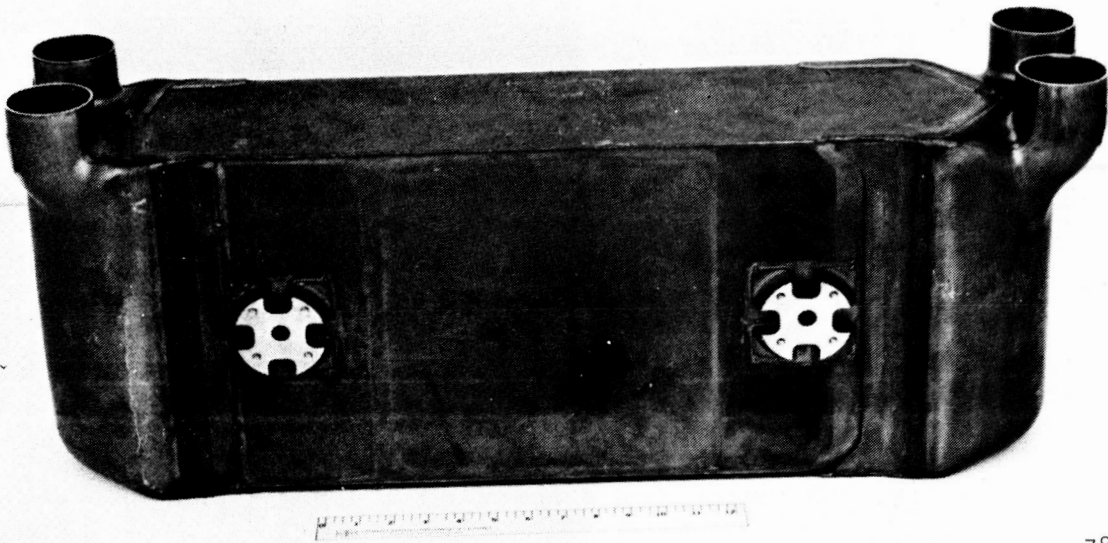
As part of its Brayton-cycle space power system advanced technology program, NASA-Lewis Research Center has been pursuing the development of power conversion equipment for use with solar, reactor, and isotope heat sources. The recuperator is a key component in these systems and has been the subject of a development program extending over the past 14 years. The history of this activity has been traced and is documented in this report.

The particular effort described in this report covers the design, fabrication, and test of the Mini-Brayton recuperator (MBR) that is part of a 2.0-kW space power system, which uses an isotope heat source. The designation of Mini-Brayton is used to distinguish this system from other, larger power systems designed for operation with isotope or reactor heat sources. The unit is fabricated from Hastelloy X and is designed for 10 years of

TABLE 1.--MINI-BRAYTON RECUPERATOR SPECIFICATIONS

Parameters	Description
Working fluid	Xenon-helium , molecular weight = 83.8
Hot, low-pressure gas flow	0.162 kg/sec (0.357 lb/sec)
Cold, high-pressure gas flow	0.159 kg/sec (0.350 lb/sec)
Hot-side inlet temperature	722°C (1332°F)
Cold-side inlet temperature	107°C (224°F)
Cold-side temperature effectiveness, ϵ	0.975
Hot-side inlet pressure	0.494 MPa (71.7 psia)
Cold-side inlet pressure	0.732 MPa (106.2 psia)
Combined pressure drop, $\Delta P/P_{inlet}$	0.70 percent
Heat transfer rate	23.75 kW (22.53 Btu/sec)
Heat transfer area	46.0 m ² (495 sq ft)
Overall dimensions	
Height	35.1 cm (13.8 in.)
Width	17.5 cm (6.9 in.)
Length	71.1 cm (28.0 in.)
Material of construction	Hastelloy X
Weight	59.4 kg (131 lb)
Design life	100,000 hr (10 years)

ORIGINAL PAGE IS
OF POOR QUALITY



78188/1

Figure 1.--MBR As-Built Configuration.

continuous operation at 1000°K (1300°F) with a xenon-helium working fluid. The primary goals are high reliability and performance with minimum weight.

The current application for the MBR is the Brayton Isotope Power System (BIPS), a space power system now being developed by the Department of Energy, Division of Advanced Systems and Materials Production, Washington, D.C. The final MBR has been delivered to the AiResearch Manufacturing Company of Arizona, where it is installed in the BIPS Ground Demonstrator System.

HISTORY AND BACKGROUND

The MBR design is the result of a recuperator development program that has extended over the past 14 years. The individual contracts between AiResearch and NASA-Lewis Research Center that comprise this effort are summarized in Table II. Highlights are discussed below.

Solar Brayton-Cycle Recuperator

Extensive parametric analyses of plate-fin and tubular heat exchanger geometries were conducted. The final selection was a plate-fin configuration-- a design used in all subsequent programs. Related design items including triangular end section design for uniform flow distribution, axial heat conduction effects, and manifold flow distribution were first analyzed here. An optimized plate-fin recuperator was built and tested to confirm the analytical design techniques. The material of construction was type series 347 stainless steel and the assembly weight was 199 kg (438 lb). Estimated performance with argon working fluid was a temperature effectiveness of 0.95 and an overall pressure drop (both sides) of 2.3 percent. The recuperator is shown in fig. 2 and the program results are documented in Reference 1.

Brayton Heat Exchanger Unit (BHXU)

The BHXU is an integral heat exchanger unit incorporating a plate-fin recuperator, a plate-fin gas-to-liquid heat sink heat exchanger, and the ducting and bellows. The assembly is shown in fig. 3. The BHXU mates with a turbine-alternator-compressor assembly, the NASA Brayton Rotating Unit (BRU). This power system, capable of producing 2.25 to 10.5 kW, has been operated by Lewis Research Center for over 30,000 hr.

Parametric analysis and design layout studies identified the plate-fin counterflow configuration as optimum for the recuperator. The recuperator was fabricated from series 347 stainless steel and the core assembly weight was 91 kg (201 lb). With xenon-helium working fluid, the predicted recuperator effectiveness was 0.941 and the overall pressure drop (both sides) was 2.99 percent. An important part of this study was the start of a comprehensive design procedure for high-temperature bellows. Three BHXU systems were delivered to NASA.

Power system tests at NASA showed that after repeated startup and shutdown cycles, the recuperator would develop cracks in the header bar-to-tube plate joints, which resulted in working fluid leakage. The cracking mechanism was identified as low-cycle fatigue. No heat transfer performance degradation has been observed in 30,000 hr of test operation. Experience gained in this program has led to improved structural designs that have been incorporated in the MBR. Results of this program are presented in References 2 and 3.

TABLE 11.--BRAYTON-CYCLE HEAT EXCHANGER DEVELOPMENT
(NASA-Lewis Research Center Sponsored Programs)

Program	Contract	Period of Performance
Solar Brayton-Cycle Recuperator Delivered development unit	NAS 3-2793	11/63 - 3/65
Solar Brayton Heat Source HX Design Study	NAS 3-8025	6/65 - 1/68
Brayton Heat Exchanger Unit (BHXU) Delivered 3 systems - recuperator, heat sink HX, ducting, and bellows Tested at Lewis for 30,000+ hr	NAS 3-10607	5/67 - 3/72
Alternate Design BHXU Delivered advanced system with Hastelloy X recuperator, tubular HSHX, and link-type bellows	NAS 3-13454	11/69 - 8/73
Heat Exchanger and Duct Assembly (HXDA) Study program for nuclear system	NAS 3-13453	11/69 - 12/70
Brayton-Cycle Heat Exchanger Technology Low-cycle fatigue test New braze alloys High-temperature bellows Thermal cycle test on submodules	NAS 3-15347	6/71 - 8/76
Mini-Brayton Recuperator Test prototype design Deliver MBR	NAS 3-18029	3/74 - 6/78

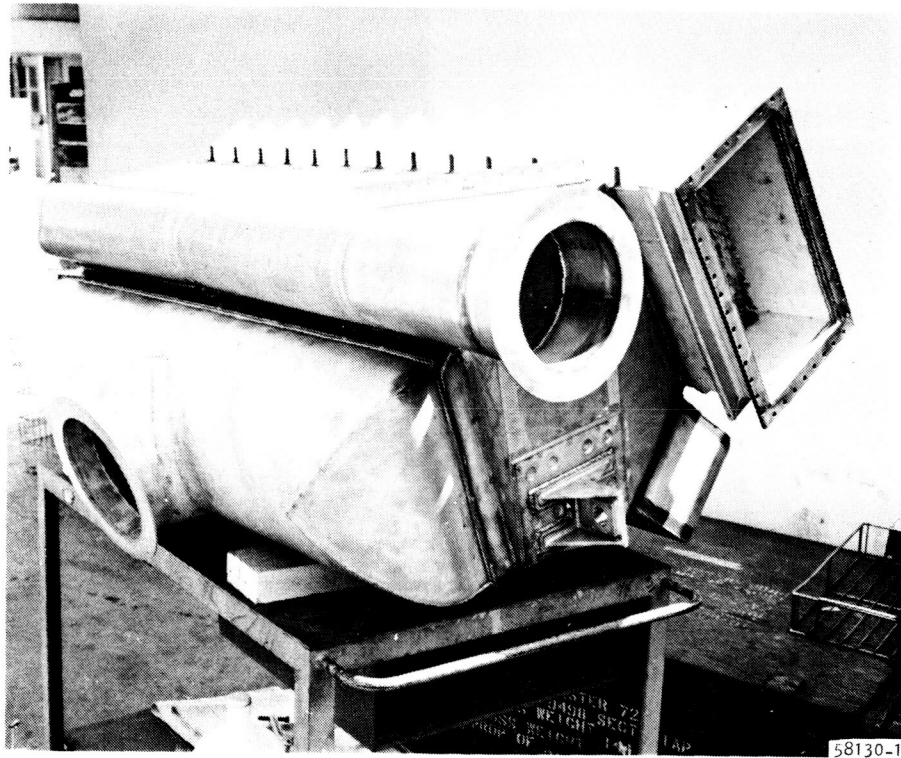
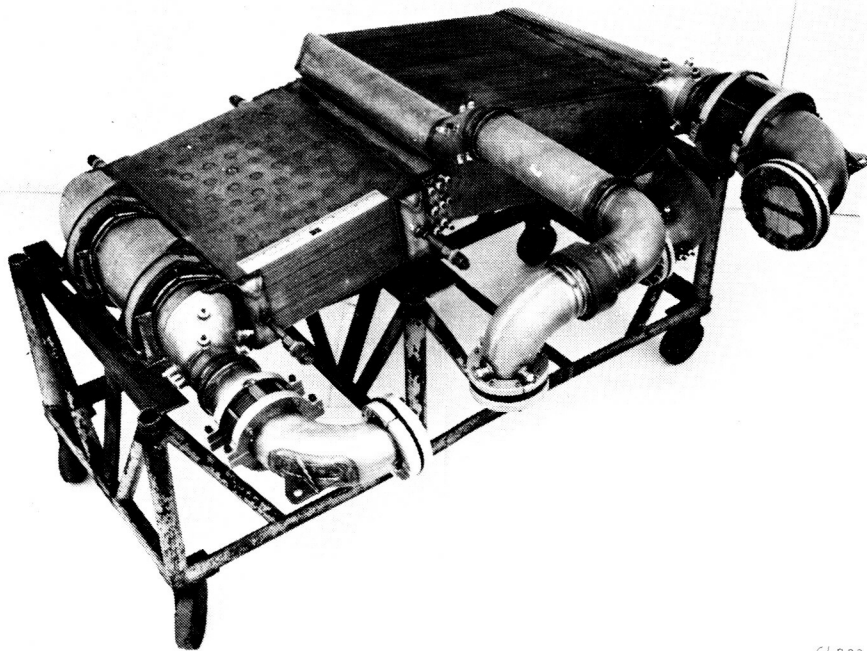


Figure 2.--Solar Brayton-Cycle Recuperator.



64203-3

F-27049

Figure 3.--Brayton-Cycle Heat Exchanger Unit.

Alternate Design BHXU

This was the second generation of the BHXU designed to be integrated with the Brayton Rotating Unit (BRU) and installed in the NASA Engine B. The program goal was to achieve greater reliability by: (1) using stronger materials and more ductile braze alloys to increase the recuperator thermal fatigue life; (2) providing double containment against external leakage of the gaseous working fluid; and (3) elimination of possible leak paths of the organic coolant into the gas stream.

Recuperator size was increased by 16 percent to provide a temperature effectiveness of 0.95. The predicted overall pressure drop was 2.68 percent (both sides). The material of construction was Hastelloy X and the recuperator core weight was 158 kg (348 lb). Double containment of the working fluid was achieved by brazing an additional cover plate to the core header bars, thus eliminating direct exposure of any braze joint to space vacuum.

Operating pressures for this unit were increased over those for the original BHXU. Utilization of a single bellows in the interconnecting ducts would have produced excessive stresses. A successful design solution was achieved by using three hinged bellows in each duct. An internal hinge in each bellows made the bellows self-sufficient for absorbing the pressure thrust load.

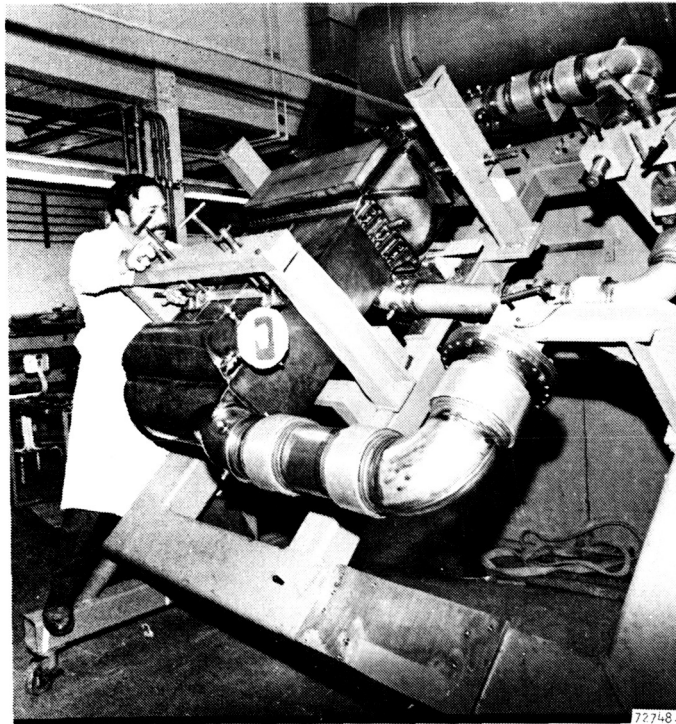
A tubular waste heat exchanger was selected for the alternate design because it offered a significant reduction in the number of leak paths for a modest increase in weight compared with the plate-fin design. Each core contained a total of 2016 stainless steel tubes helically wrapped with a copper fin.

A complete BHXU assembly was manufactured and delivered to NASA. The final assembly is shown in fig. 4. Results of the parametric analyses are presented in Reference 4 and a description of the fabrication development and manufacturing operations in Reference 5.

Heat Exchanger and Duct Assembly (HXDA)

As part of advanced space power systems studies, NASA investigated the performance characteristics of Brayton power conversion systems in the 35- to 150-kW class (Reference 6). These systems, which employ a liquid metal cooled reactor, use three heat exchangers: waste heat exchanger, heat source heat exchanger, and the recuperator. These heat exchangers and their interconnecting ducting comprise the HXDA.

The Phase I AiResearch effort was concerned with the selection of basic types of heat transfer surfaces for each heat exchanger and the development of minimum weight designs. Four designs were selected for final optimization and the recuperator was in all cases a counterflow plate-fin design with triangular end sections; the heat source heat exchanger was a cross-counterflow



ORIGINAL PAGE IS
OF POOR QUALITY

Figure 4.--Alternate Design BHXU.

finned tubular design; and the waste heat exchanger was a cross-counterflow plate-fin unit with two independent liquid cooling circuits in the core. Concept optimization studies are presented in Reference 7.

Experimental data regarding the pressure containment capabilities of plate-fin matrixes operating at conditions typical for advanced power systems were obtained in Phase II. Specimens fabricated from series 347 stainless steel and Hastelloy X with nickel- and gold-braze alloys were burst and creep-rupture tested at temperatures up to 1140°K (1600°F). Test results were published in Reference 8.

The Phase III studies were directed to the development of two HXDA preliminary designs: one associated with the SNAP-8 reactor temperature capabilities--about 920°K (1200°F) maximum temperature--and the other with a more advanced system operating at about 1200°K (1700°F). These two preliminary designs are presented in Reference 9.

In June 1971, the fabrication of the HXDA was initiated with a program to design, fabricate, and test a heat exchanger and duct assembly for a Brayton power system in the 15- to 80-kW class. Preliminary component designs were established based on the design point conditions in Reference 10. The final recuperator design was plate-fin counterflow with triangular end sections and constructed of Hastelloy X. With a xenon-helium working fluid (molecular weight = 39.94), the design point effectiveness was 0.925 and the overall pressure drop for both sides was 1.15 percent. Estimated recuperator weight was 382 kg (842 lb).

Small-scale tests were performed to evaluate recuperator braze joint strength and the characteristics of an alternate braze alloy (Nicuman 23) for the waste heat exchanger. At this stage of development it was clear that low-cycle fatigue was the most critical structural design factor. Accordingly, a series of reverse bending, strain-controlled, fatigue tests were performed to obtain basic design data on the cycle life of parent metal, parent metal weld joints, and brazed and welded heat exchanger joint sections. Results of the small-scale tests and the preliminary design efforts are documented in Reference 11.

Brayton Cycle Heat Exchanger Technology

In January 1972, the HXDA program was reoriented from the development of a specific power system to a technology program for advanced Brayton-cycle heat exchangers and associated equipment. The detail design of the HXDA was terminated; the small-scale tests and fabrication technology efforts were continued and ultimately directed specifically to the development of the Mini-Brayton Recuperator (MBR).

Specific accomplishments of the technology program were: (1) heat transfer and pressure drop data were obtained for a finned-tube heat transfer matrix representative of the heat source heat exchanger; (2) a modularized, plate-fin waste heat exchanger with means to verify double containment was developed; (3) twenty-two high-temperature braze alloys were evaluated to find a low-cost alloy with the desirable attributes of a gold-based alloy; the final selection was Nicrobraz 30; and (4), bellows designs suitable for operation at 1400°K (1600°F) and 1.4 MPa (200 psia) for 1000 cycles and 50,000 hours were determined to be feasible. Bellows design techniques developed here were believed to be an advancement in the state of the art.

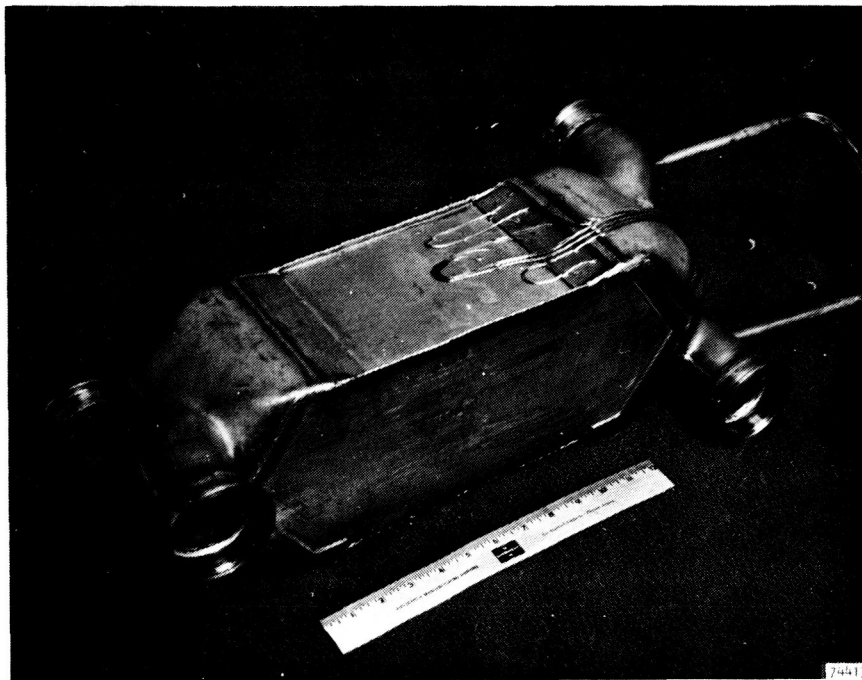
The basic MBR design for a 2-kW power system was first established as part of this technology program. Special attention was paid to flow distribution and axial conduction effects to ensure meeting the 0.975 temperature effectiveness requirement. A thorough transient temperature analysis was performed to identify those areas within the recuperator structure where excessive temperature gradients are developed. High-temperature gradients can occur when adjacent structural elements respond at different rates to a system startup or shutdown transient. These data were the basis for a prediction of thermal fatigue life, and also were used to develop alternate structural concepts with increased fatigue life.

The final design incorporated new manifold construction and header bar shapes designed to alleviate the thermal stress. Double-containment side plates, a scheme originally developed for the alternate design BHXU, were incorporated in the MBR design. Hastelloy X was specified for construction because of its superior strength and fabricability compared with a 300-series stainless steel. Gold-base braze alloys were selected because of their high strength and ductility compared with nickel-base alloys.

Two submodules, half the flow length and half the stack height of the full-size MBR, were constructed. One of the units is shown in fig. 5. The structural design was similar to the full-size unit. The first submodule was performance tested to verify the thermal design and was then subjected to repeated thermal cycles. Test parameters, i.e., the time to reach peak operating temperature, were purposely set at off-limit conditions to rapidly induce fatigue cracking. In this manner any weak areas could be isolated, the failure mechanism identified, and appropriate design modifications instituted. The second submodule was modified to reinforce weak areas detected in the first submodule and was subjected to thermal cycle testing.

The first submodule accumulated 80 thermal cycles before the test was stopped. Internal bypass leakage was observed but the unit was externally helium leak tight. The second submodule displayed similar results, but in this test external helium leakage was detected after 100 thermal cycles. These leaks, which occurred in a corner of the manifold attachment flange, were repaired and testing continued. After 278 cycles the test was stopped. There was no external leakage except in the corner areas, which continued to crack after several repair operations. After a detail metallurgical examination, it was concluded that with appropriate modification the MBR could withstand at least 100 cycles without internal or external leakage. Results of the technology program are presented in Reference 12.

ORIGINAL PAGE IS
OF POOR QUALITY



F-27048

Figure 5.--Brayton-Cycle Heat Exchanger,
Recuperator Submodule.

HEAT EXCHANGER DESIGN

The basic design features are shown in the recuperator outline in fig. 6 and the flow and configuration schematics in fig. 7. The heat exchanger is of all-brazed and welded construction and is fabricated entirely of Hastelloy X. The internal construction is typical for counterflow heat exchangers. Heat transfer takes place predominately in the rectangular counterflow section where high-performance rectangular offset fins are used. Triangular end sections are used to distribute and collect the gas flow to and from the counterflow section. Plain rectangular fins are used in the end sections to minimize pressure drop. Total heat transfer area (hot and cold sides) is 46.0 m^2 (495 sq ft).

Design Features

The Mini-Brayton Recuperator (MBR) incorporates several unique features directed towards increasing heat exchanger reliability and cyclic life. They are described below.

Manifold construction.--Manifolds are not directly welded to the core as is the case for a typical plate-fin heat exchanger. Separate manifold attachment strips are brazed to the core sides. These strips are purposely set back from the corners of the core assembly because of the high temperature gradients that exist in this area. As shown in fig. 1, a cylindrical manifold extends across the core and is welded to the attachment strips. This shape provides for ideal pressure containment. A splitter plate separates the hot and cold gas streams within the manifold. The splitter is dished to better withstand the pressure differential between streams.

Braze alloy.--Gold-base braze alloys are specified for all operations because of their superior ductility and strength compared with nickel-base alloys.

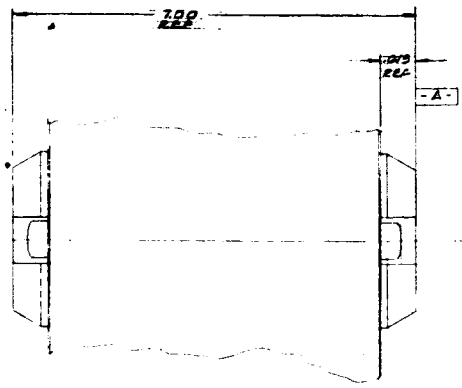
Channel header bars.--To reduce the difference in thermal mass between the thin tube sheet and the header bars, the bars are machined in a channel shape as shown in fig. 8.

Seal plate.--After the first braze operation wherein the plates, bars, and fins are joined, the braze joints along the sides of the core are exposed. A defect in any of these exposed braze joints could result in leakage of cycle working fluid to space and eventual shutdown of the power system. To reduce the number of exposed joints and potential leak paths, seal plates are brazed to the sides of the core as shown in fig. 8. After the seal plates are brazed in place, the edges are welded to provide a double containment seal.

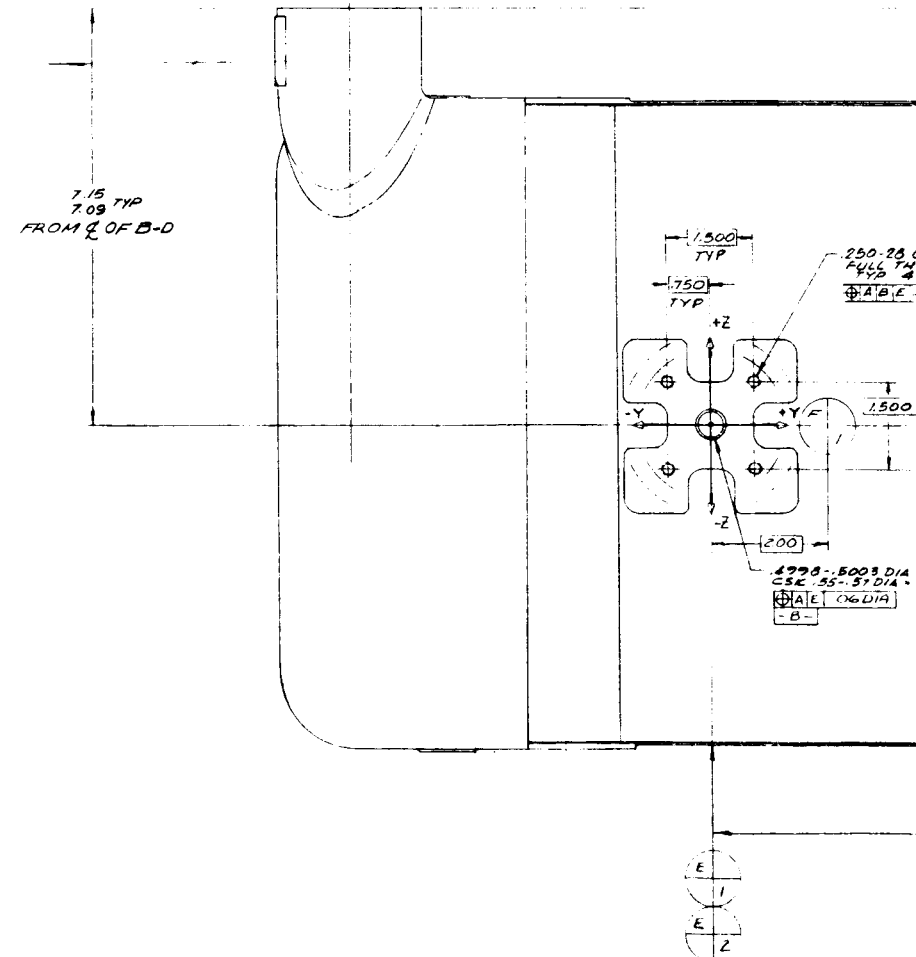
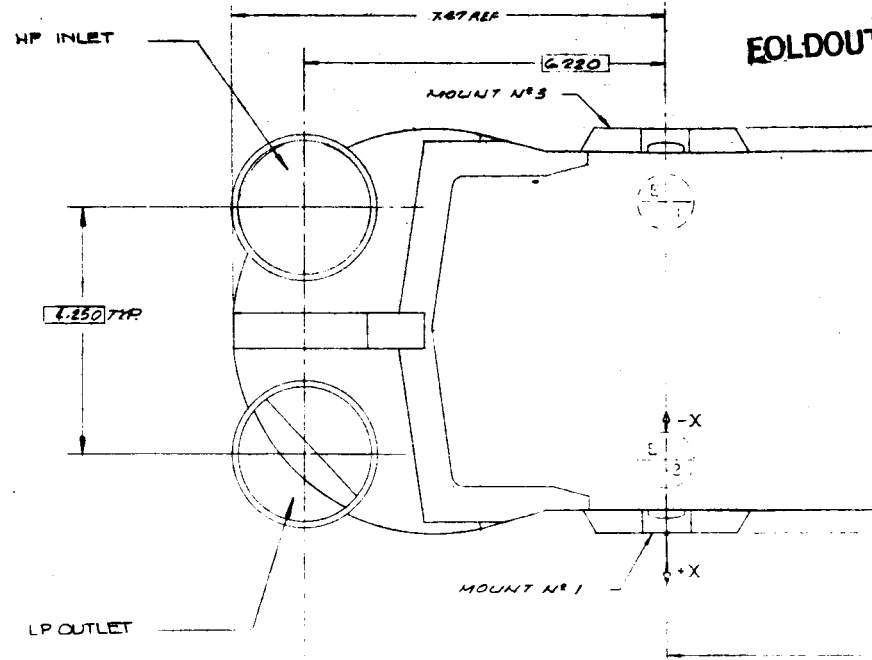
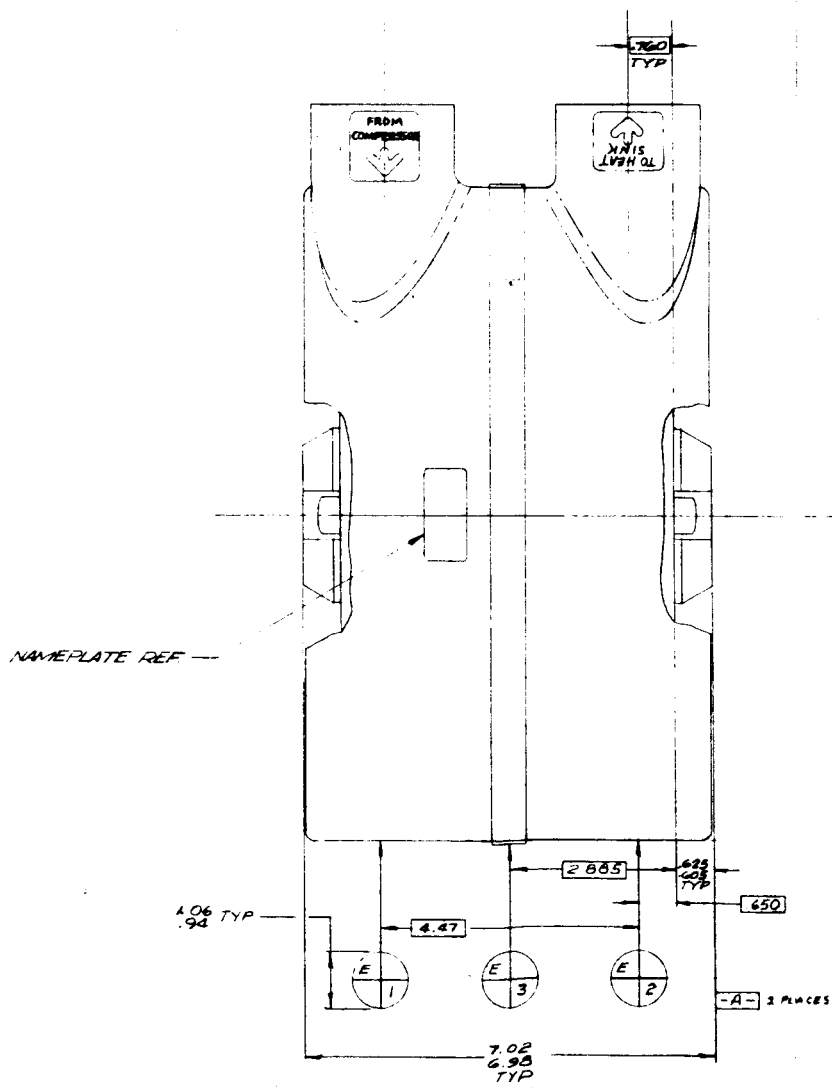
After the first braze, the core sides are machined flat to receive the seal plates. The corner radii are matched to the seal plate bend radius. The seal plate also provides a surface for joining of the manifold attachment flanges and mounting brackets to the core matrix.

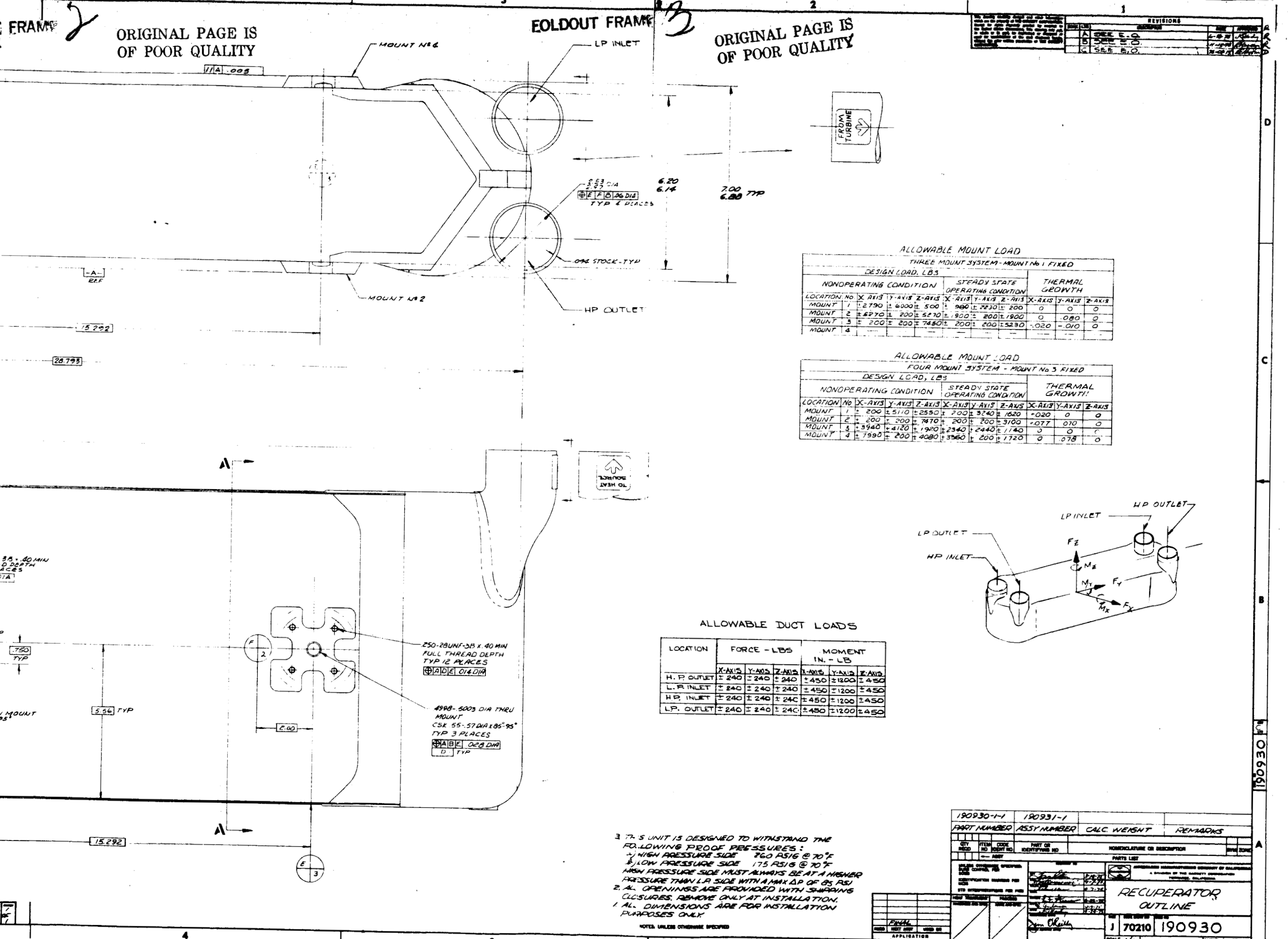
FOLDOUT FRAME

ORIGINAL PAGE IS
OF POOR QUALITY



SECTION A-A





ORIGINAL PAGE IS OF POOR QUALITY

ORIGINAL PAGE IS OF POOR QUALITY

REVISIONS			
NO.	DATE	BY	DESCRIPTION
A	SEE E.O.		
B	SEE E.O.		
C	SEE E.O.		

ALLOWABLE MOUNT LOAD
THREE MOUNT SYSTEM - MOUNT N#1 FIXED

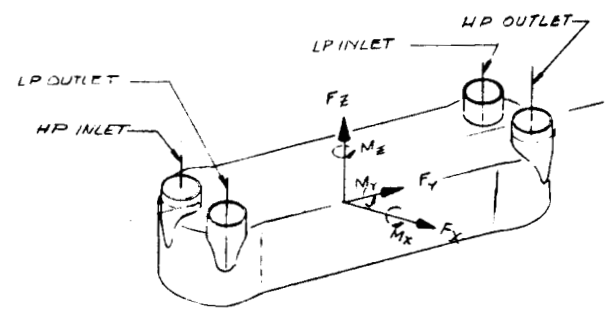
DESIGN LOAD, LBS												
NONOPERATING CONDITION				STEADY STATE OPERATING CONDITION				THERMAL GROWTH				
LOCATION No	X-AXIS	Y-AXIS	Z-AXIS	X-AXIS	Y-AXIS	Z-AXIS	X-AXIS	Y-AXIS	Z-AXIS	X-AXIS	Y-AXIS	Z-AXIS
MOUNT 1	2790	± 6000	± 500	960	± 2230	± 200	0	0	0	0	0	0
MOUNT 2	± 6270	± 200	± 5270	± 900	± 200	± 1900	0	0	0	0	0	0
MOUNT 3	± 200	± 200	± 7450	± 200	± 200	± 5230	0	0	0	0	0	0
MOUNT 4												

ALLOWABLE MOUNT LOAD
FOUR MOUNT SYSTEM - MOUNT N#3 FIXED

DESIGN LOAD, LBS												
NONOPERATING CONDITION				STEADY STATE OPERATING CONDITION				THERMAL GROWTH				
LOCATION No	X-AXIS	Y-AXIS	Z-AXIS	X-AXIS	Y-AXIS	Z-AXIS	X-AXIS	Y-AXIS	Z-AXIS	X-AXIS	Y-AXIS	Z-AXIS
MOUNT 1	± 200	± 5110	± 2550	± 700	± 3240	± 1620	0	0	0	0	0	0
MOUNT 2	± 200	± 200	± 7470	± 200	± 200	± 3100	0	0	0	0	0	0
MOUNT 3	± 3940	± 4120	± 1920	± 2340	± 2440	± 1140	0	0	0	0	0	0
MOUNT 4	± 1990	± 200	± 4080	± 3360	± 200	± 1720	0	0	0	0	0	0

ALLOWABLE DUCT LOADS

LOCATION	FORCE - LBS			MOMENT IN. - LB		
	X-AXIS	Y-AXIS	Z-AXIS	X-AXIS	Y-AXIS	Z-AXIS
H. P. OUTLET	± 240	± 240	± 240	± 450	± 1200	± 450
L. P. INLET	± 240	± 240	± 240	± 450	± 1200	± 450
H. P. INLET	± 240	± 240	± 240	± 450	± 1200	± 450
L. P. OUTLET	± 240	± 240	± 240	± 450	± 1200	± 450

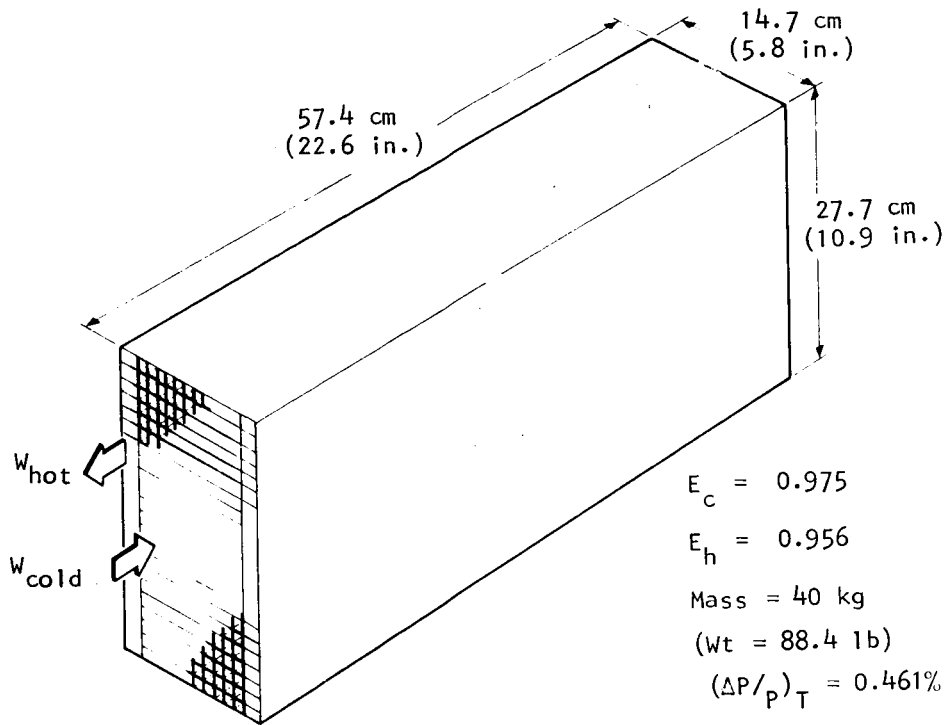


3 THIS UNIT IS DESIGNED TO WITHSTAND THE FOLLOWING PROOF PRESSURES:
 1. HIGH PRESSURE SIDE 260 PSIG @ 70°F
 2. LOW PRESSURE SIDE 175 PSIG @ 70°F
 HIGH PRESSURE SIDE MUST ALWAYS BE AT A HIGHER PRESSURE THAN LP SIDE WITH A MAX ΔP OF 85 PSI
 2. ALL OPENINGS ARE PROVIDED WITH SHARPING CLOSURES, REMOVE ONLY AT INSTALLATION. ALL DIMENSIONS ARE FOR INSTALLATION PURPOSES ONLY.

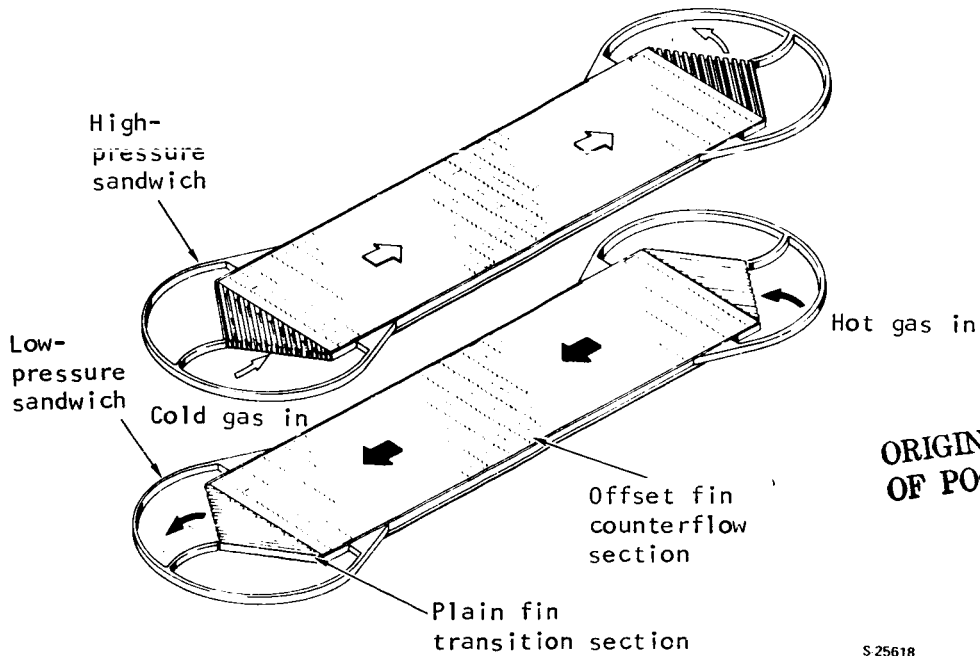
NOTES: UNLESS OTHERWISE SPECIFIED

190930-1-1		190931-1	
PART NUMBER	ASSY NUMBER	CALC. WEIGHT	REMARKS
QTY REQD	ITEM CODE	PART OR IDENTIFYING NO	NOMENCLATURE OR DESCRIPTION
PARTS LIST			
<p>190930-1-1</p> <p>RECUPERATOR OUTLINE</p> <p>1 70210 190930</p> <p>SCALE 1/1</p>			

Figure 6. --Recuperator Outline.

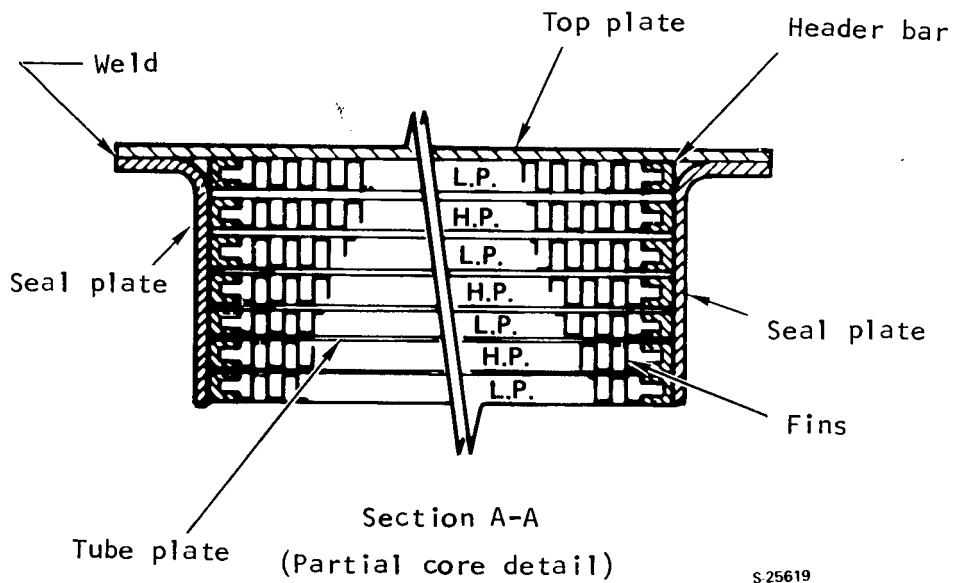
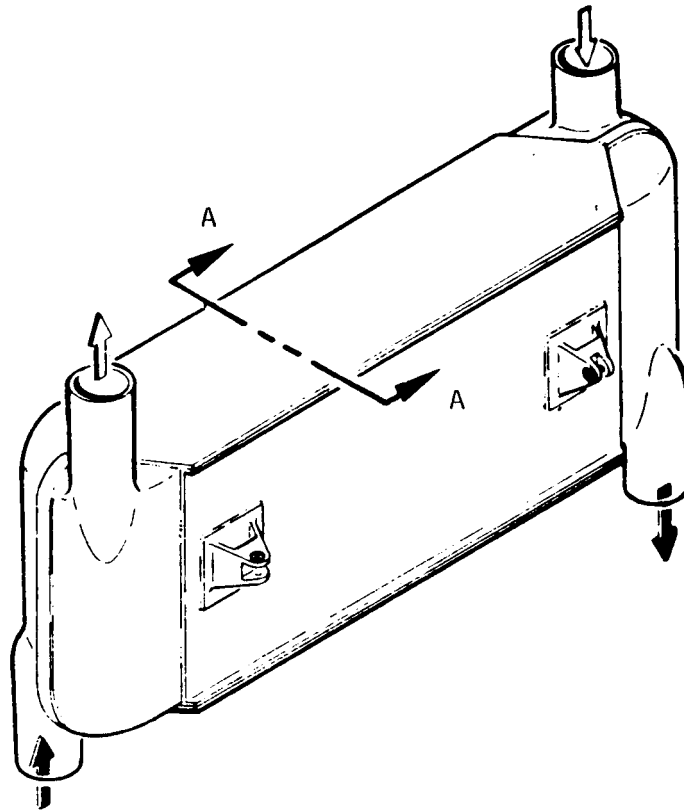


(a) Counterflow Section.



(b) Gas Flow Path and Fin Configuration

Figure 7.--MBR Preliminary Design.



S 25619

Figure 8.--Core Construction.

Graduated tube plate thickness.--Tube plate thickness increases from a nominal dimension of 0.2 mm (0.008 in.) in the center portion of the core to 0.81 mm (0.032 in.) adjacent to the 1.0-mm-thick (0.040-in.) sideplate. This feature, shown in fig. 8, provides a gradual transition between thick and thin plates and thereby provides improved load distribution during a thermal transient.

Splitter-to-core joint.--To withstand the high tensile loads developed at this location, a tongue-in-groove joint design as shown in fig. 9 was developed. Each header bar incorporates a paddle-shaped end and when stacked and brazed, a monolithic structure is formed at the core apex. A tapered groove-and-tongue arrangement is used to facilitate a close fit for brazing. The splitter overlaps the sideplates to prevent direct exposure of a primary braze joint.

Weld over braze.--As previously described, the manifolds are not welded directly to the core matrix. The cylindrical manifold is welded to an attachment strip that has been previously brazed to the core. This scheme avoids welding over the core braze joints, which is not desirable because the process can result in cracks in the weld nugget as well as cracks in the core braze joints away from the weld zone.

Sideplate thickness.--The sideplates are chemically machined to obtain the nominal thickness of 1.0 mm (0.040 in.) while maintaining the edges, which attach to the manifolds at 2.3 mm (0.090 in.). Thus, the weld joint between the manifold and sideplates is effected in material of identical thickness.

Manifold attachment flange.--To correct a weakness observed in the submodule tests, the flanges were reinforced by adding a gusset where the flanges join to the sideplate (hot end only).

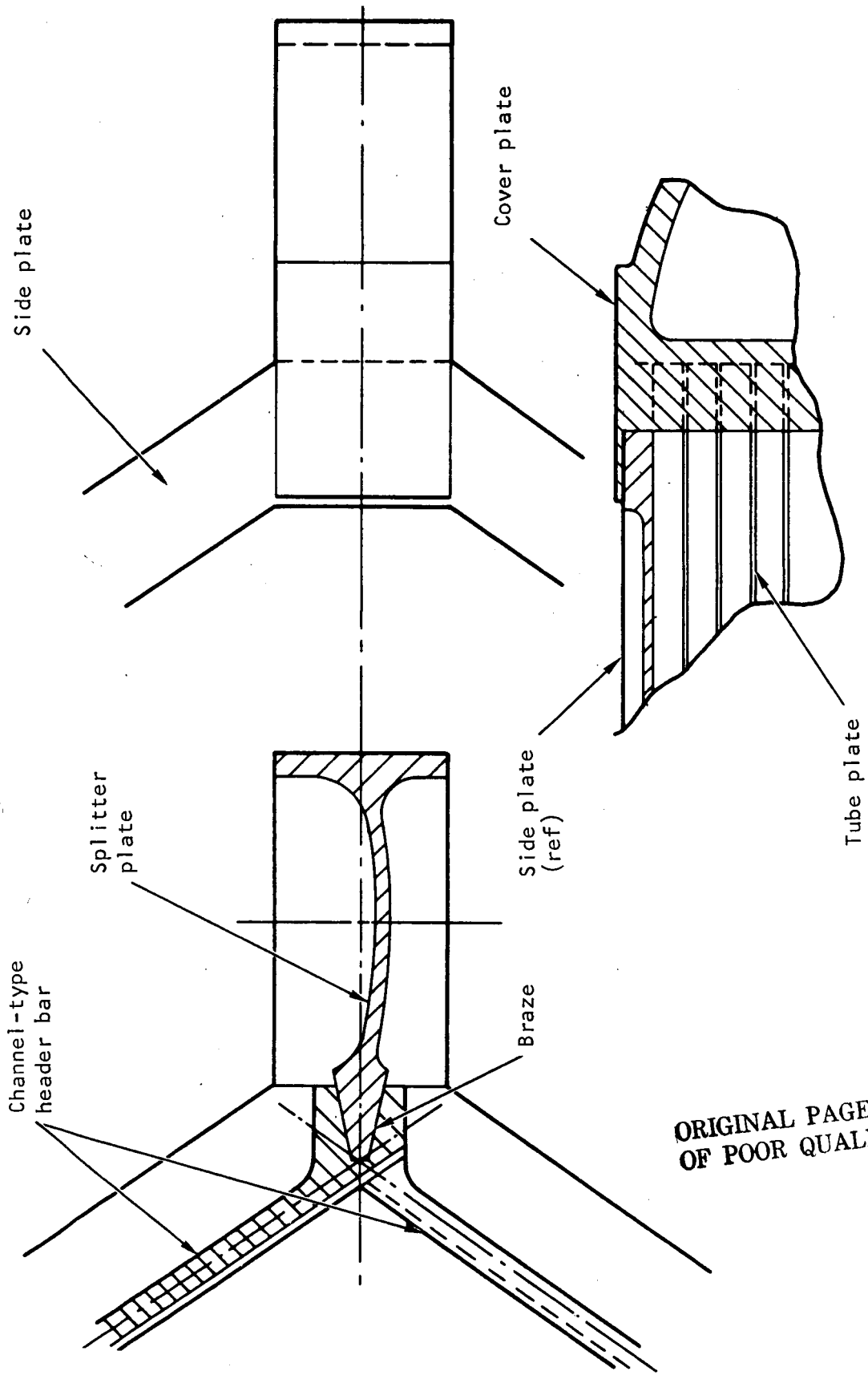
Thermal Design

Design point conditions are presented in Table III. The unit is designed for a closed Brayton power system capable of producing a gross power output of 2345 W.

Thermal design optimization of the MBR was first conducted as part of the Brayton-Cycle Heat Exchanger Technology Program (Reference 12). Optimum fin geometries were selected for the counterflow section and the triangular end section. The manifold was designed to provide uniform flow distribution.

Results of this optimization, which were used in the final MBR design, are presented in Table IV.

Test results obtained in the technology program using submodules--heat exchangers with half the flow length and half the stack height of the final MBR--indicated several areas for improvement or further analysis. These continued studies are reported here.



S-25657

Figure 9.--Splitter-Core Joint Design.

ORIGINAL PAGE IS
OF POOR QUALITY

TABLE III.--THERMAL DESIGN REQUIREMENTS

Parameter	Hot Side	Cold Side
Fluid	Xe-He*	Xe-He*
Flow, g/s (lb/sec)	162 (0.357)	159 (0.350)
Inlet temperature, °C (°F)	722 (1332)	107 (224)
Inlet pressure, MPa (psia)	0.494 (71.7)	0.732 (106.2)
Effectiveness	-	0.975
Combined pressure drop, $\Delta P/P$, percent	0.700	

*Molecular weight = 83.8 grams/mole

TABLE IV.--PROTOTYPE HEAT EXCHANGER DESIGN CHARACTERISTICS

Nominal overall dimensions, cm (in.)	
Height	35.0 (13.8)
Width	17.5 (6.9)
Length	73.2 (28.8)
Estimated weight, kg (lb)	594 (131.2)
Material	Hastelloy X
Header bar type	Channel
Thickness, mm (in.)	2.5 (0.10)
Nominal plate thickness, ⁽¹⁾ mm (in.)	0.20 (0.008)
Counterflow core fins ⁽²⁾ type	Rectangular, offset
Count, fins/cm (fins/in.)	7.87 (20)
Height, mm (in.)	2.5 (0.100)
Thickness, mm (in.)	0.10 (0.004)
End section configuration	
Height hot/cold end, cm (in.)	1.27/5.08 (0.5/2.0)
Width hot/cold end, cm (in.)	14.22/14.22 (5.6/5.6)
Split hot/cold end, percent	50
Fin type ⁽²⁾	Rectangular, plain
Count, fins/cm (fins/in.)	6.30 (16)
Height, mm (in.)	2.5 (0.100)
Thickness, mm (in.)	0.15 (0.006)
Number of plate-fin sandwiches, hot/cold	50/49
Ports, number	4
OD, cm (in.)	6.35 (2.5)

Notes:

- (1) Plate thickness is variable for the outer sandwiches.
- (2) Fin type is the same for both high- and low-pressure passages.

End section design.--Achievement of a high temperature effectiveness is especially dependent on obtaining uniform flow distribution across the passage width. Flow distribution is controlled by the end section design parameters as illustrated in fig. 10. Sizing for uniform flow usually results in asymmetrical, unequal end section geometries at the two recuperator ends. Use of the same geometry at each end would result in poor distribution because the pressure drop would not be equal for the same mass velocity even though the flow path lengths are equal. Nonuniformity along parallel paths results from the large density difference, and to a smaller extent from the viscosity difference, that occurs from the inlet to outlet.

Three parallel gas flow paths through the heat exchanger low-pressure passages are identified by dashed lines in fig. 10(a). For uniform core flow distribution, the total (inlet-to-outlet) pressure drop along each flow path should be the same for a constant value of the gas mass velocity. Since the entrance, exit, and turn losses are equal for all three flow paths, regardless of end section geometry, this requirement reduces to a requirement for equal frictional losses, i.e.,

$$\Delta P_f 1A + \Delta P_f 1B = \Delta P_f 2A + \Delta P_f 2B = \Delta P_f 3A + \Delta P_f 3B$$

where ΔP_f = friction pressure drop.

Since $\Delta P_f 1B = \Delta P_f 3A$, this is equivalent to the condition

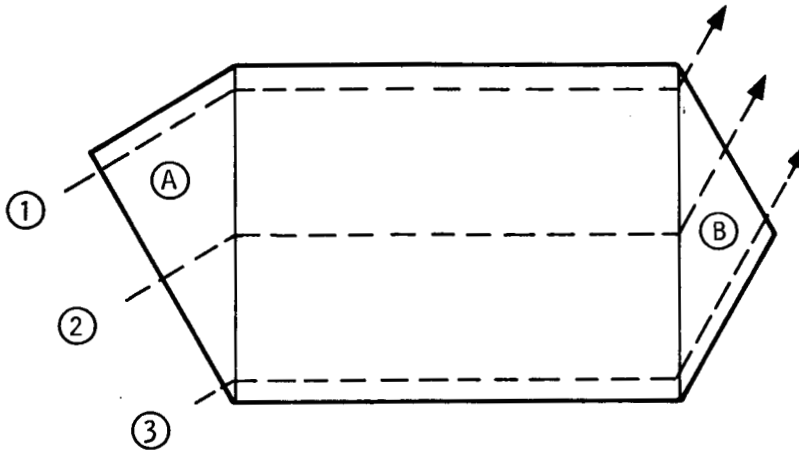
$$\Delta P_f 1A = \Delta P_f 3B, \text{ or } \Delta P_f 2A = \Delta P_f 2B.$$

That is, for uniform flow distribution, the average frictional pressure loss in the inlet end should be equal to the average frictional pressure loss in the outlet end. This is not equivalent to requiring the average total pressure drops to be equal because kinetic losses at opposite ends are not equal.

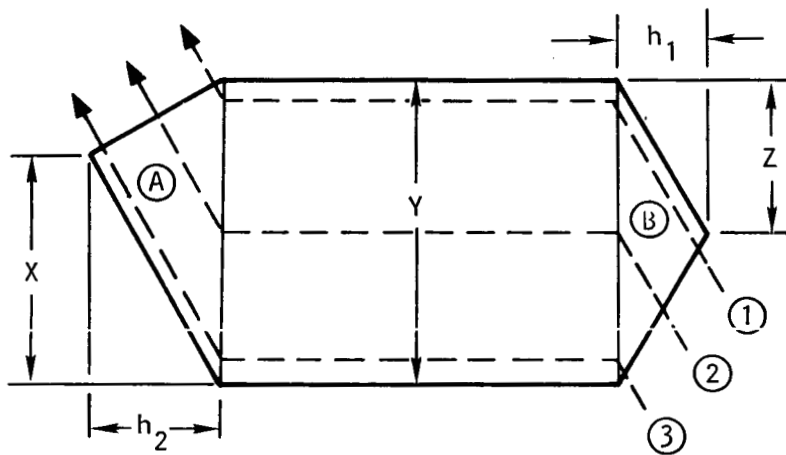
Fig. 10(b) shows the high-pressure-side fin sandwich for the same recuperator. Similar considerations as those discussed for flow distribution on the low-pressure side apply to the high-pressure side. Thus, to obtain uniform flow distribution throughout the heat exchanger, the end section geometries must be such that the inlet frictional loss equals the outlet frictional loss on each side of the exchanger. Within this requirement, a number of design solutions exist, because for each geometry selected at one end of the exchanger, there is a geometry at the other end (obtained by varying the parameters defined in fig. 10(c)) that results in balanced pressure drops.

For the MBR it is best to use symmetrical end sections, i.e., the ratios x/y and z/y are both equal to 0.5. This locates the splitter plate in the center of the manifold, thereby reducing the stress developed in the splitter and manifold to a minimum. For the submodules described in Reference 12, the height h was set equal and, hence, the end sections were symmetrical and identical; it was elected to accept the resultant flow maldistribution and performance loss.

ORIGINAL PAGE IS
OF POOR QUALITY



(a) Low-Pressure Gas Passage



(b) High-Pressure Gas Passage

<u>Hot End</u>	<u>Cold End</u>
x/y and h_2	x/y and h_1

(c) Geometry Parameters

S-25653

Figure 10.--End Section Design.

For the prototype heat exchanger, end section pressure drops were calculated, combined with those in the counterflow section, and the flow distribution along the recuperator width that gives equal pressure drop (impedance) was then determined. The resultant flow distribution shown in fig. 11 indicates nonuniform flow characteristics with a flow variation from one side of the recuperator to the other of approximately 8 percent. This flow variation is induced by a pressure drop variation of approximately 11 percent along the flow width if the flow were uniformly distributed. The net effect of the flow maldistribution is to create a local unbalance in the capacity rate ratio, $(W_{cp})_{cold}/(W_{cp})_{hot}$, which degrades the performance.

Heat exchanger performance with the fig. 11 flow distributions was determined and compared with the uniform flow solution. The results for the high-pressure side are shown in Table V.

TABLE V.--RECUPERATOR PERFORMANCE FOR HIGH-PRESSURE SIDE

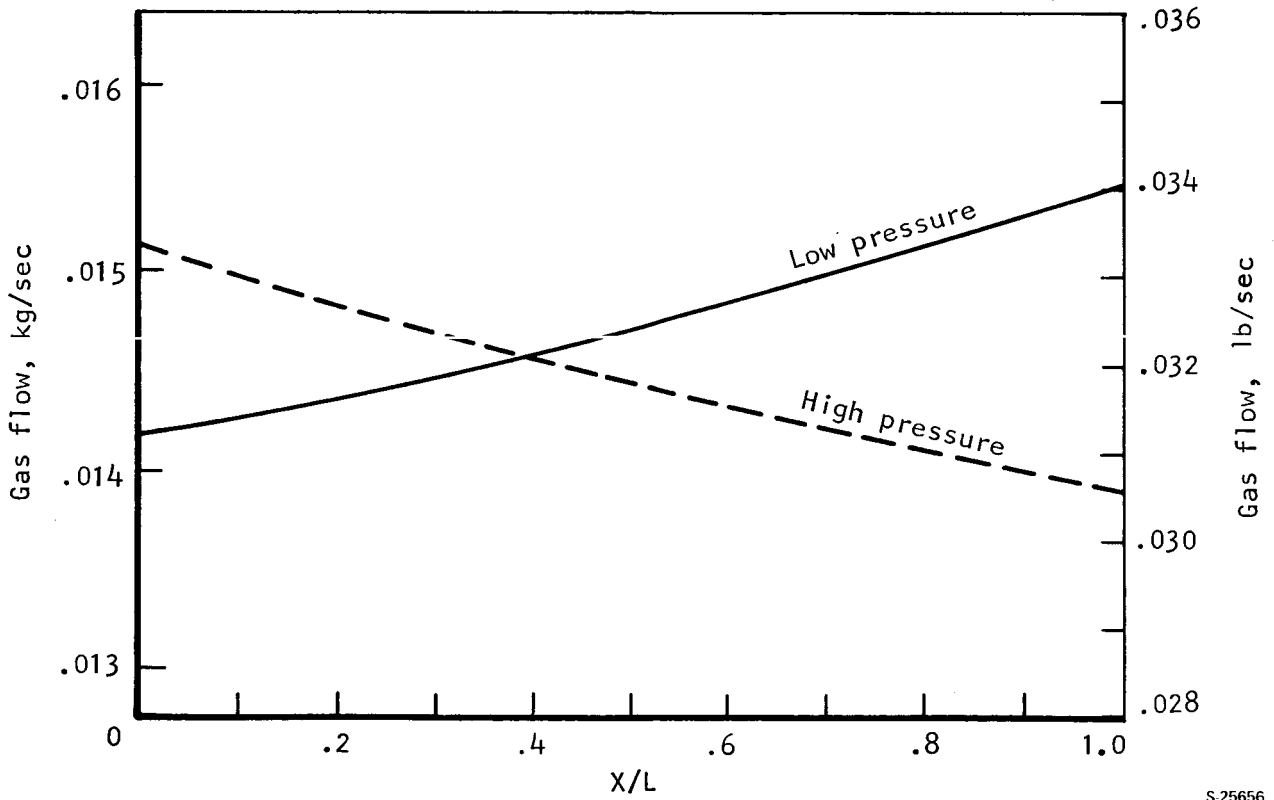
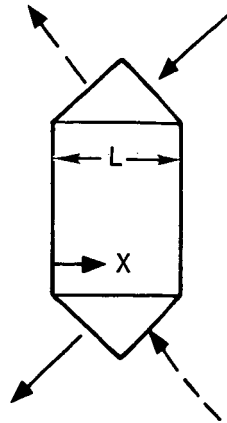
	Uniform Flow	Nonuniform Flow*
Inlet temperature, °C (°F)	107 (224)	107 (224)
Outlet temperature, °C (°F)	710.4 (1310.7)	706.3 (1303.3)
Effectiveness	0.9808	0.9741

*Flow distribution shown in fig. 11

The reduction in temperature effectiveness caused by the nonuniform flow is small (0.68 percent); however, because of the high effectiveness required of the recuperator, the nonuniform flow degrades the thermal conductance, UA, by 24 percent. This performance penalty is unacceptable.

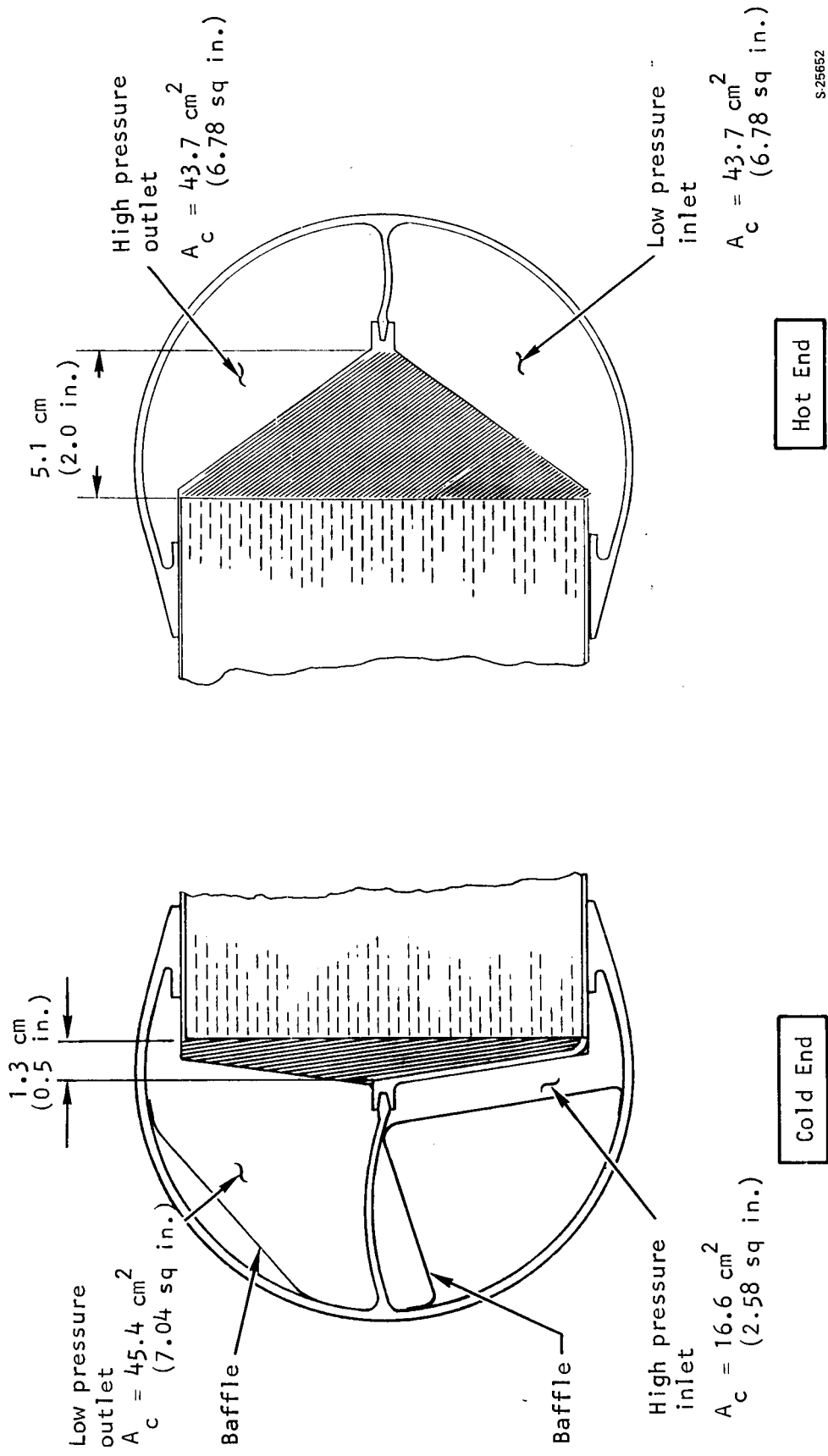
Further parametric studies were conducted. The end sections were kept symmetrical (ratio = 0.5), but the section height h was varied. It was determined that a reasonable solution could be obtained by setting the section heights on the hot and cold ends at 51 and 13 mm (2.0 and 0.5 in.) respectively. This configuration, shown in fig. 12, limits the flow maldistribution to less than 2 percent.

Manifold flow distribution.--The heat exchanger manifolding must be carefully sized to promote uniform flow into each passage. As discussed above, flow uniformity is especially important for a high-effectiveness application. The problem is illustrated in fig. 13. In a U-flow configuration, the static pressure rise due to flow deceleration in the inlet manifold must be matched to static pressure drop due to flow acceleration in the outlet manifold. In this fashion, the static pressure differential is maintained equal across each passage, and uniform flow results. In



S-25656

Figure 11.--Flow Distribution with an 11 Percent Pressure Drop Imbalance.

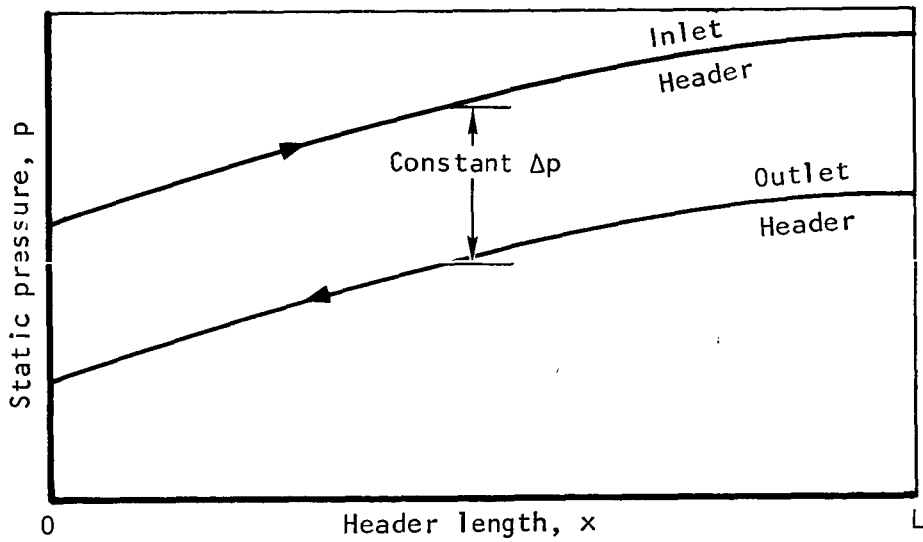
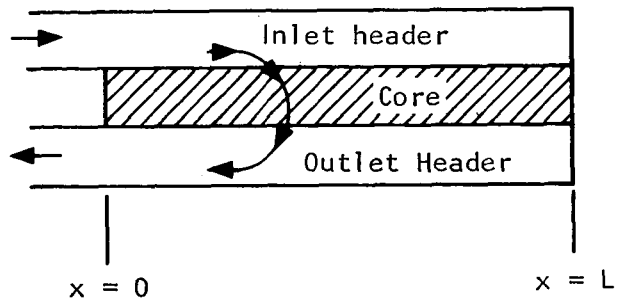


S-25662

Figure 12.--Flow Distribution Provisions.

ORIGINAL PAGE IS OF POOR QUALITY

ORIGINAL PAGE IS
OF POOR QUALITY



S-25654

Figure 13.--Manifold Pressure Gradients.

a U-flow design it is possible to match the pressure gradients by using constant flow area manifolds and adjusting the area ratio between manifolds.

Based on analytical techniques developed in References 13 and 14, the manifolds were sized to promote uniform core flow. The resultant flow areas, A_c , are shown in fig. 12. Gross manifold flow area is controlled by the shape of the cylindrical manifold, which is fixed. The calculated net flow area is achieved by locating sheet metal baffles within the manifold as indicated in fig. 12. The baffles are vented, and hence, they merely direct the flow, and pressure containment is by the manifold structure.

Predicted performance.--The MBR specification and the predicted performance are compared in Table VI. Heat transfer performance is based on zero heat loss to ambient. A positive margin in the overall thermal conductance, UA, of 19.5 percent is indicated; however, known factors of flow maldistribution and manufacturing tolerances can be expected to reduce the UA margin to 12.0 percent. Based on the submodule results reported in Reference 12, the net UA margin is adequate.

The recuperator pressure drop is predicted to be equal to the specification limit without margin. This is considered acceptable because the analytical technique has been shown to produce a conservative result when used to predict the submodule performance (Reference 12).

TABLE VI.--PREDICTED PERFORMANCE

Performance	Required	Predicted (No margin)
Cold side effectiveness	0.975	0.9798
Equivalent thermal conductance, UA, kW/°C (Btu/sec°F)	1.406 (0.741)	1.748 (0.921)
Total $\Delta P/P_{inlet}$, percent UA margin = 19.5 percent Pressure drop margin = 0	0.700	0.696
<p>Factors predicted to decrease equivalent UA</p> <p>Up to 2 percent flow maldistribution: 4.0 percent UA</p> <p>Manufacturing tolerance: 3.5 percent UA</p> <hr/> <p>Total 7.5 percent UA</p> <p>Net UA margin = 12 percent</p>		
Predicted Pressure Drop Breakdown	Hot side (low pressure) $\Delta P/P_{in}$, percent	Cold side (high pressure) $\Delta P/P_{in}$, percent
Core	0.248	0.109
End sections	0.130	0.056
Inlet-outlet ducts*	0.071	0.022
Manifolds	<u>0.029</u>	<u>0.031</u>
Total	0.478	0.218
Total for both sides	0.696 percent	

*1.5 duct velocity heads 6.17 cm (2.43 in.) ID duct

Structural Design

The unit must be capable of 100,000 hr (10 years) continuous operation at a maximum operating temperature of 1000°K (1330°F). Life requirements further specify that the recuperator must endure 1000 operating cycles without failure. A cycle is defined as startup of the system, followed by sustained steady-state operation at maximum conditions and finally, shutdown of the system until ambient conditions are obtained. In general, thermal stresses exceeding the material yield strength will occur during the startup transient. Cyclic life is determined by comparing the accumulated plastic strain per cycle to the critical plastic strain to cause crack initiation in the heat exchanger structure.

Results of the submodule test program (Reference 12) identified low-cycle fatigue as the most critical design problem. Analyses were performed to predict transient temperature distributions throughout the core assembly, the resultant thermal stresses, and the cycle life at critical sections; results were reported in Reference 12. Because of the critical nature of low-cycle fatigue-induced cracking, these initial studies were extended and the results for the MBR are presented in a separate section.

Inertia loads, shock, vibration, and acceleration are considered to be possible during any phase of the operating cycle. The mounting brackets must, therefore, be designed to endure the required loads at the elevated temperature condition. Inertia loads occur for a relatively short time, such as vehicle launch, and, therefore, short time material properties are applicable.

Design criteria are summarized in Table VII. After consideration of possible load amplification, a combined load factor of 50 g was specified for vibration, shock, and acceleration loads. This maximum loading is considered to act independently along any one axis. Proof and burst pressure tests are specified to verify heat exchanger integrity and to ensure a capacity for withstanding short-term overpressure conditions.

Loads induced by pressure containment were analyzed and the results presented in Reference 12. Additional analysis performed on the manifold splitter-to-core joint and the recuperator installation is described below.

Splitter-core joint.--Results of the thermal cycle test conducted on the first submodule (Reference 12) showed a deficiency at the splitter/core joint. After 10 cycles of operation, a fatigue crack developed at the point where the manifold splitter plate is brazed to the apex of the triangular end section, thereby permitting interpass leakage to occur.

TABLE VII.--STRUCTURAL DESIGN CRITERIA

Requirement	Condition	Design Criteria
Operating life	100,000 hr (10 yr) at maximum temperature and pressure	Total distortion does not exceed 1 percent creep
Cyclic life	1000 cycles; transient startup and shutdown with 400 sec to reach maximum gas inlet temperature	Accumulated plastic strain is less than critical failure strain
Proof pressure test	150 percent overpressure for short time	Stresses must be less than material yield strength
Burst pressure test	250 percent overpressure for short time	Stresses must be less than material ultimate strength
Inertia loading	150 percent load factor for short time	Stresses must be less than material yield strength

To gain a better understanding of the stresses developed at this location, a two-dimensional finite element model of the manifold configuration was constructed using beam elements. Temperature distributions associated with a 100-second and a 300-second startup ramp* were imposed on the model, together with boundary displacements from the core stress analysis.

Results showed that the thermal stresses developed in the manifold structure were below the material yield strength. The predicted tensile strength at the splitter/core joint for the test conditions (60-second startup ramp) was 18.6 MPa (2700 psi). This stress level is believed to be below the yield point of the braze joint (Hastelloy X brazed with Palniro RE filler alloy), although specific data are lacking.

Metallographic examination of the splitter/core joint showed that cracks had developed in the bar-to-plate joints at the core apex, indicating that a high-tensile loading in the stack-height direction occurred during the test. Thus, it was decided to perform a three-dimensional analysis to account for the manifold restraint in the stack height direction.

The finite element model is shown in fig. 14. Results for pressure-related loading showed lower distortions than predicted by a two-dimensional analysis, indicating that the specified manifold gauges are conservative.

Results of the analysis are shown in fig. 15 in the form of thermal distortions that occur 70 sec after the beginning of the 100-sec startup

*Time for hot gas (low pressure) inlet temperature to reach maximum operating temperature from a cold start.

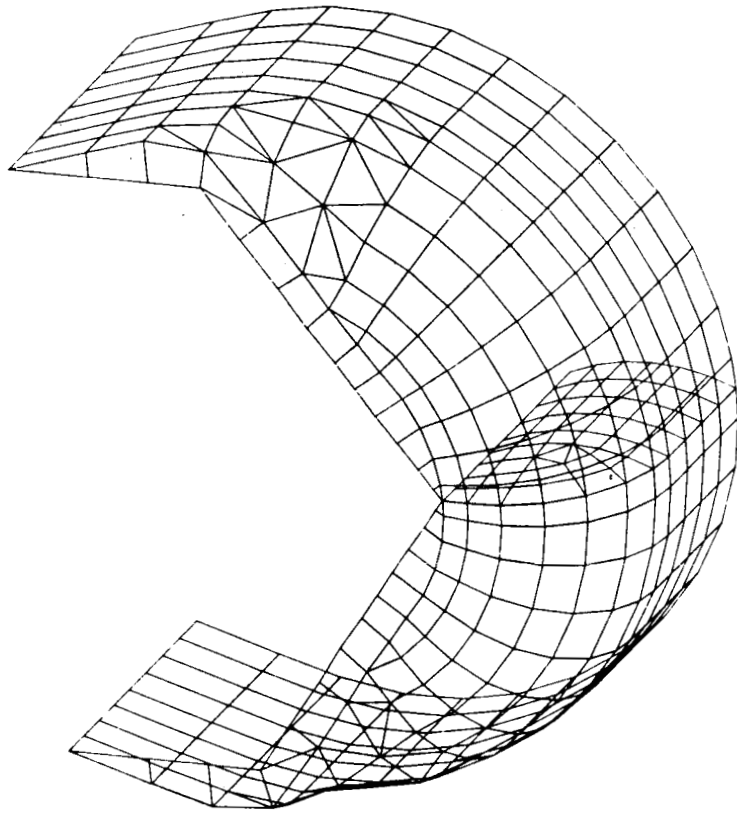


Figure 14.--Three-Dimensional Finite Element Model.

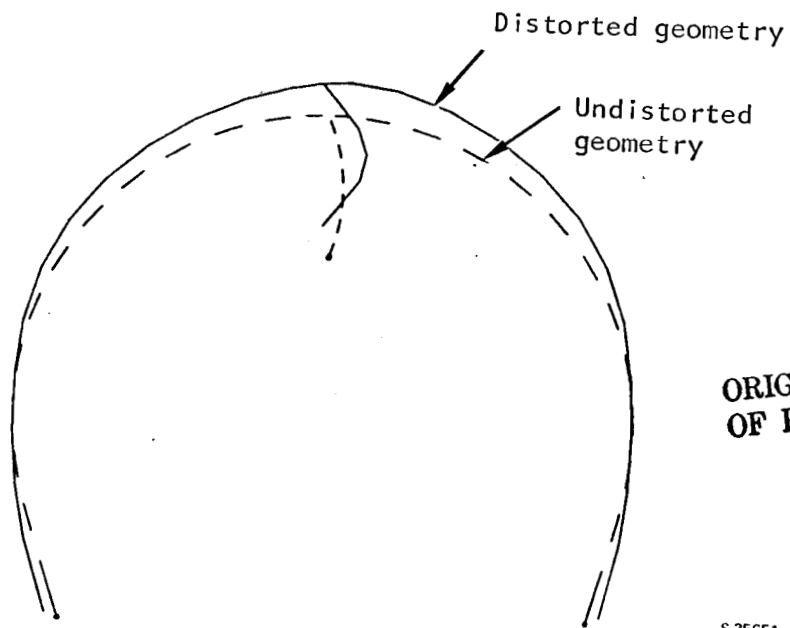


Figure 15.--Thermal Distortions of MBR Manifold at Mid-Stack Height Section.

transient. At this time the core had expanded more than the manifolds, thereby imposing a compressive loading on the manifold splitter plate. Typical stress contours are shown in fig. 16. These results show significantly higher stress levels than shown by the previous two-dimensional thermal stress analysis. The increased stresses can be attributed to the end effects caused by the rigid side plates. The apparent elastic stress exceeds the material yield strength at certain locations and some plastic deformation will occur; however, no failure in the parent material or the weld joints over the heat exchanger cyclic life is predicted based on the Hastelloy X ductility characteristics.

Thermally induced loads on the critical splitter-core braze joint are tabulated in fig. 17, which shows the load variation along the stack height direction. These loads are much greater than those obtained with a two-dimensional analysis and increase significantly at the manifold ends where the ends are brazed to the side plate.

As a result of this analysis the splitter joint design shown in fig. 9 was evolved. This joint provides sufficient shear area to react the thermal- and pressure-induced loads.

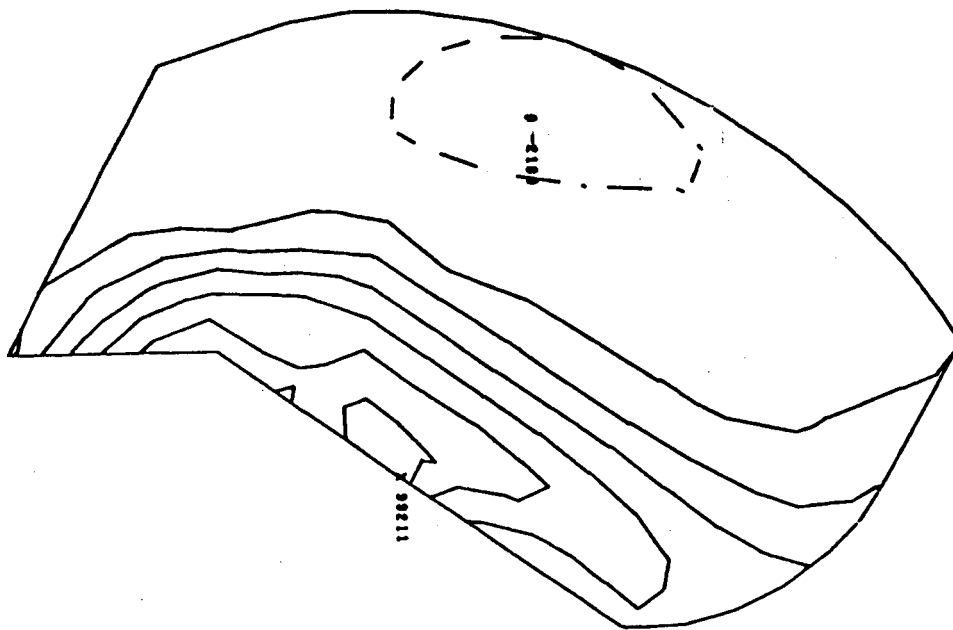
The three-dimensional analysis explains why fatigue cracks developed in the splitter-core joint during the submodule thermal cycle test. During the startup temperature transient, the core matrix responds faster than the manifolds because the matrix contains fins that enhance the heat transfer rate. The matrix wants to expand in the core stack height direction as well as outward from the core apex, but is restrained by the stiff manifold structure. A high compressive load is produced in the core matrix, especially at the apex, and the material yield strength is probably exceeded during a portion of the cycle. During the latter stages of the transient, the manifolds start to respond and the load at the core apex is reversed and a high tensile stress is developed. During the steady state portion of the cycle, the tensile stress relaxes and a measure of creep damage is incurred. Thus, a plastic loop is produced, which, after a number of operating cycles, causes a low-cycle fatigue crack to develop.

Installation.--The recuperator mounts were designed to withstand a 50 g load applied independently along any axis. The allowable loads for both a 3- and 4-mount system are defined in outline drawing 190930 (see fig. 7). Allowable duct loads and the thermal growths were calculated and the results are also shown on drawing 190930.

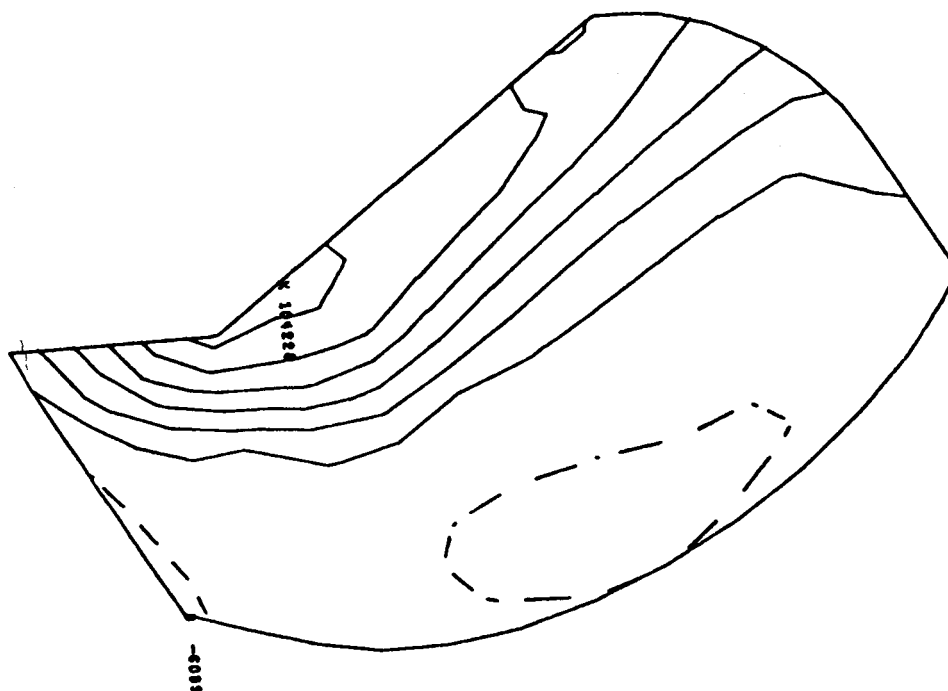
Failure Mode, Effect, and Criticality Analysis (FMEA)

A failure mode, effect, and criticality analysis was performed for the recuperator considering the component and the system installation, and the results are presented in Reference 15. No serious design deficiencies were found. A number of recommendations were advanced, including the following:

1. System controls should prevent imposing off-limit pressures or temperatures on the recuperator.



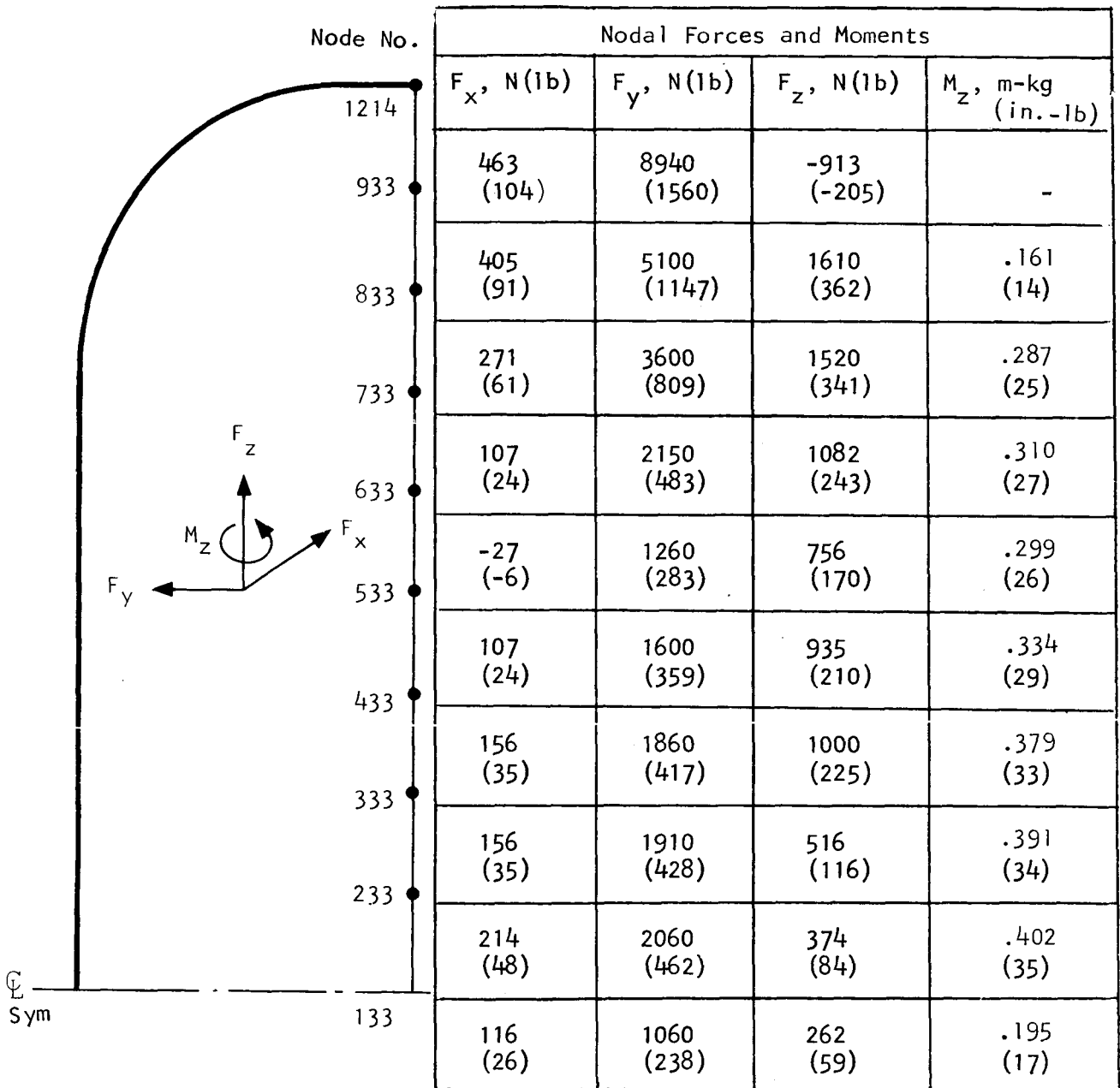
(a) Low-Pressure Manifold.



(b) High-Pressure Manifold

S 25521

Figure 16.--Maximum Principal Thermal Stress Contours.



S-25620

Figure 17.--Thermally Induced Loads in the Splitter/Core Braze Joint Due to System Startup Transient.

2. An inspection technique should be developed to verify full braze alloy flow on the manifold attachment flange-to-core braze joint.
3. System integrator should verify that loads applied to the ducts or mounts do not exceed the design allowables.
4. A qualification test should be performed to substantiate the recuperator mounting arrangement.

PROTOTYPE HEAT EXCHANGER

A prototype MBR was fabricated to develop fabrication techniques and to verify the performance and cyclic life predictions. The unit was equivalent to the final MBR in all respects except for the mounting pads, which were not used on the prototype.

Fabrication

The heat exchanger core was assembled in a three-step brazing procedure. In the first operation, Palniro 1 braze alloy (AMS 4784, 50 Au25Ni25Pd) in the form of 0.025-mm foil was cut to size and tack-welded to the individual tube sheets. The header bars were then attached to the foil-coated tube plates using a fixture to maintain the bars within 0.25 mm of true position along their entire length. A partial passage assembly with the fins in place is shown in fig. 18. The solid header bar is stopped about 18 mm short of the end of the passage on the core side next to the passage inlet. This provides for additional flexibility in the corners of the core where the transient temperature gradients are high. A thin sheet metal baffle is used to prevent flow from bypassing.

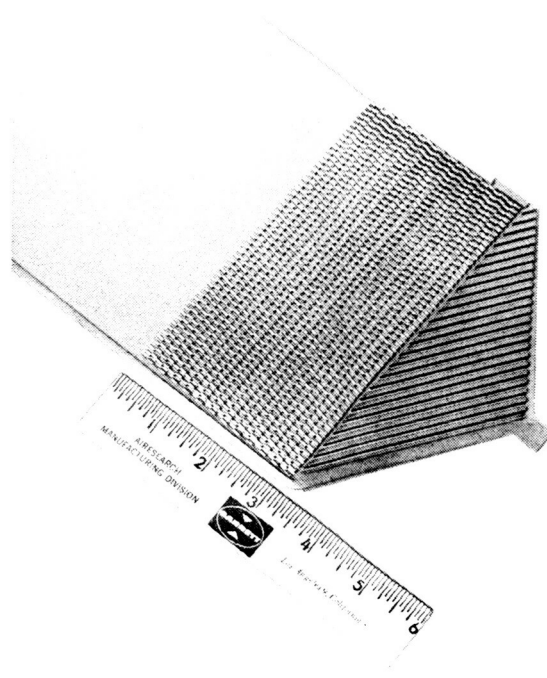
Individual passages were assembled in a stacking fixture and held in place using temporary ties. The assembly was transferred to a graphite fixture and brazed in a vacuum furnace.

After brazing, the sides of the header bars are machined flat and a tapered groove is cut at the apex to receive the manifold splitter plate. The machined core assembly is shown in fig. 19. The heavier section, chemically machined in the sideplate for manifold attachment, is also visible.

In the second braze operation, the seal plates and manifold splitters (fig. 20) are joined to the core assembly using Palniro RE (55Au37Ni8Pd) braze alloy. Fig. 21 shows the core assembly after completion of this operation.

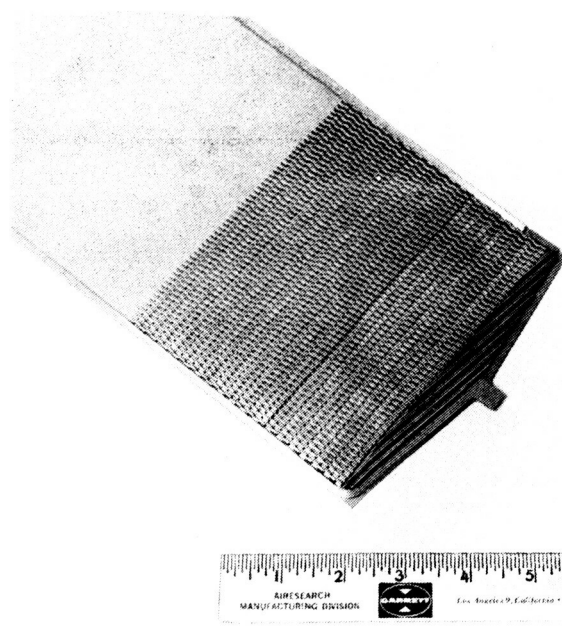
In a third and final braze operation, using Palniro 7 alloy (70Au22Ni8Pd), the manifold pan attachment flanges (fig. 22) are brazed to the seal plate to form the complete core assembly (fig. 23).

The manifold pans were fitted and welded to the core assembly. All welds were visually checked for cracks using 20X magnification and were then radiographically inspected. A photograph of the completed prototype unit is shown in fig. 24. Conoseal flanges are installed on the duct ends to facilitate testing.



76359-5

(a) Hot End.



76369-4

F-27052

(b) Cold End.

Figure 18.--Passage Assembly.

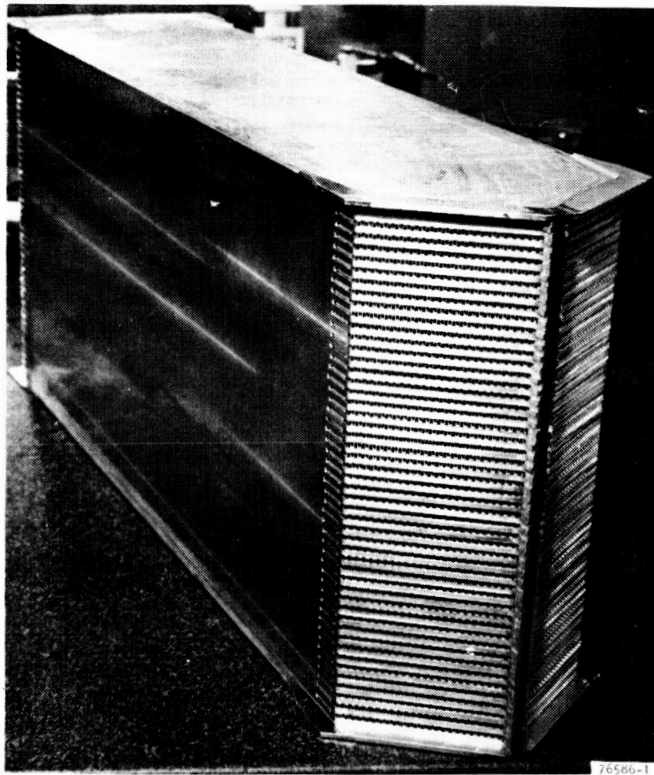
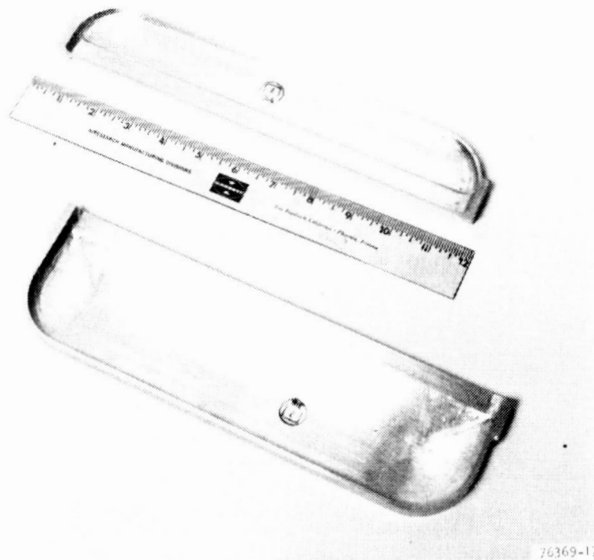


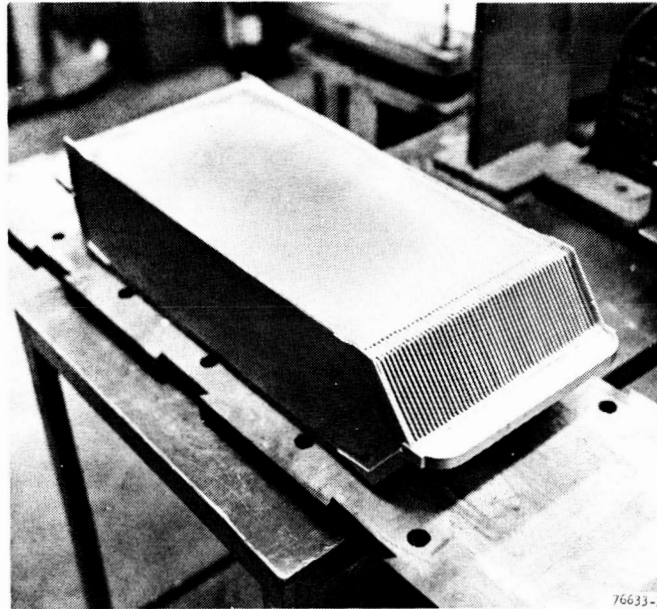
Figure 19.--Core Assembly After Machining of the Header Bar Surface and Manifold Splitter Groove.



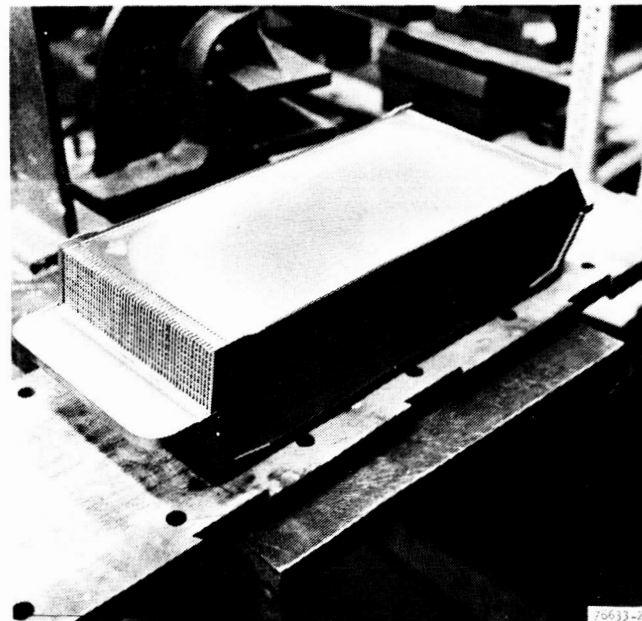
F-27054

Figure 20.--Manifold Splitter Plates.

ORIGINAL PAGE IS
OF POOR QUALITY



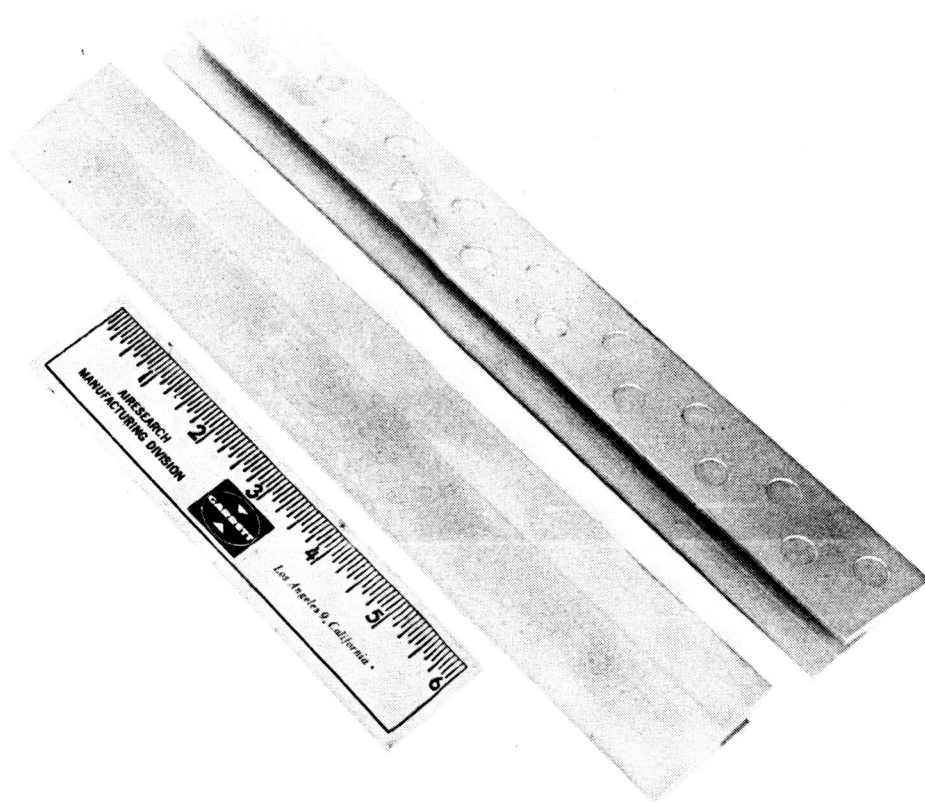
(a) Core Assembly, Hot End View.



F-27053

(b) Core Assembly, Cold End View.

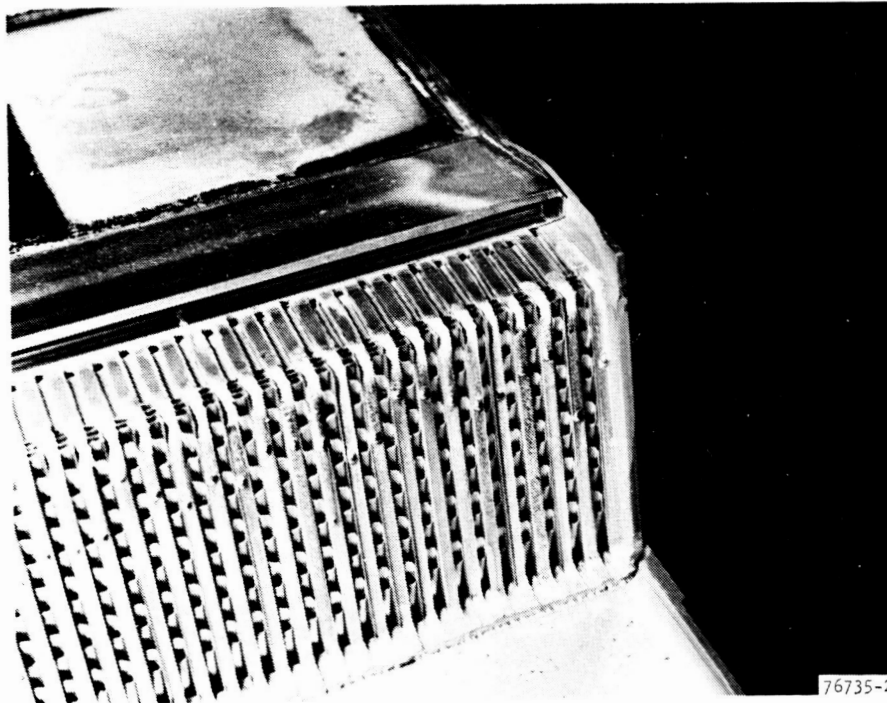
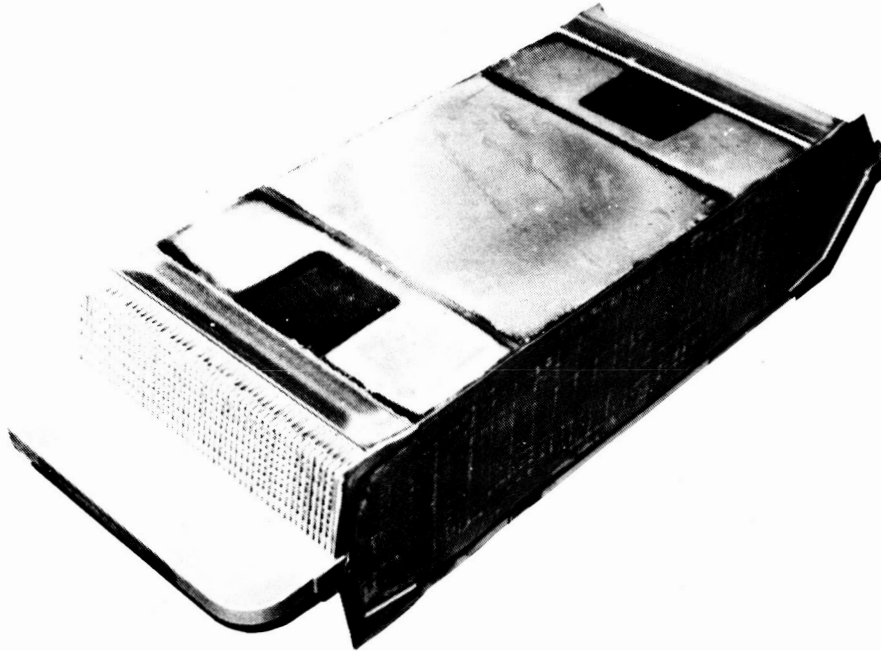
Figure 21.--Core Assembly Following Braze to
Attach Seal Plates and Splitters.



76362-1

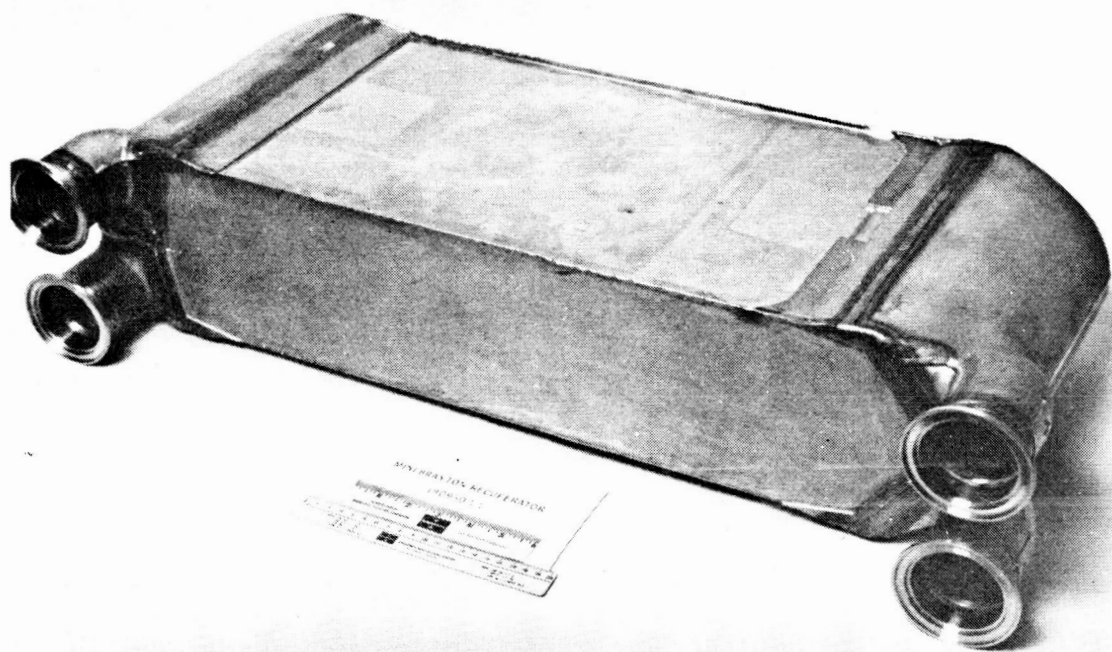
Figure 22.--Manifold Attachment Flange.

ORIGINAL PAGE IS
OF POOR QUALITY



F-27046

Figure 23. Core Assembly Following Braze to Attach the Manifold Side Flanges.



77183-1

Figure 24.--Mini-Brayton Recuperator, Prototype Assembly.

Performance Test

Proof pressure test.--A proof-pressure test was conducted at laboratory ambient temperature. Pressure was applied to both circuits at the same time. The following pressure levels were held for five minutes:

Lower pressure (hot) 1.21 + 0.03, -0 MPa (175 + 5, -0 psig)

High pressure (cold) 1.79 + 0.03, -0 MPa (260 + 5, -0 psig)

During the pressurization and subsequent pressure release, the circuit differential pressure was not allowed to rise above 0.59 MPa (85 psi).

No visible deformation or leakage was noted during these tests.

Helium leak check.--Following a thorough trichlorotrifluoroethane cleaning of the internal surfaces of the assembly, a helium leak check was made to determine the leakage rate between the high- and low-pressure circuits of the unit and from the unit to the surroundings. The objective for the intercircuit and external leakage is 10^{-7} atmospheric cc/sec or less.

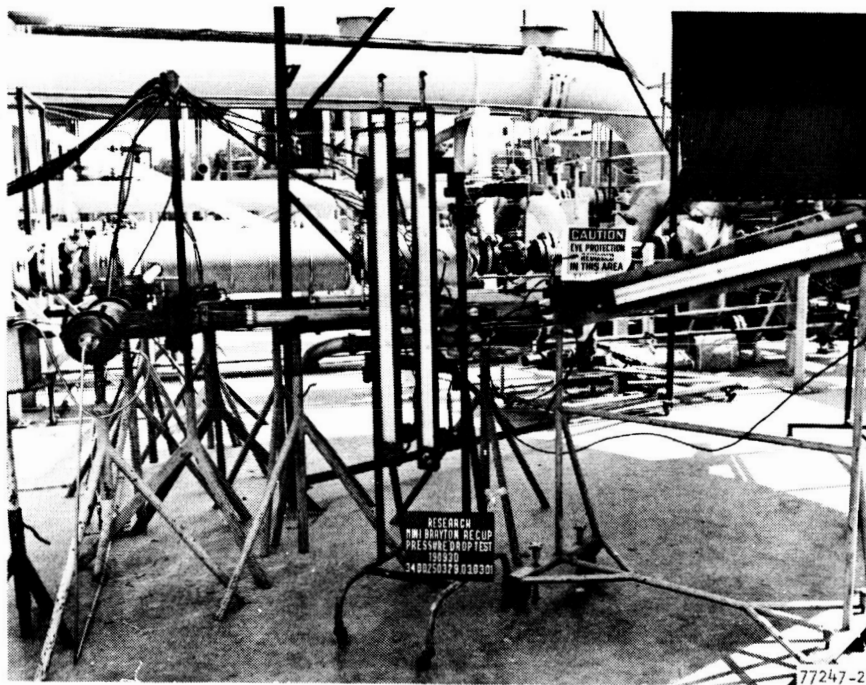
For the external leakage determination, both circuits were evacuated and the external surfaces of the unit were enveloped with helium at a slight positive pressure. The leakage rate measured was 1.0×10^{-8} atmospheric cc/sec.

The intercircuit leakage rate was determined by evacuating the low-pressure circuit of the unit and filling the high-pressure circuit with helium at a maximum differential pressure of 1 atm. In this check, the measured leakage rate was 3×10^{-8} atmospheric cc/sec.

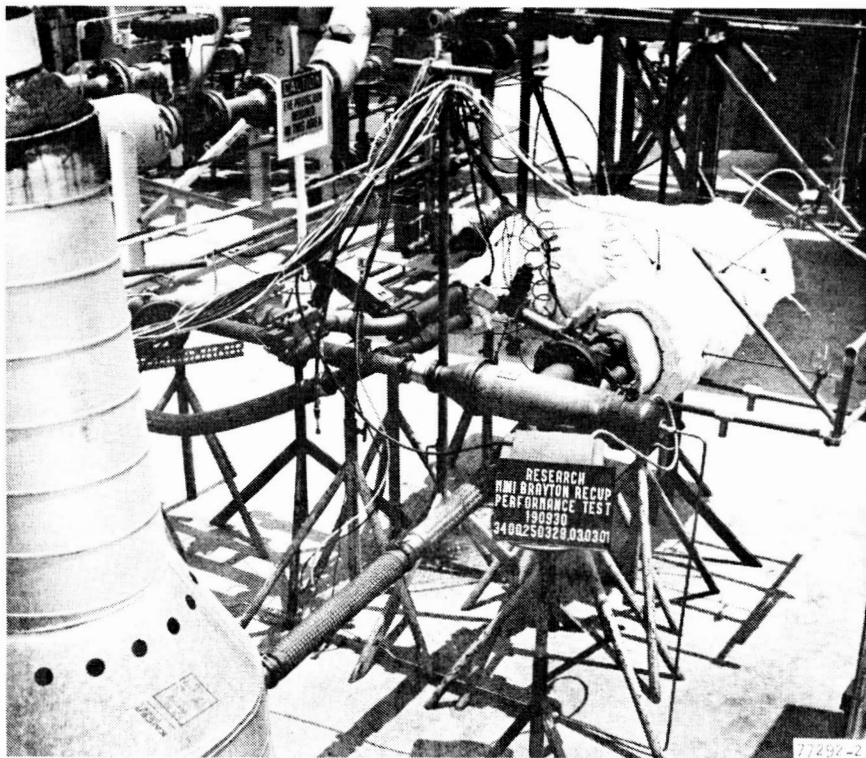
Isothermal pressure drop test.--The pressure drop tests were performed with laboratory air at ambient temperature exhausting to sea-level ambient pressure. Data were obtained at eight flow points in each circuit and the flow range covered 20 to 400 percent of the design point Reynolds number. Fig. 25 shows a photograph of the test setup.

The predicted pressure drop with xenon-helium based on the air data corrected for Reynolds number effects is shown in fig. 26. At the design point flow, this particular unit exhibited a pressure drop 10 percent above the design value.

Heat transfer performance test.--In actual operation, the Mini-Brayton Recuperator will be in a space vacuum environment with xenon-helium as the working fluid. Heat transfer performance testing under these conditions was ruled out because of cost considerations. Calibration tests, therefore, were run using laboratory compressed air with the unit exposed to a sea-level pressure environment and the test data corrected to design point conditions using analytical techniques.

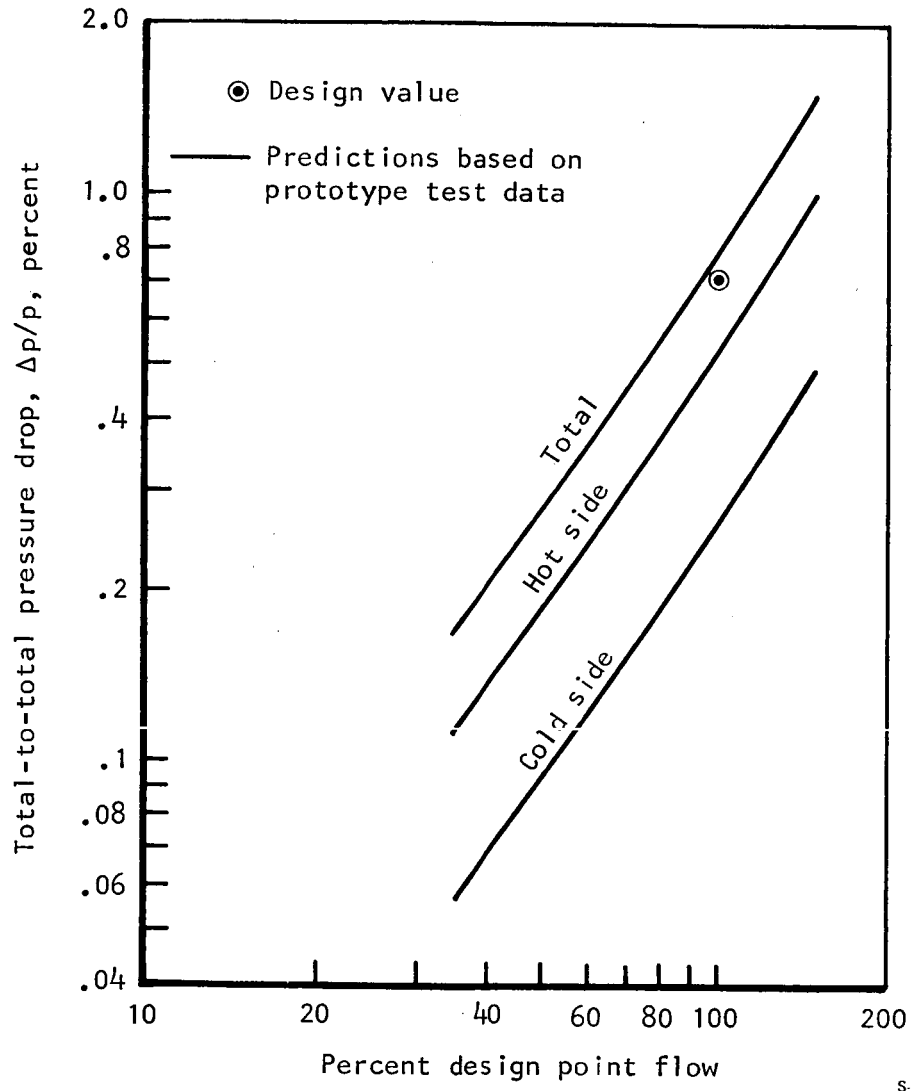


(a) Isothermal Pressure Drop.



(b) Heat Transfer.

Figure 25.--Performance Test Setup.



S-25646

Figure 26.--Pressure Drop with XeHe for the Prototype Mini-Brayton Recuperator.

The design point effectiveness is $E_C = 0.975$. At this high effectiveness level, small variations in heat transfer surface characteristics, axial conduction, and core flow distribution tend to produce large changes in the thermal conductance (UA). Small heat leaks to ambient that otherwise would be negligible must be accounted for. For example, using 150 mm (6.0 in.) thickness of a high-temperature fibrous insulation around the heat exchanger would limit the heat loss to 1.0 percent of the heat transferred. For the MBR, using air as the test fluid, this small heat loss would reflect a 15 percent decrease in the overall thermal conductance, UA (with xenon-helium, the UA degradation would exceed 35 percent).

The basic approach used to correct the heat leak was to test at flows much larger than the full-scale flow rates, but at the design temperature level. In this case the heat leak is about the same as at the design point flow but the effect on UA is much less and an analytical correction for heat leak is reasonable. The exact procedure was as follows:

1. Test at air flows that exceed the design point Reynolds number by a factor of four.
2. Correct the test results for heat leak (estimated to be a 2 percent or less correction to the measured UA value).
3. Predict recuperator performance at the high air flow test condition. Use the same design data and coefficients as originally used to design the MBR.
4. Compare the predicted performance to test performance. Since heat leak has been accounted for, any remaining discrepancy is attributed to flow maldistribution, manufacturing tolerances, or other related factors.
5. The percent discrepancy in UA, plus or minus, was assumed constant over the flow range of interest and this factor was used when converting the test data to performance with Xe-He.

The success of this procedure depends on the ability to scale the losses other than the heat leak. If calibration tests are performed at full-temperature, then complex and non-linear temperature functions are eliminated from the process. Reynolds number effects on the heat transfer and pressure drop performance can be accounted for because test data are available over the range of interest. The friction factor (f) and Colburn modulus (j) are monotonic functions of the Reynolds number; there are no transition regions.

Flow distribution in the core and manifolds at the high airflow condition was checked using the previously described techniques, and no significant maldistribution effects were found. A detail discussion of the test plan is presented in Reference 16.

Test setup.--A view of the overall setup for the heat transfer tests is shown in fig. 25. Here, the test unit is insulated with 150 mm (6 in.) of Kaowool. A schematic of the test arrangement and instrumentation is given in fig. 27.

Special consideration was given to temperature measurement because at high effectiveness levels, small temperature variations cause a substantial change in UA. For example, at design point Reynolds number conditions, a 3°C error in the hot gas inlet temperature (nominally at 722°C) yields an 18 percent change in UA. The following special procedures were followed:

1. Premium grade chromel-alumel wire was used and the junctions were calibrated using melting point standards.
2. For the high-temperature locations (cold outlet and hot inlet), aspirating-type probes were used. This particular probe design is effective in eliminating thermocouple radiation and conduction errors. The probes were calibrated to obtain the recovery factor.
3. Thermocouple output was read on a precision potentiometer.

With this installation, it was predicted that uncertainties in the temperature measurements were limited to 0.25 percent, which corresponds to $\pm 1.8^\circ\text{C}$.

Data analysis and results.--Heat transfer data were obtained over a flow range corresponding to a core Reynolds number range of 100 to 400 percent of the design point condition. Heat loss corrections were applied and the test performance with air was matched on a heat exchanger performance computer program. Results are shown in fig. 28.

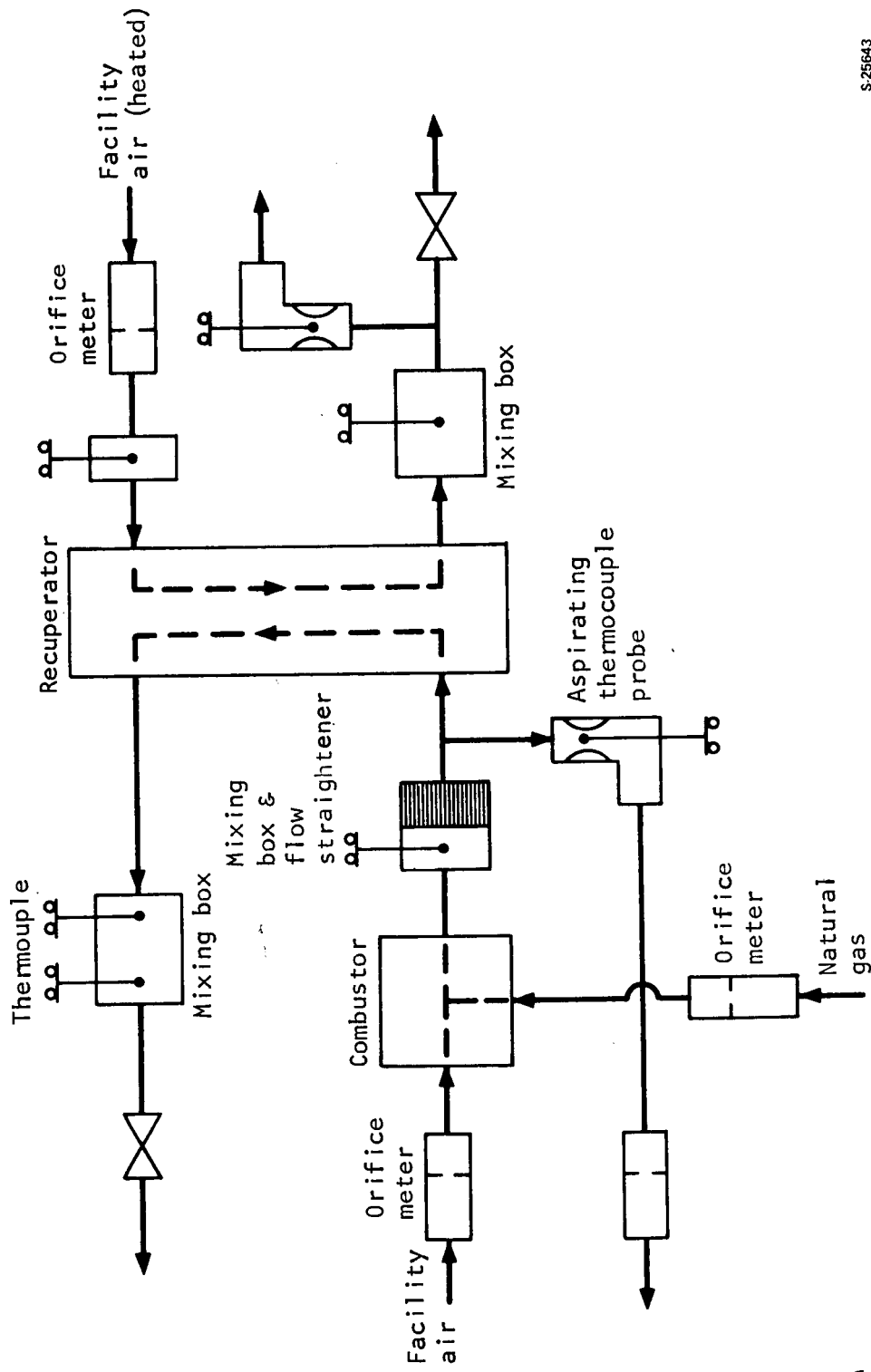
Once an accurate match was achieved with air, the performance with Xe He was determined merely by changing the fluid property input data. Fig. 29 shows the results of this scaling procedure. The predicted thermal performance, exceeds the required effectiveness by 0.0015 units and the equivalent UA by 11 percent.

The increased heat transfer performance tends to compensate for the excess pressure drop noted in fig. 26.

After completing the performance test, the unit was helium leak checked. The measured intercircuit leakage was 6.4×10^{-9} atmospheric cc/sec, and the measured external leakage was 6.0×10^{-9} atmospheric cc/sec. These rates were thus well below the allowable leakage rate of 1×10^{-7} atmospheric cc/sec.

Thermal Cycle Test

Test objectives were to verify the cyclic life predictions. Test parameters, i.e., the time to reach peak operating temperature, were purposely set at off-limit conditions to induce premature fatigue cracks. Thus, the test becomes a shakedown of the structural design in which any potentially weak areas can be isolated, the failure mechanism identified, and appropriate design modifications instituted.

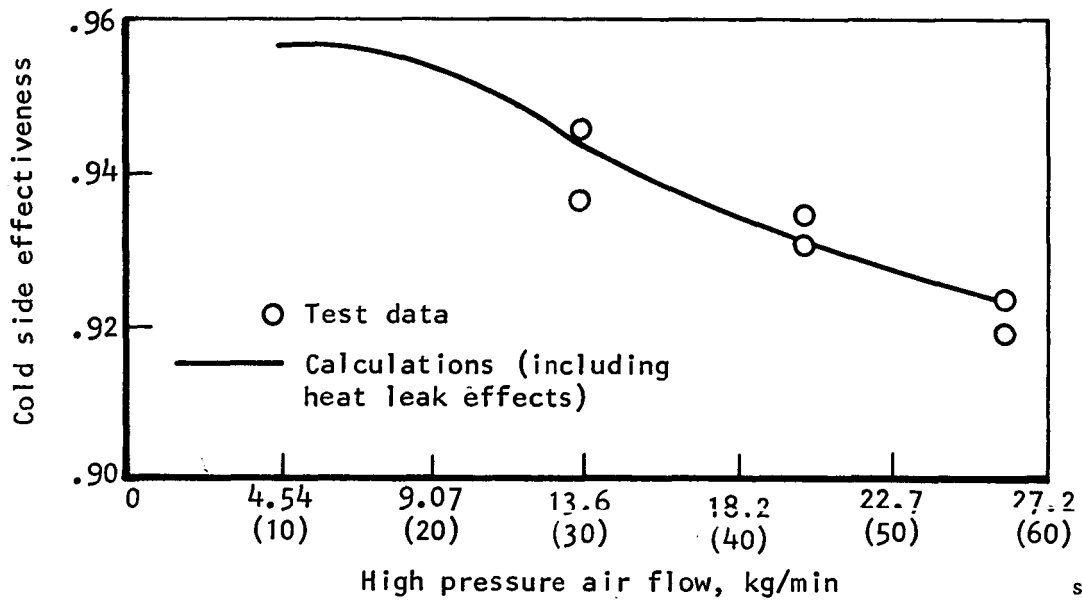


S-25643

Figure 27.--Performance Test Setup.

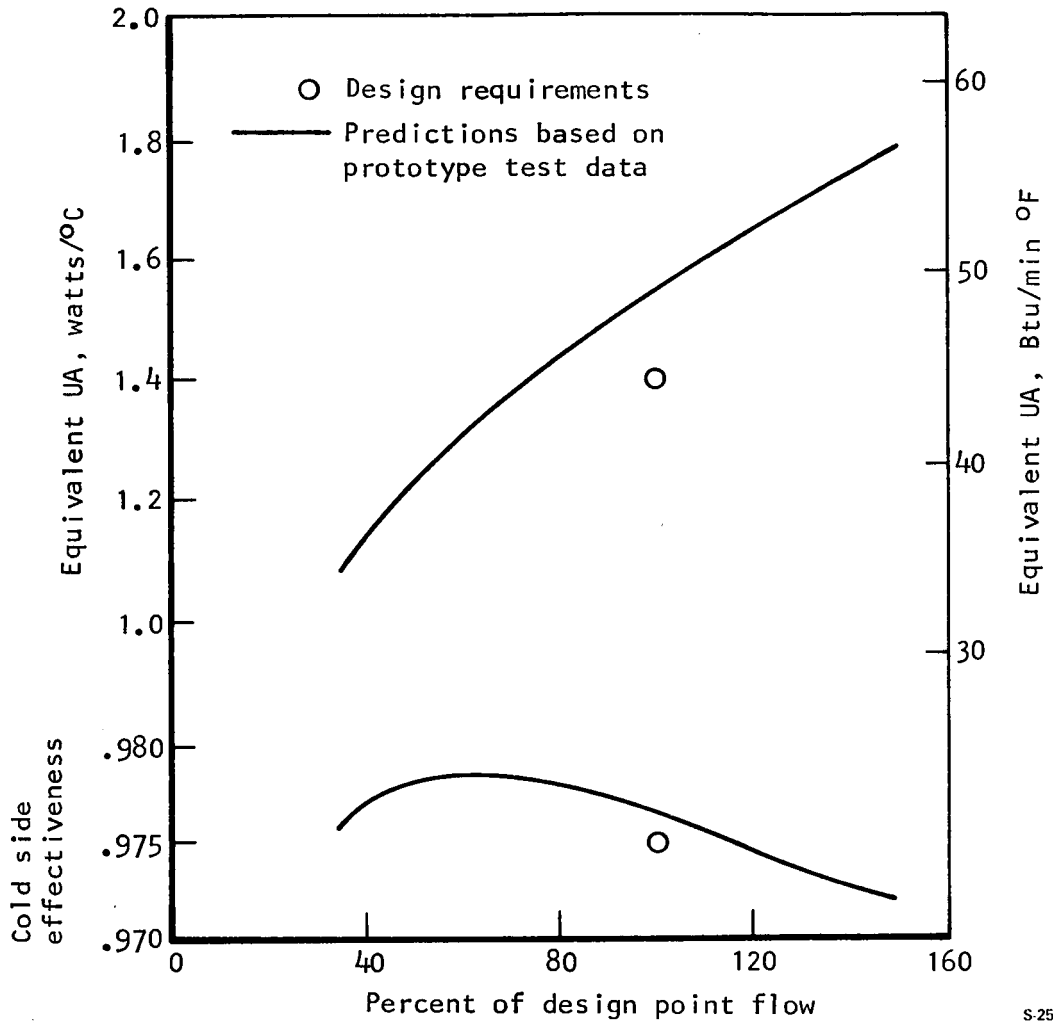
ORIGINAL PAGE IS
OF POOR QUALITY

<u>Test conditions</u>	<u>Hot side</u>	<u>Cold side</u>
Fluid	Natural gas product of combustion	Air
Inlet temp, °C (°F)	722(1332)	107(224)
Inlet pressure, MPa (psig)	0.393(57)	0.631(91.5)



S-25647

Figure 28.--Thermal Performance with Air.



S-25648

Figure 29.--Predicted Thermal Performance with XeHe.

Test conditions, defined in fig. 30, are equivalent in severity to those used in the recuperator submodule tests of Reference 12. The hot gas temperature profile is identical to that used in the submodule test. The hot and cold gas flows are double those of the submodule test, corresponding to the increase in stack height; flow velocity is identical. The hot and cold gas pressures are also identical. The step increase in the cold gas inlet temperature from lab ambient to 107°C (224°F) was deleted for the prototype tests. Because of the increased performance of the prototype (longer flow length), excessive stresses during the hot gas cool-down period do not occur, and a reduction of the hot-to-cold gas temperature differential was not required.

The test setup was similar to that for performance testing. Process control equipment was used to vary the air and natural gas flows to achieve the specified hot gas inlet temperature transient in a precise, repeatable fashion.

After completing 5, 10, 20, 40, 70, and 100 cycles of operation, the unit was checked for external leakage by pressurizing both sides of the unit to 0.21 MPa (30 psig) and observing for pressure decay. A soap solution was also used to help detect any visible leakage. A pressure decay test at 0.21 MPa (30 psig) was also made to detect any evidence of internal bypass leakage. There was no indication of leakage at any time.

After the 100th cycle the unit was cleaned and subjected to a helium leak check. Results were as follows:

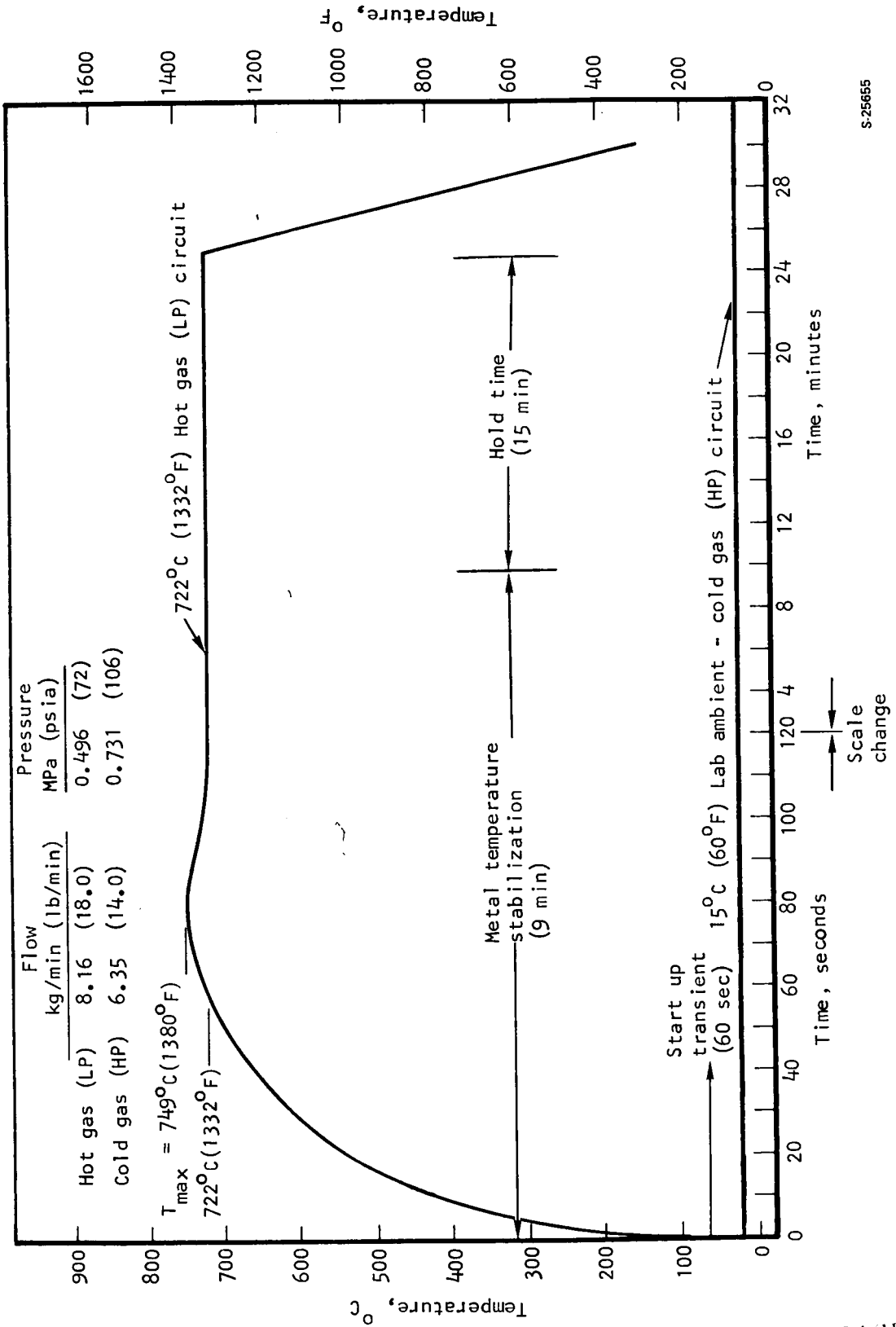
External	2.5×10^{-9} scc per sec
Internal bypass	$>10^{-6}$ scc per sec

The unit was within the specification for maximum allowable external leakage (1×10^{-7} scc/sec), but there was evidence of a small internal bypass leak. The pressure decay test with air was repeated with the following results:

Initial pressure	0.21 MPa (30 psig)
Pressure after 40 minutes	0.21 MPa (30 psig)
Pressure after 48 hours	0.14 MPa (20.9 psig)

There was definitely a small internal leak but the rate was too small to be visible. This leak rate would result in an undetectable change in system power output.

Testing was resumed and an additional 33 cycles were accumulated for a total of 133 cycles. There was no visible external leakage at 0.21 MPa (30 psig). With the high-pressure side of the unit pressurized to 0.21 MPa (30 psig), the pressure decayed to 0.14 MPa (20.7 psig) in 30 minutes. Upon examination a small internal crack was detected in a tube plate just behind the solid mass that constitutes the manifold splitter-to-core joint.



S-25655

Figure 30. ---Thermal Cycle Test Conditions.

ORIGINAL PAGE
OF POOR QUALITY

Testing was continued until a total of 200 cycles had been accumulated. At this point, the external helium leakage was less than 2.25×10^{-10} scc/sec. This leak rate is less than that recorded after 100 cycles; the difference is attributed to diffusion of helium through the rubber stoppers used to seal the ports, which was less for the test after 200 cycles.

The amount of internal bypass leakage continued to increase; the test history is summarized below:

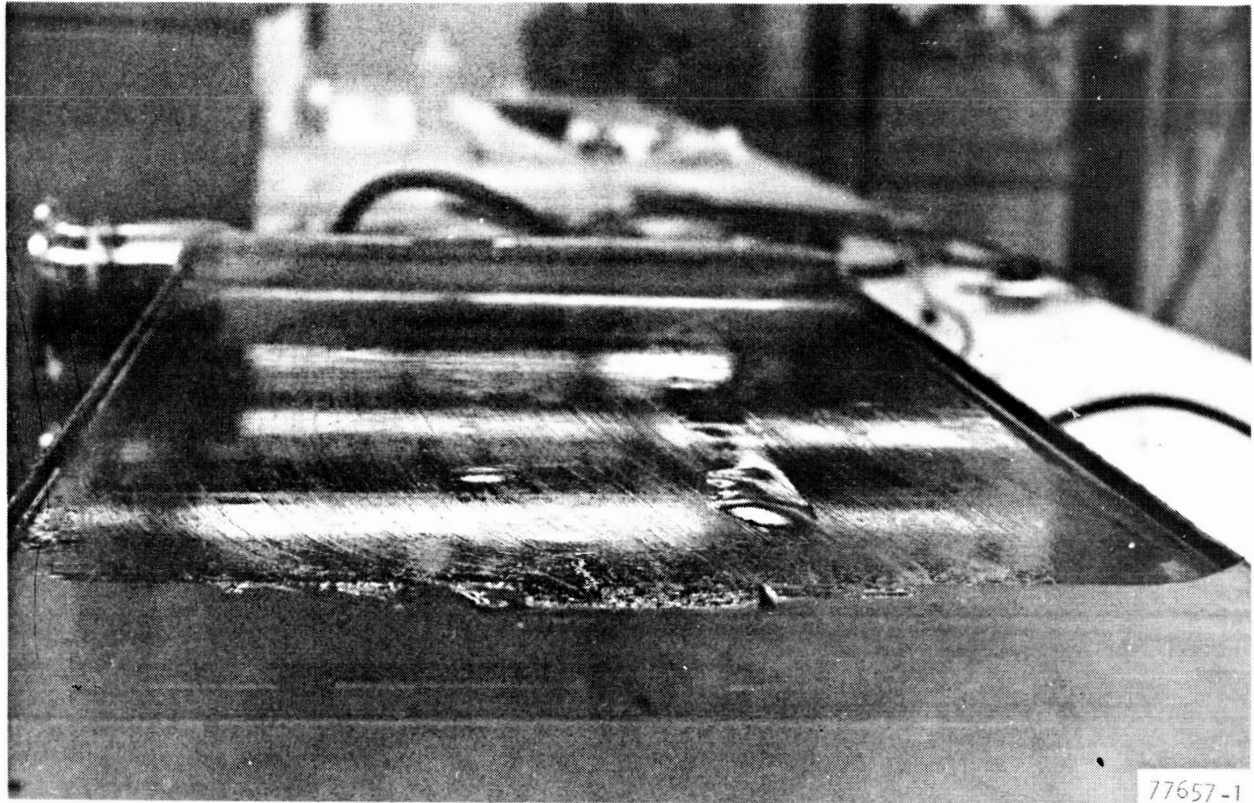
<u>Time</u>	<u>Internal Bypass Leakage</u>
Start of testing	Less than 6.4×10^{-9} scc/sec
100 cycles	Pressure decay from 0.21 to 0.14 MPa (30 to 20.9 psig) in 48 hr
133 cycles	Pressure decay from 0.21 to 0.14 MPa (30 to 20.7 psig) in 30 min
170 cycles	Pressure decay from 0.21 to 0.10 MPa (30 to 14.2 psig) in 5 min
200 cycles	Pressure decay from 0.21 to 0.15 MPa (30 to 21.8 psig) in 30 sec

A flow check was performed and based on these data, it was estimated that the bypass flow of high-pressure xenon-helium gas would be 0.31 gm/s (6.9×10^{-4} lb/sec) at design point conditions. This bypass is about 0.2 percent of the total flow, which appears to be negligible from the point of view of recuperator performance.

The appearance of the seal plate after 200 cycles is shown in fig. 31 (the surface was moistened with alcohol to make the blisters more apparent). The largest blister (7 cm long by 2.5 cm wide by 0.08 cm high and located 7 cm from the hot end attachment flange) was first detected after 170 cycles. It did not appear to have grown after being subjected to another 30 cycles. Another smaller blister, which is evident on the left side of fig. 30, was not detected during the 170th cycle examination.

Voids were known to exist in the seal-plate braze prior to testing. Apparently, a crack developed in the header-plate braze joint in an area that coincides with a seal-plate braze void. Gas pressure acting in the void area caused the blister to develop. Since the unit remained helium leaktight, the concept of double containment using a seal plate was effective.

The corner area where the manifold attachment flange is joined to the side plate on the hot end of the core was known to be critical. During the previous submodule test, low-cycle fatigue cracks developed in this area; based on these observations, the corner area was strengthened by the addition of gussets. This area on the prototype unit was closely examined and small cracks were detected in the weld joint. The cracks were barely visible to the naked eye,



ORIGINAL PAGE IS
OF POOR QUALITY

Figure 31.--Blisters in Seal Plate Observed After 200 Cycles.

but could be observed with 7X magnification. The crack location is defined in fig. 32. The cracks were in the weld joint on the corners of the assembly and were on both sides of the side plate located closest to the ports. No cracks were detected on the opposite side plate.

The cracks, which appear to be the result of low-cycle fatigue, did not extend through the side plate because the unit still was helium leakproof.

Conclusions

The completion of 100 cycles of thermal cycle testing with no external leakage and a minute amount of internal bypass flow validates the structural design of the heat exchanger. Minor modifications were incorporated on the deliverable MBR to improve the low-cycle fatigue performance.

MINI-BRAYTON RECUPERATOR

The Mini-Brayton Recuperator (MBR) that was assigned for delivery to NASA-Lewis Research Center is identical to the prototype design except for the following:

- Four mounting pads were installed to permit recuperator installation in the Brayton power system. These mounts were designed for low thermal inertia, and were configured to accept a fitting that incorporates a spherical (self-aligning) bearing. This mounting arrangement is required to permit thermal growth without binding or application of bending moments at the mount location.
- The side plate doublers were extended past the ends of the gussets on the manifold attachment flanges to reduce the strain concentration and thereby alleviate the potential for fatigue cracking observed on the prototype cycle test.

No other changes were believed necessary based on the results of the performance and thermal cycle shakedown tests.

Changes were also made to the manufacturing operations to improve the unit quality. These included:

- Addition of a glass bead peening process performed on each detail fin to remove any burrs produced during the fin-forming operation. Any burrs that separate from the fins during actual operation could become a source of contamination to the power system turbocompressor assembly.
- Modified braze tooling to improve seal-plate brazing. Pressure-bag fixturing was used to obtain more uniform loading compared with the dead-weight loading technique used on the prototype heat exchanger.

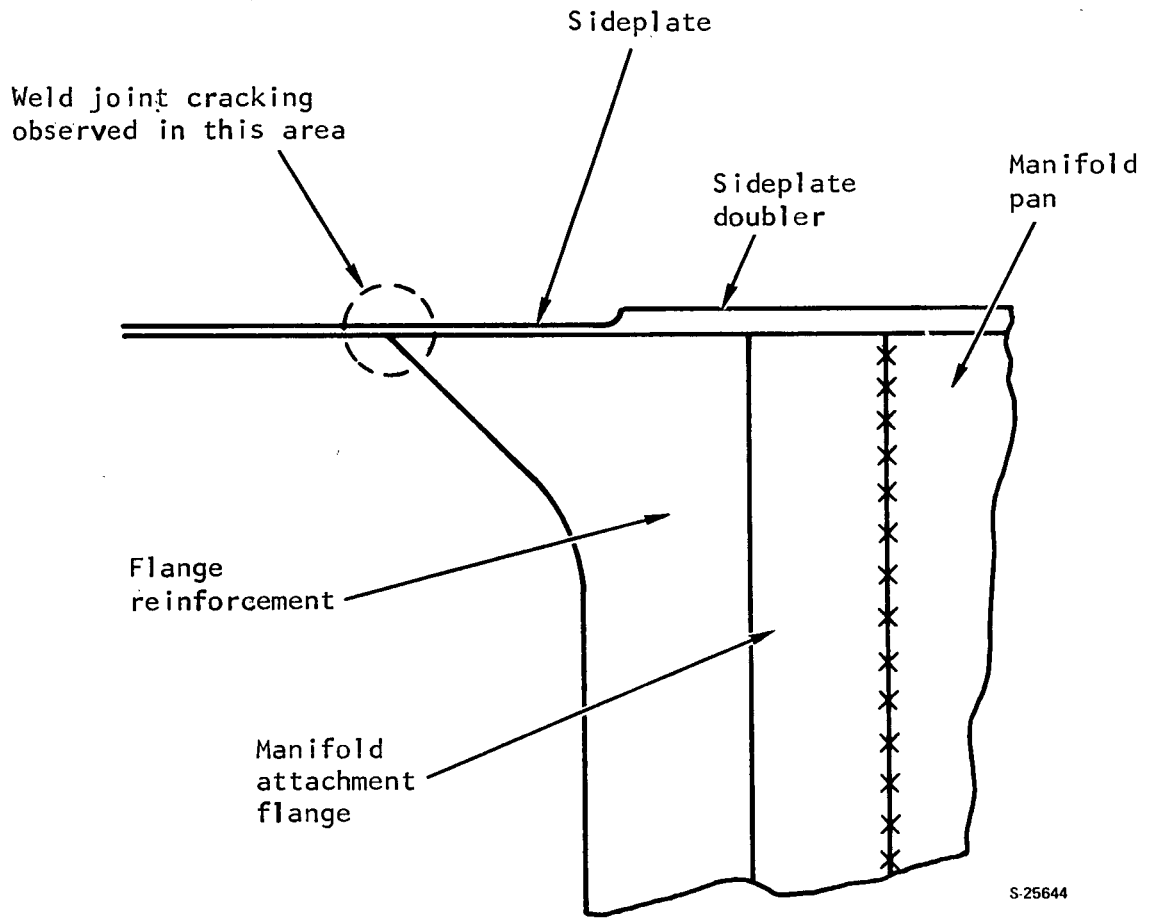


Figure 32.--Location of Fatigue Cracks.

- A cleaning specification using trichlorotrifluoroethane to achieve the following standard: (1) no particles greater than 500 microns, (2) 5 particles maximum, 175 to 500 microns, (3) 2.2 micrograms per sq cm total filterable solids, and (4) 1.1 micrograms per sq cm non-volatile residue.
- A stress-relieving heat treatment was performed on the welded assembly prior to final machining operations to ensure that no unaccounted-for stresses were imposed on the recuperator installation during operation.

The as-brazed core assembly is shown in fig. 33. A view of the corner construction showing the braze joints between the machined bar and plate matrix, the seal plate, and the manifold attachment flange is presented in fig. 34. The close fit is evident; the possibility of a virtual leak in this corner has been eliminated.

The completed recuperator is shown in figs. 35 and 36. The flange gussets and extended side plate doubler are evident in the view of the hot end construction, fig. 33.

Acceptance Test

Acceptance testing consisted of: (1) a proof pressure test, (2) a helium leak check, (3) weight determination, (4) isothermal pressure drop (flow calibration), (5) dimensional check, and (6) a final cleaning operation. Details of the test procedure are presented in Reference 17; results are discussed below.

For the proof pressure test, the low- and high-pressure circuits were pressurized to 1.21 and 1.79 MPa (175 and 260 psig), respectively, at room temperature. Maximum pressure difference across the manifold splitter plate is 0.58 MPa (85 psi). These pressure levels are the respective ambient temperature equivalents of 0.84 MPa and 56°C (122 psig and 133°F) and 1.20 MPa and 707°C (174 psig and 1304°F). No visible deformation was noted on the unit following these tests.

Results of the helium leak check were as follows.

<u>Location</u>	<u>Measured Leak Rate, scc per sec</u>	<u>Leak Rate Objective, scc/sec</u>
External	$<3.4 \times 10^{-8}$	$<1 \times 10^{-7}$
Internal bypass	1.0×10^{-4}	$<1 \times 10^{-7}$

Although the bypass leakage exceeds the objective, the unit is acceptable; the absence of any visible leakage indicated that the internal braze joints are structurally sound. The amount of bypass flow during operation will not produce a detectable effect on system power output.

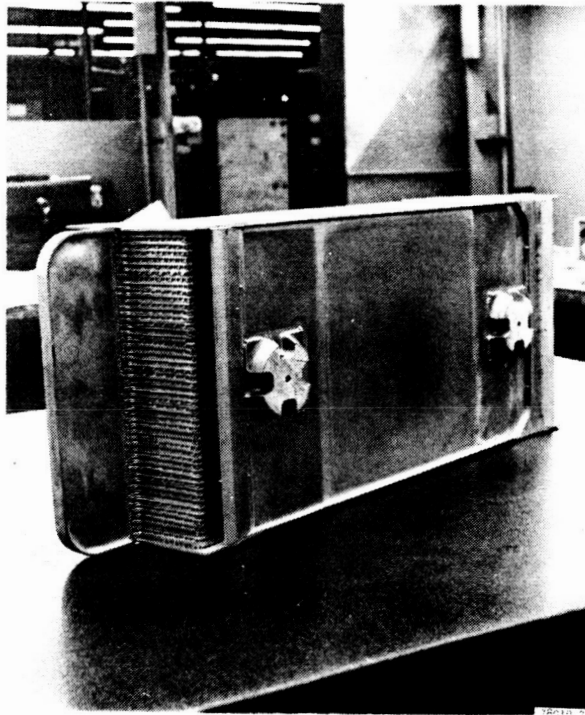
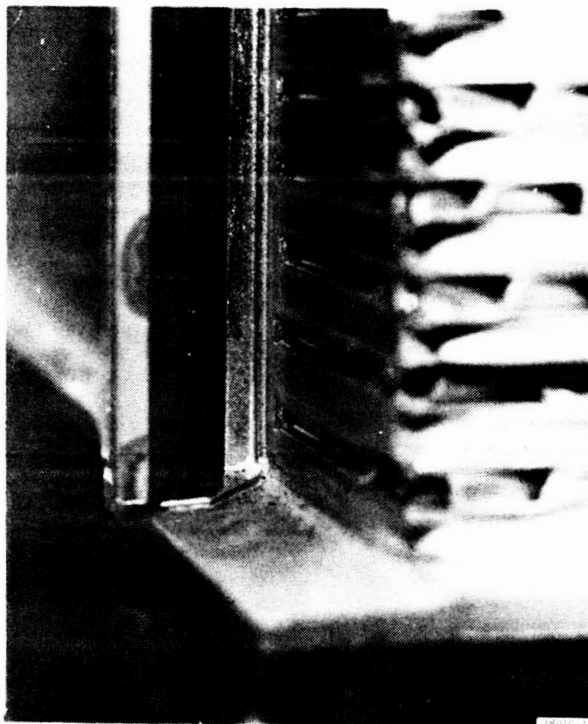


Figure 33.--MBR Core Assembly.

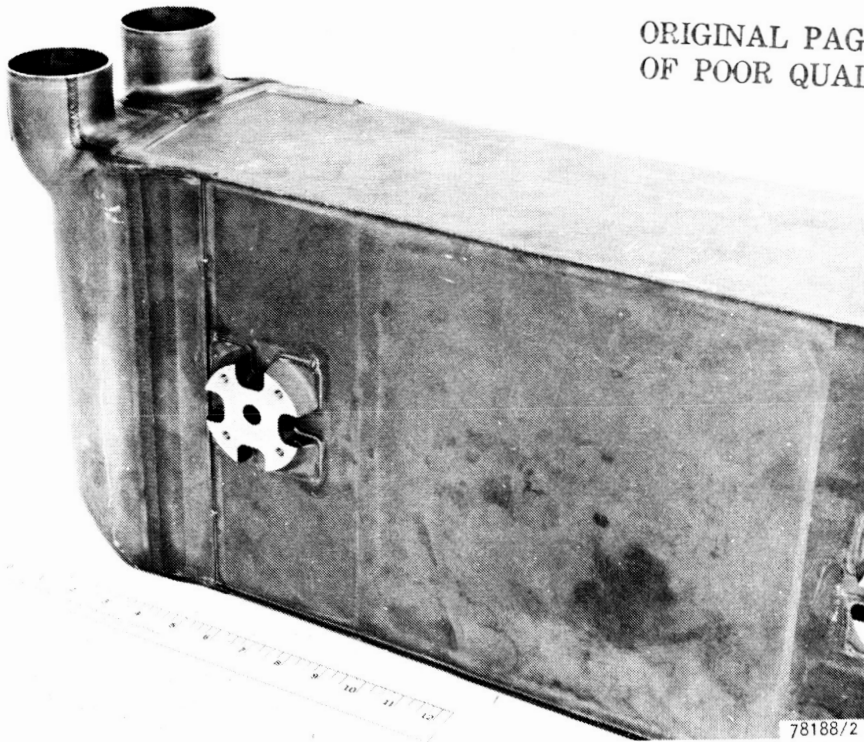


ORIGINAL PAGE IS
OF POOR QUALITY

F-25067

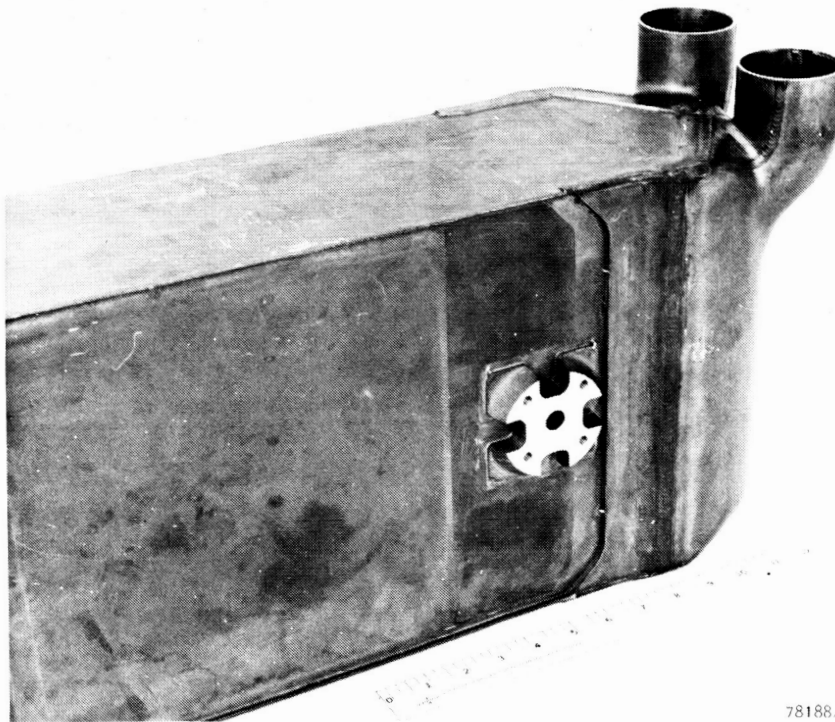
Figure 34.--Closeup View of Corner Braze Joint Area.

ORIGINAL PAGE IS
OF POOR QUALITY



78188/2

(a) Cold End.

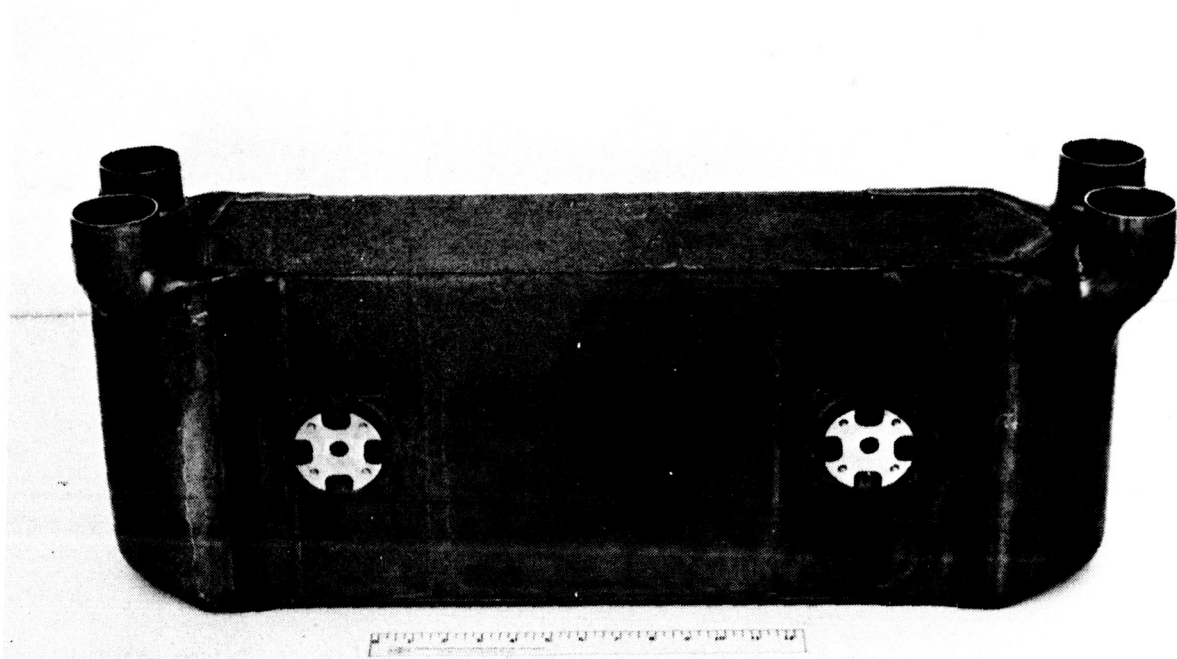


78188/3

(b) Hot End.

F 27045

Figure 35.--MBR Construction.



78188/1

ORIGINAL PAGE IS
OF POOR QUALITY

Figure 36.--MBR As-Built.

Total weight of the MBR was 56.5 kg (128.8 lb). This compares quite well with the predicted weight of 59.6 kg (131.2 lb).

Isothermal pressure drop tests for both the high- and low-pressure circuits were conducted at room temperature with air as the test fluid; the results are plotted in figs. 37 and 38. The data are converted to standard conditions using the factor

$$\sigma = 2.84 \frac{P}{T}$$

where P = pressure, kPa

and T = temperature, °K

For comparison purposes, the results of the prototype pressure drop tests are also plotted in these figures. The MBR pressure drop is slightly lower than the corresponding prototype pressure drop. This reduction may in part be attributed to the glass-bead cleaning performed on the fins of the MBR unit.

Design point scaling of the above pressure drop data indicates that the recuperator would have an overall pressure drop (both sides combined) $\Delta P/P = 0.73$ percent compared with 0.78 for the prototype unit (see fig. 26).

CYCLIC LIFE ANALYSIS

During the system startup transient, the recuperator temperature response varies in the fins, plates, header bars, and manifolds. Large temperature differences can be produced in adjacent structures due to the difference in their mass and in the local heat transfer coefficient. This results in high thermal stresses that can produce plastic deformation in local areas. Damage produced by plasticity and creep during each operating cycle accumulates, and after a sufficient number of cycles, a low-cycle fatigue crack develops; this crack can propagate through the parent metal, weld, or braze joint. Cracking can result in internal bypassing of the working fluid (loss in system power output) or in loss of working fluid to space (system shutdown).

Low-cycle fatigue was identified as the failure mechanism on the NASA Engine B recuperator. In this test, cracks were observed to develop in the header bar-to-tube plate joints after 15 to 30 cycles of operation.

Submodule thermal cycle tests reported in Reference 12 showed that low-cycle fatigue was the mechanism responsible for the cracks that developed in the manifold splitter-to-core joint. Fatigue cracks were also observed in the heat exchanger structure at the conclusion of the prototype MBR thermal cycle test. Indeed, low-cycle fatigue is the mechanism responsible for limiting the recuperator life.

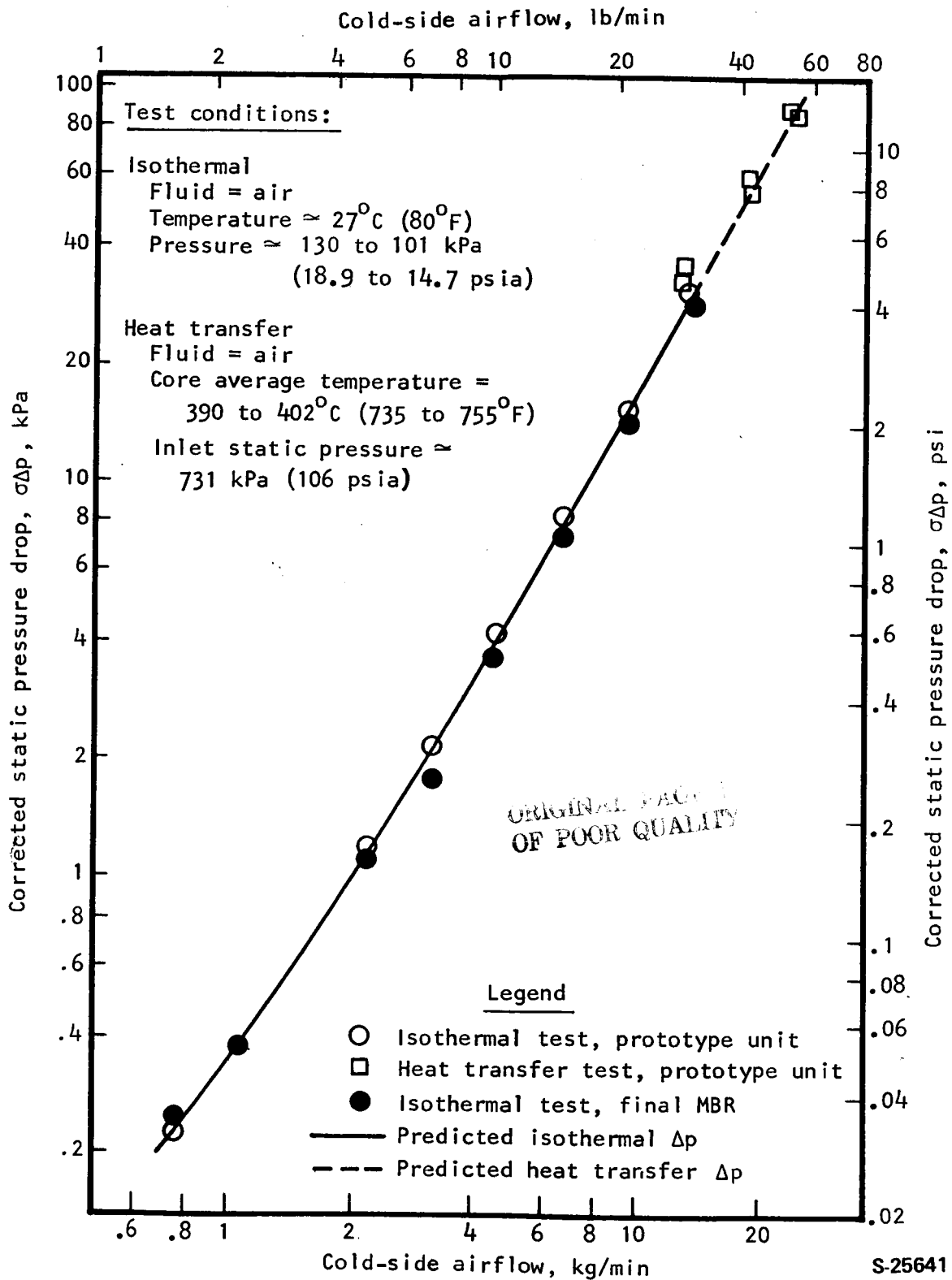


Figure 37.--High-Pressure (Cold) Side Pressure Drop.

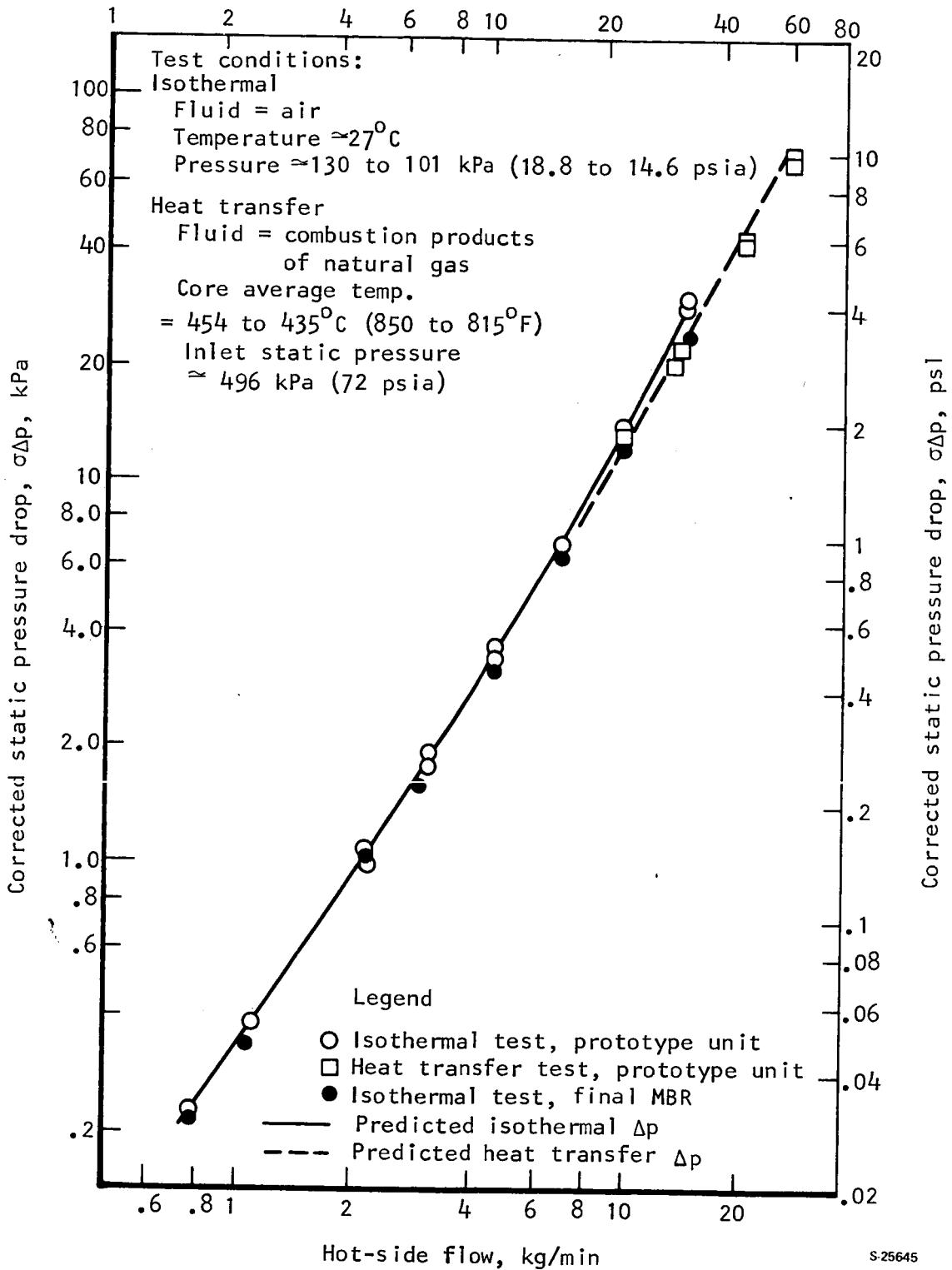


Figure 38.--Low-Pressure (Hot) Side Pressure Drop.

A thorough understanding of the fatigue mechanism can lead to an improved design. Identification of critical areas and means to alleviate the thermal stress can increase fatigue life. It is entirely possible to develop a recuperator design that can withstand the imposed cyclic life requirement. This section presents the results of a continuing series of analyses directed towards an understanding of the fatigue mechanism and a prediction of the cyclic life of the Mini-Brayton recuperator (MBR). The studies are a follow-on to the effort described in Reference 12.

Startup Transient

The startup transient is characterized by time required for the hot, low-pressure gas to reach a steady-state condition at the recuperator inlet. Gas and metal temperatures at the cold end of the recuperator respond much less readily, and hence the temperature differentials and resulting thermal stresses are minor and not considered in the analysis. Hot gas inlet transients are presented in fig. 39. Here, the NASA-specified transient with xenon-helium gas is shown to take 400 seconds to reach steady state. The flow responds quickly and reaches rated flow within 18 seconds. Under these conditions, the cycle life is stipulated to be 1000 cycles.

The thermal cycle test condition is shown for comparison in fig. 39. This transient was imposed on the Reference 12 submodules as well as the prototype MBR. The test fluid was air and it was estimated that because of the increased rate of the inlet temperature ramp (60 seconds to reach maximum temperature compared with 400 seconds for the design transient), the test unit cyclic life would be reduced to less than 100 cycles compared with a design life of 1000 cycles. As previously discussed, the prototype heat exchanger did develop an internal fatigue crack after 100 thermal cycles.

Preliminary BIPS Analysis

Power system transient analyses have been conducted by the AiResearch Manufacturing Company of Arizona (AIRPHX) in support of the Brayton Isotope Power System (BIPS). This program, sponsored by the Department of Energy, will be the ultimate application for the MBR. Preliminary results are reported in Reference 18.

Various system startup modes were examined and startup cycle 101 conditions were selected as the preferred mode because they imposed the least stress on the recuperator. The recuperator inlet transient for startup cycle 101 is also shown in fig. 34. The conditions are considerably more severe than the NASA-specified inlet transient. The BIPS transient is based on an analytical model in which it is presumed that the isotope heat source has reached a maximum operating temperature of 930°C (1707°F) when the start button is energized. The turbine-alternator-compressor assembly (Mini-BRU) is motored to a self-sustaining speed and then accelerates on

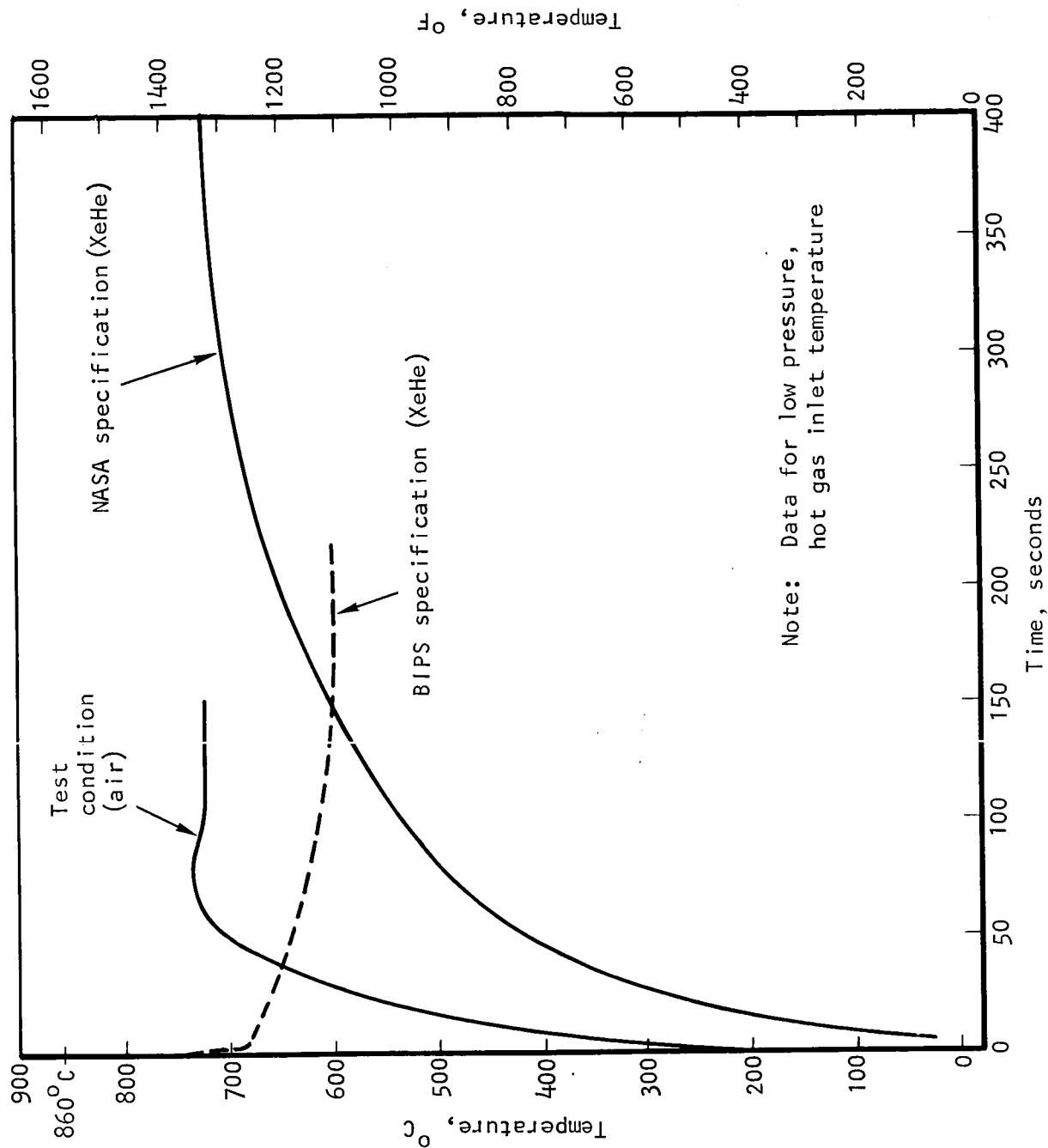


Figure 39. --Comparison of Transient Temperature Profiles.

its own to rated speed. Total time to reach rated speed is only 5 seconds. Under these conditions, it is predicted that the recuperator will be exposed to an initial temperature of 860°C (1580°F).

A detailed transient temperature analysis of the MBR in response to start cycle 101 conditions was performed. The peak stresses were determined, and an estimate of the cycle life was established. This work was performed under Department of Energy contract EY-76-C-03-1123, and the results are presented in Reference 19. This was basically a two-dimensional analysis of the recuperator thermal stresses. At the core-to-manifold joints, however, the highest stresses were developed in the stack height direction. An estimate of the stack height stresses was combined with the 2-D analysis using the 3-D von Mises formula for equivalent stress, and the cyclic life was determined. The most critical area was located at the junction between the core and low-pressure manifold pan. The computed fatigue life was 15 to 40 cycles and dependent on the mean stress correction method used in the analysis. A fatigue crack at this critical location would permit an internal bypass flow. It was predicted, however, that no external fatigue cracks would develop that would result in external leakage in less than 100 startup cycles at cycle 101 conditions.

Improved BIPS Analysis

The implications of fatigue cracking are considerable. Hence, it was decided as part of the NASA-sponsored effort to conduct further analysis to improve the cycle life prediction. In addition, the continuing power system transient analyses performed by AIRPHX have resulted in better estimates of the actual flight system startup mode. The latest startup analysis, identified as Run 600, was provided by the BIPS program office at AIRPHX (B. Minshall, BIPS-GDS Coordination Memo A06009, April 21, 1978). These startup conditions are preliminary, as the flight system scenario has not been finalized. The recuperator inlet temperatures from Run 600 are shown in fig. 40. Comparison with fig. 39 shows that as far as the recuperator is concerned, Run 600 represents a less severe condition than does Run 101.

Using the startup information from Run 600, thermal analyses using AiResearch computer programs HXT4 and H0910 were conducted to produce complete temperature maps for the recuperator. Maps were constructed at five-sec increments up to 170 sec of the startup cycle, and at steady state. The working fluid outlet temperatures predicted by these analyses are shown in fig. 40.

For the stress analysis, the cross section of the recuperator indicated in fig. 41 was simulated by the 2-D finite element model shown in fig. 42. The model is similar to those previously used and is discussed in detail in Reference 19. The three boundary conditions shown in fig. 42 allow for freedom of expansion in the X and Y directions.

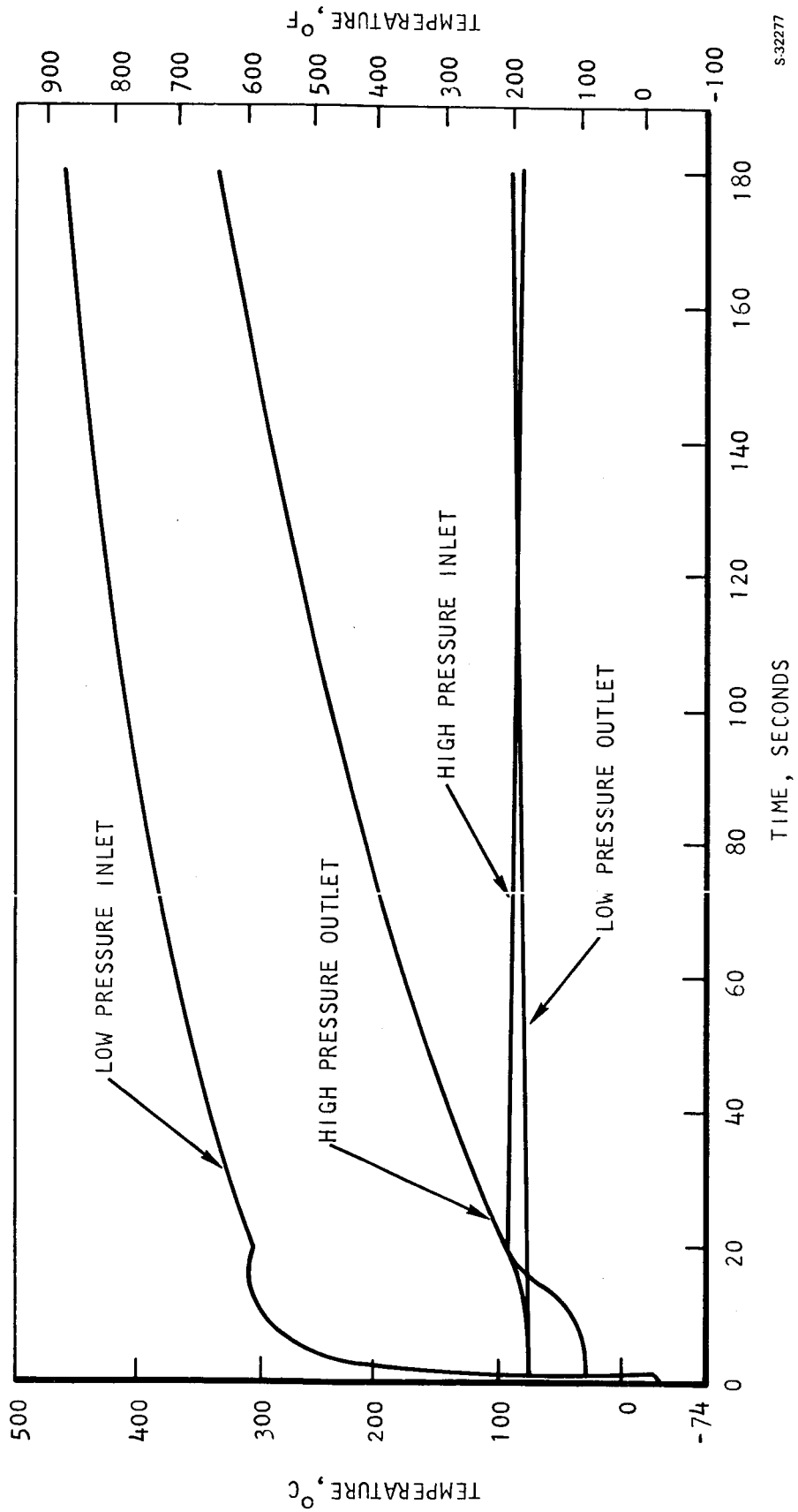


Figure 40.--Run 600 MBR Inlet Conditions and Calculated Outlet Conditions.

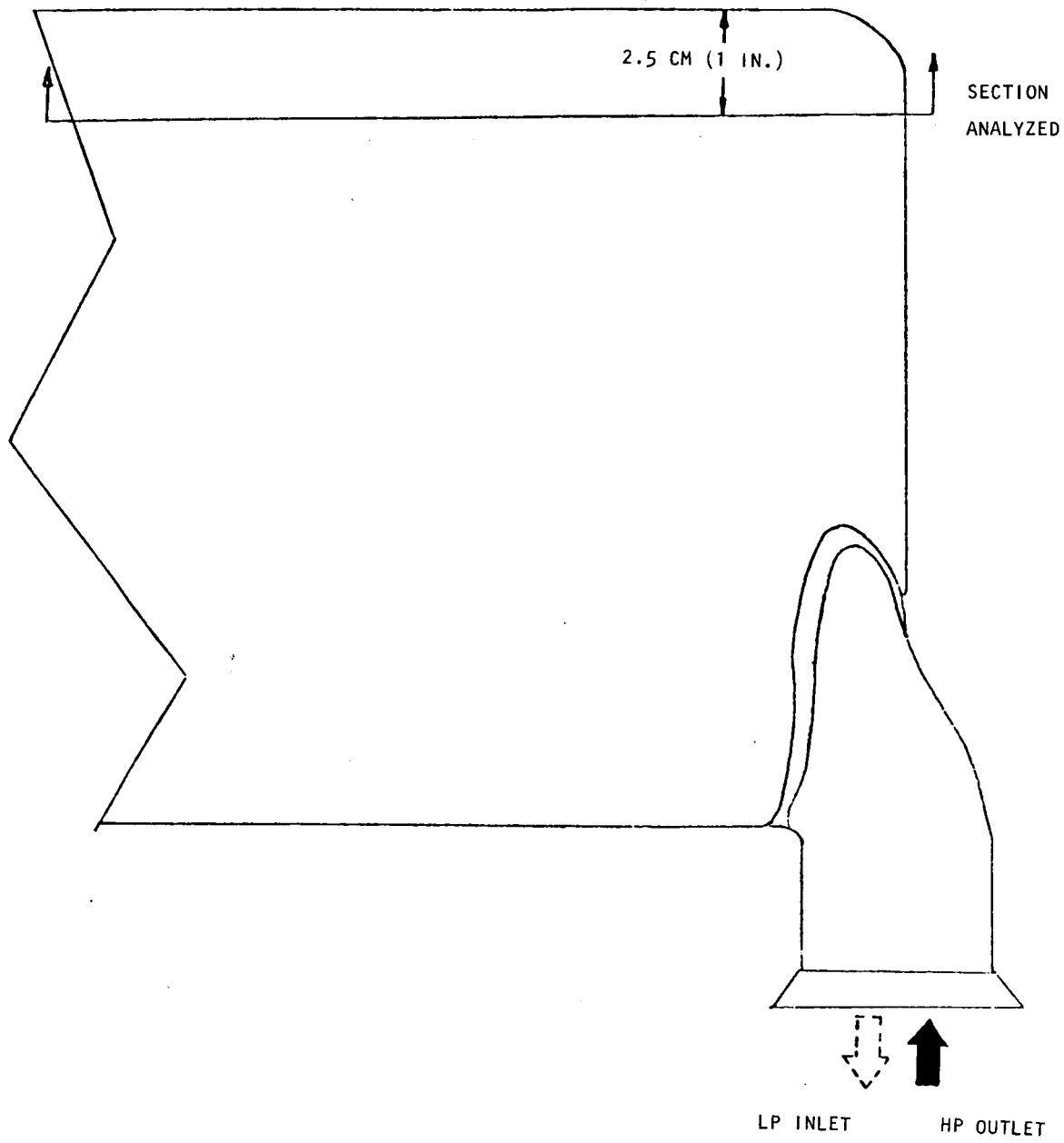


Figure 41.--Location of MBR Section Analyzed.

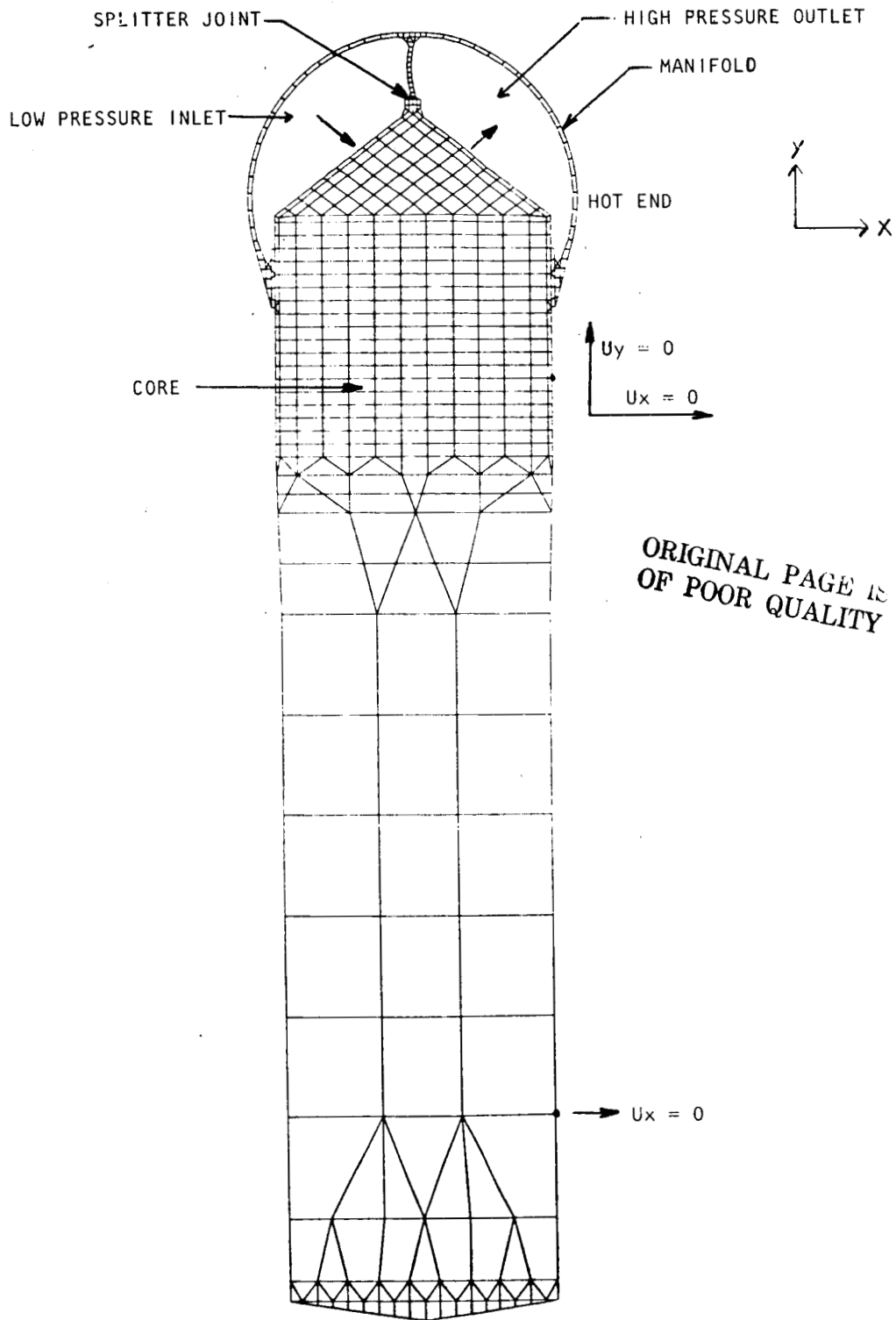


Figure 42.--2-D Finite Element Model with Boundary Conditions

The stresses and displacements in the model were determined using a finite element computer program, ANSYS. Stresses were calculated for the time intervals supplied by the thermal analysis; the maximum stress was found to occur at 30 sec. Figs. 43 through 51 show temperatures, displacements, and stresses for the hot end of the MBR at 30 sec, 170 sec, and steady state.

The most highly stressed area, shown as the shaded element 496 in fig. 52, reaches a maximum 2-D von Mises stress of 249 MN/m^2 (36,120 psi) at 30 sec. Maximum 2-D stresses at the brazed splitter joint and at the brazed pan joints are much smaller than the maximum stress in the core. Since only a 2-D stress analysis was performed, the maximum 2-D stress of 249 MN/m^2 (36,120 psi) was multiplied by a factor of 1.2 to give an equivalent 3-D von Mises stress of 299 MN/m^2 (43,340 psi). A stress concentration factor of 2.0 was applied to the equivalent 3-D stress. Fig. 53 shows the variation of von Mises stress, temperature, and yield strength with time for the critical element 493. The level of stress required to cause 1 percent creep at the steady-state temperature of 596°C (1105°F) is also shown.

With the aid of a schematic diagram of stress vs time for the critical element 493 (see fig. 54), the low-cycle fatigue (LCF) life was evaluated using AiResearch computer program X0875. Also included are the diurnal cycles, which occur twice every 24 hr when the BIPS passes through sunlight and shadow. Over the 7-yr life, around 5200 diurnal cycles are required. Each startup cycle was assumed to require approximately 3 hr. Creep damage was considered to occur at the steady-state temperature of 596°C (1105°F). Minimum values of material properties at the steady-state temperature were taken from Reference 21. Creep data were taken from the three standard deviation (minimum) Larson-Miller curves shown in fig. 55. A linear interaction formula for the life cycles due to plasticity and creep damage was used.

The estimated life of the MBR for Run 600 conditions is 220 to 785 startup cycles. This is, of course, in addition to the diurnal cycling. The minimum value, 220 cycles, is based on a factor of 10 percent applied to the life cycles due to plasticity. The expected value, 785 cycles, is based on 100 percent of the plasticity life cycles and 50 percent creep damage. For the BIPS requirement of 100 startup cycles and 5200 diurnal cycles, 46 percent of the predicted life would be used up. This is indicated in fig. 54.

These values of LCF life are based on the maximum values of creep properties. If the nominal (typical) values of creep properties shown in fig. 56 are used, the corresponding minimum and expected values of LCF life are 450 and 3150 cycles, respectively.

It should be noted that the above LCF life predictions, which meet the BIPS requirement, are for the most highly stressed region of the MBR, element 493. Failure in this region would result in internal bypassing only. The minimum cycle life for external leakage has not been explicitly determined, but should be considerably above the 220 cycle internal leakage minimum.

ORIGINAL PAGE IS
OF POOR QUALITY

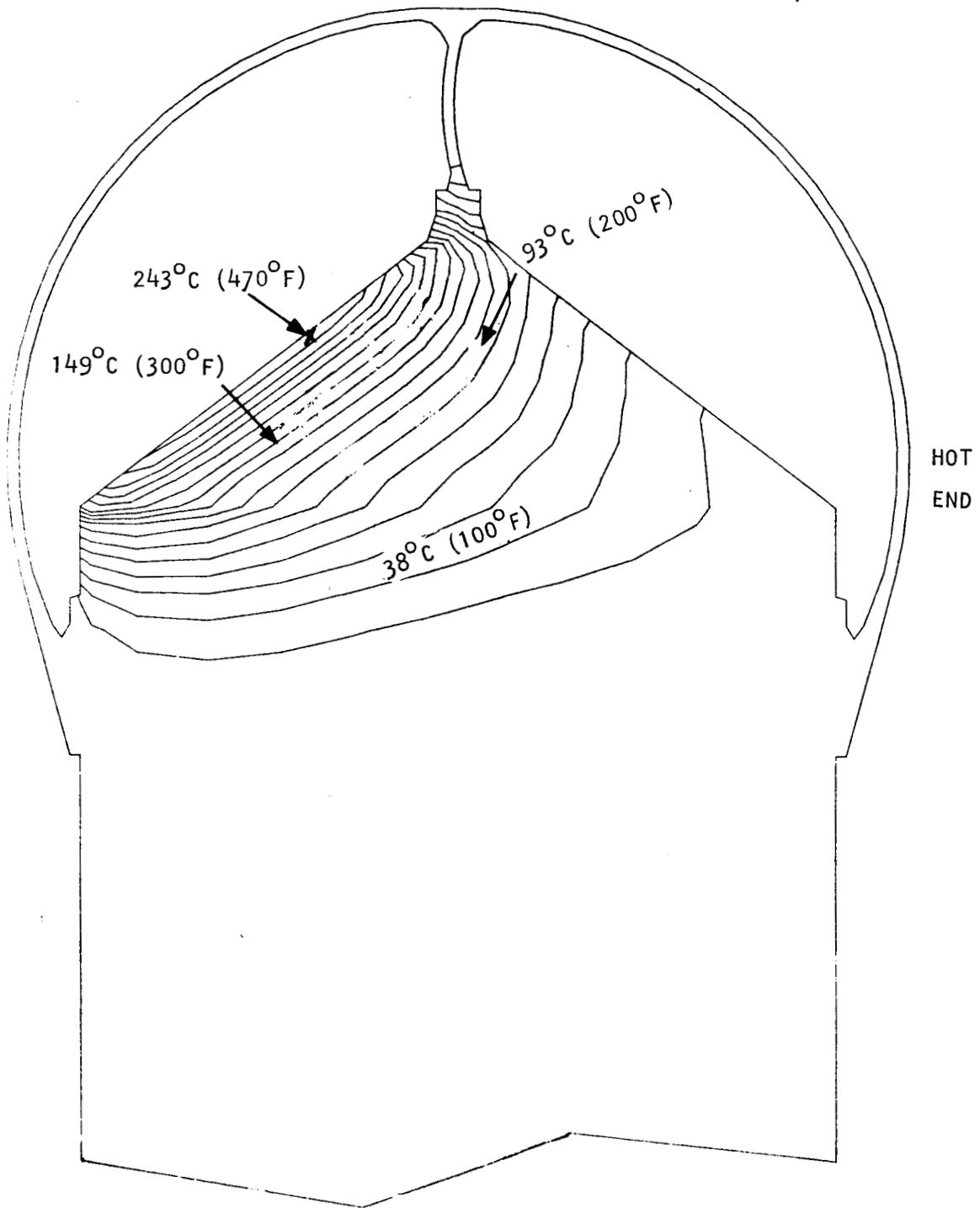


Figure 43.--Temperature Map at 30 Seconds.

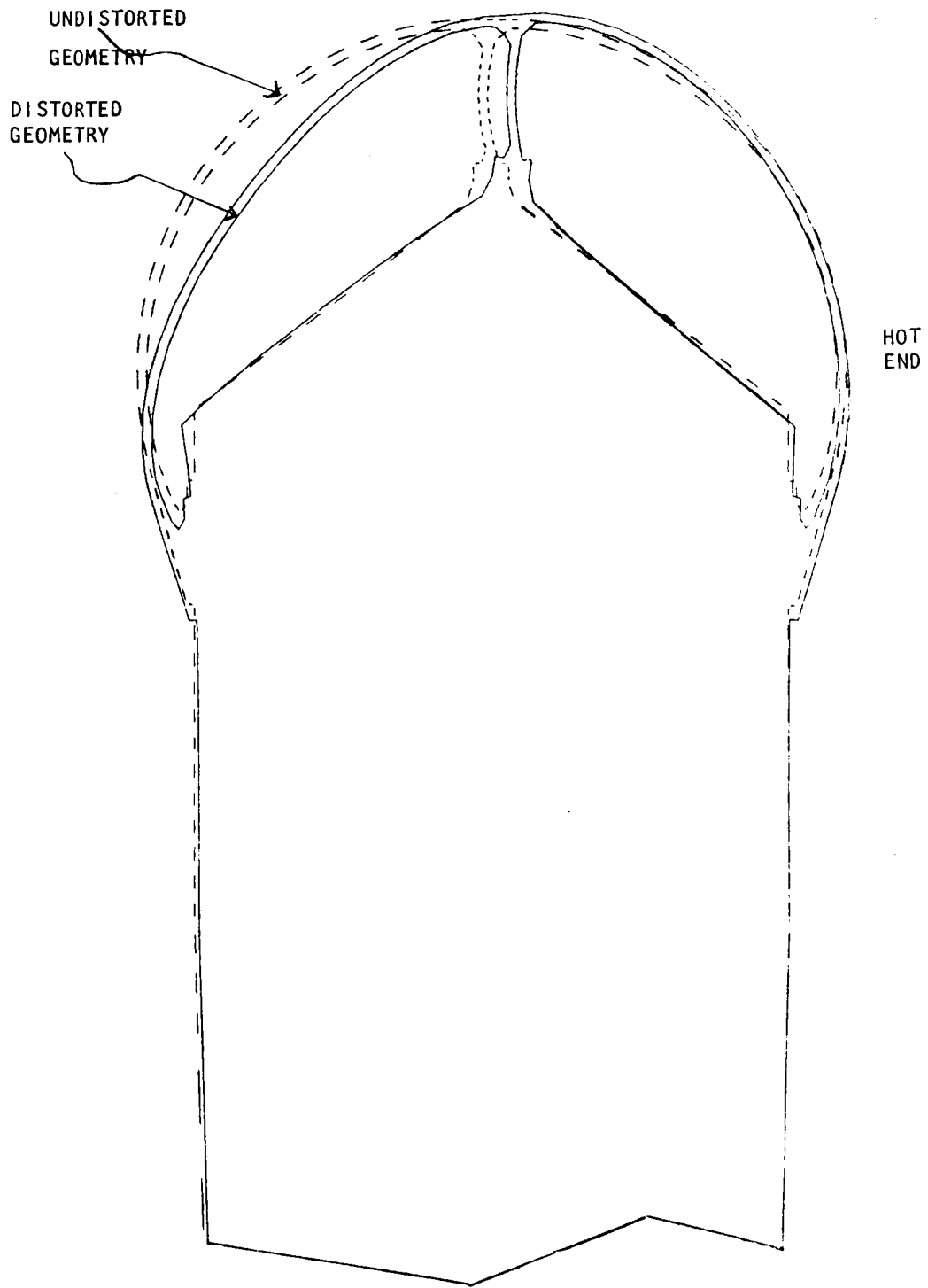


Figure 44.--Distorted Geometry at 30 Seconds.

ORIGINAL PAGE IS
OF POOR QUALITY

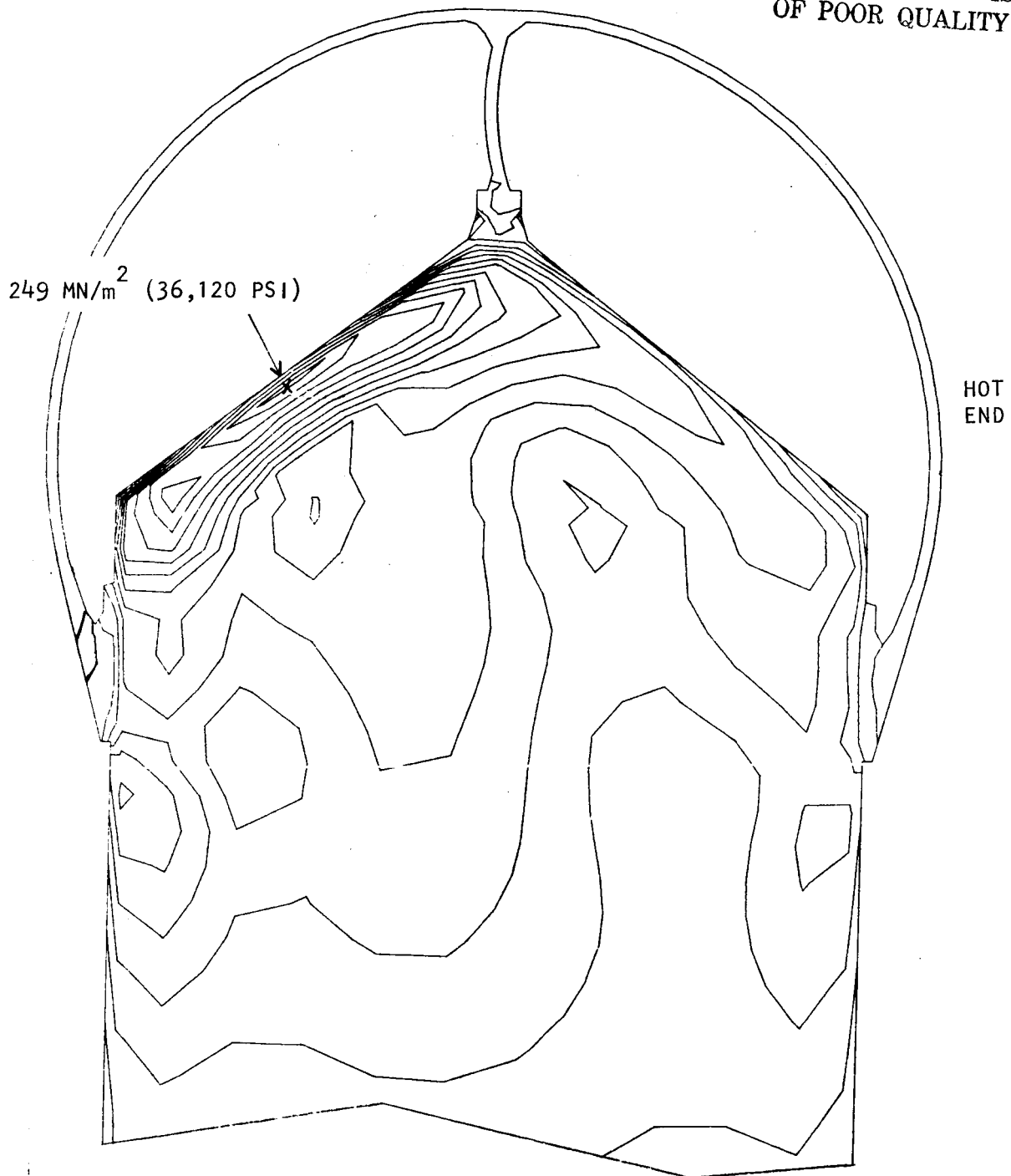


Figure 45.--2-D Von Mises Stress Map at 30 Seconds.

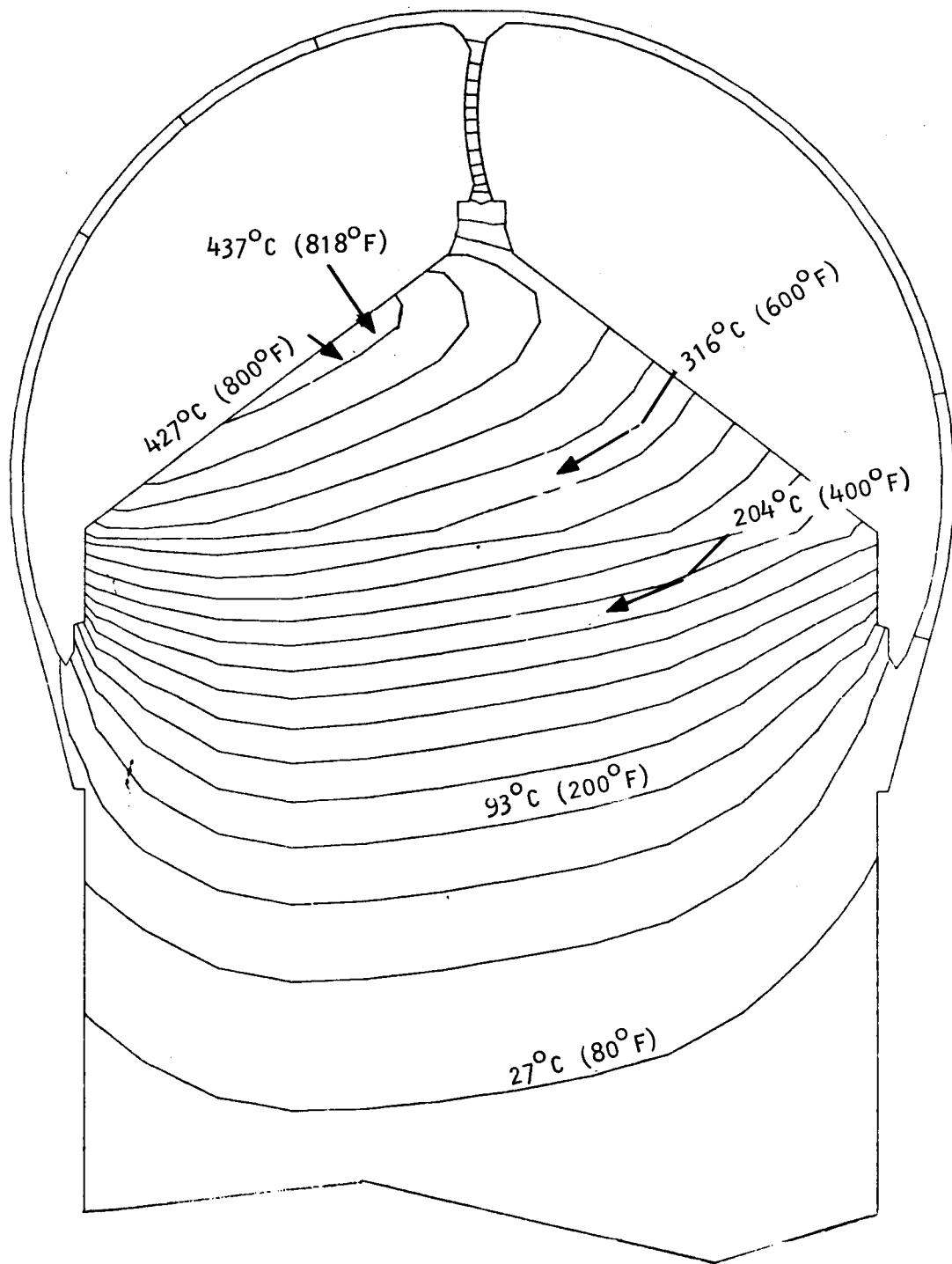


Figure 46.--Temperature Map at 170 Seconds.

ORIGINAL PAGE IS
OF POOR QUALITY

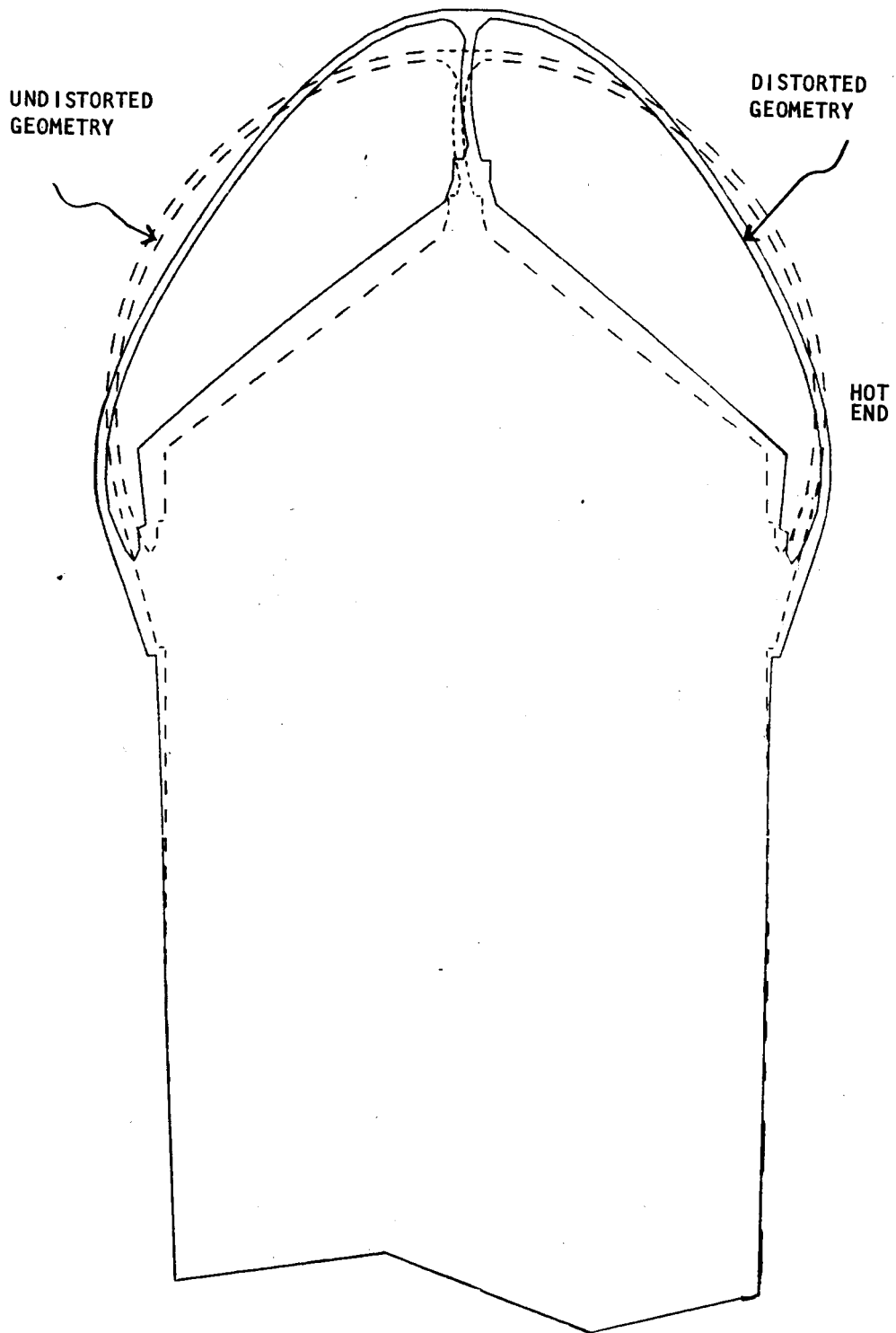


Figure 47.--Distorted Geometry at 170 Seconds.

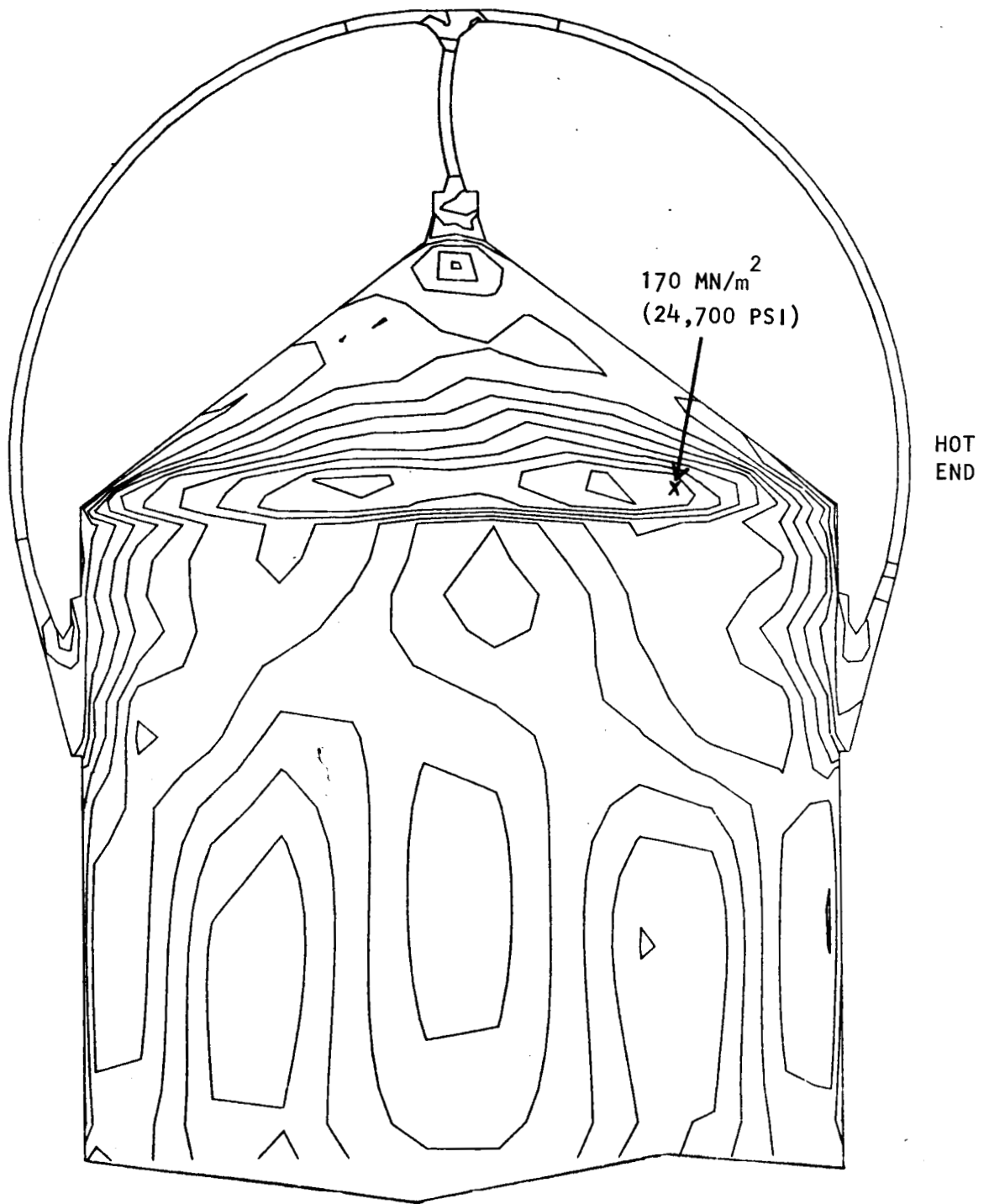


Figure 48.--2-D Von Mises Stress Map at 170 Seconds.

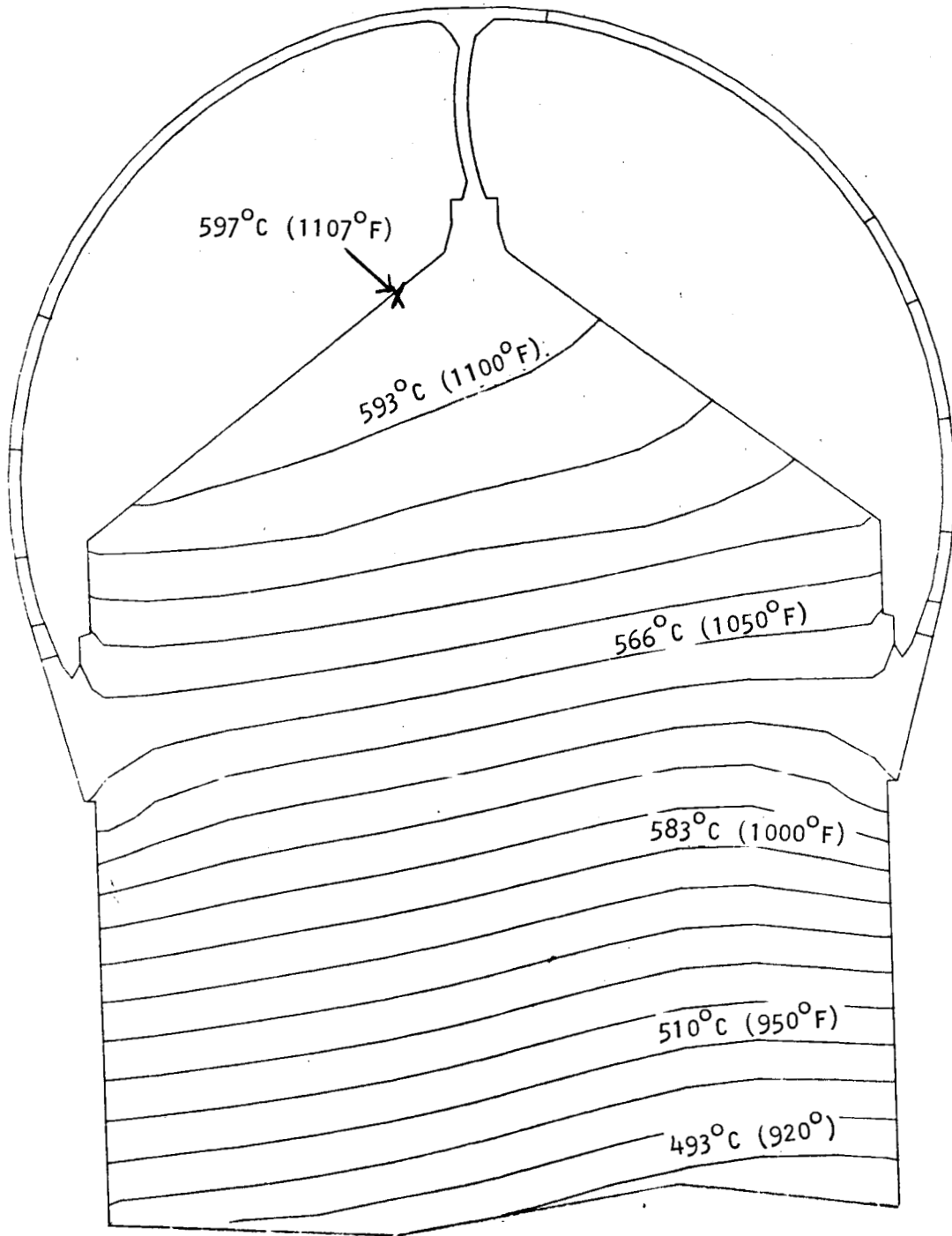


Figure 49.--Temperature Map at Steady State.

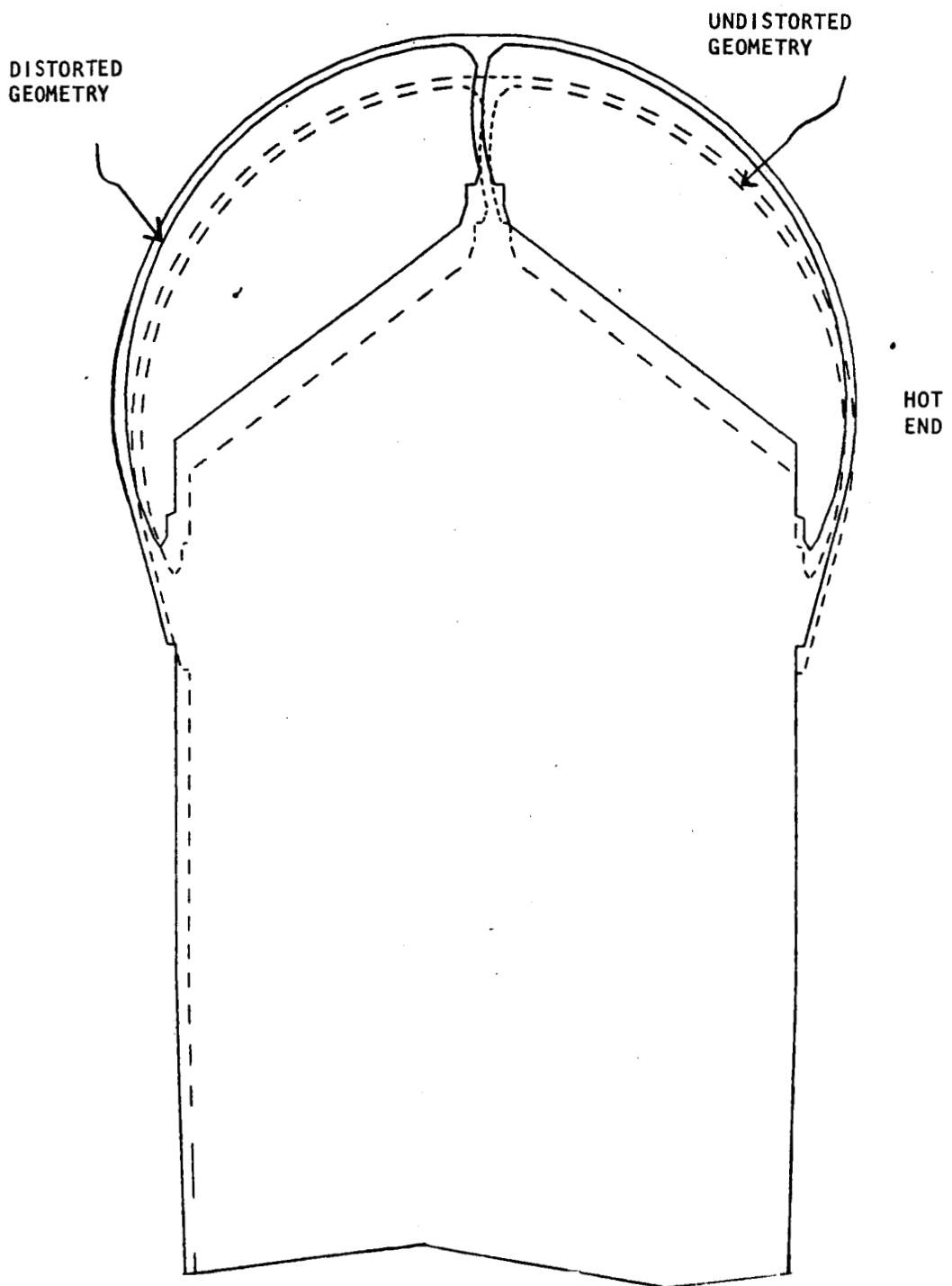


Figure 50.--Distorted Geometry at Steady State.

ORIGINAL PAGE IS
OF POOR QUALITY

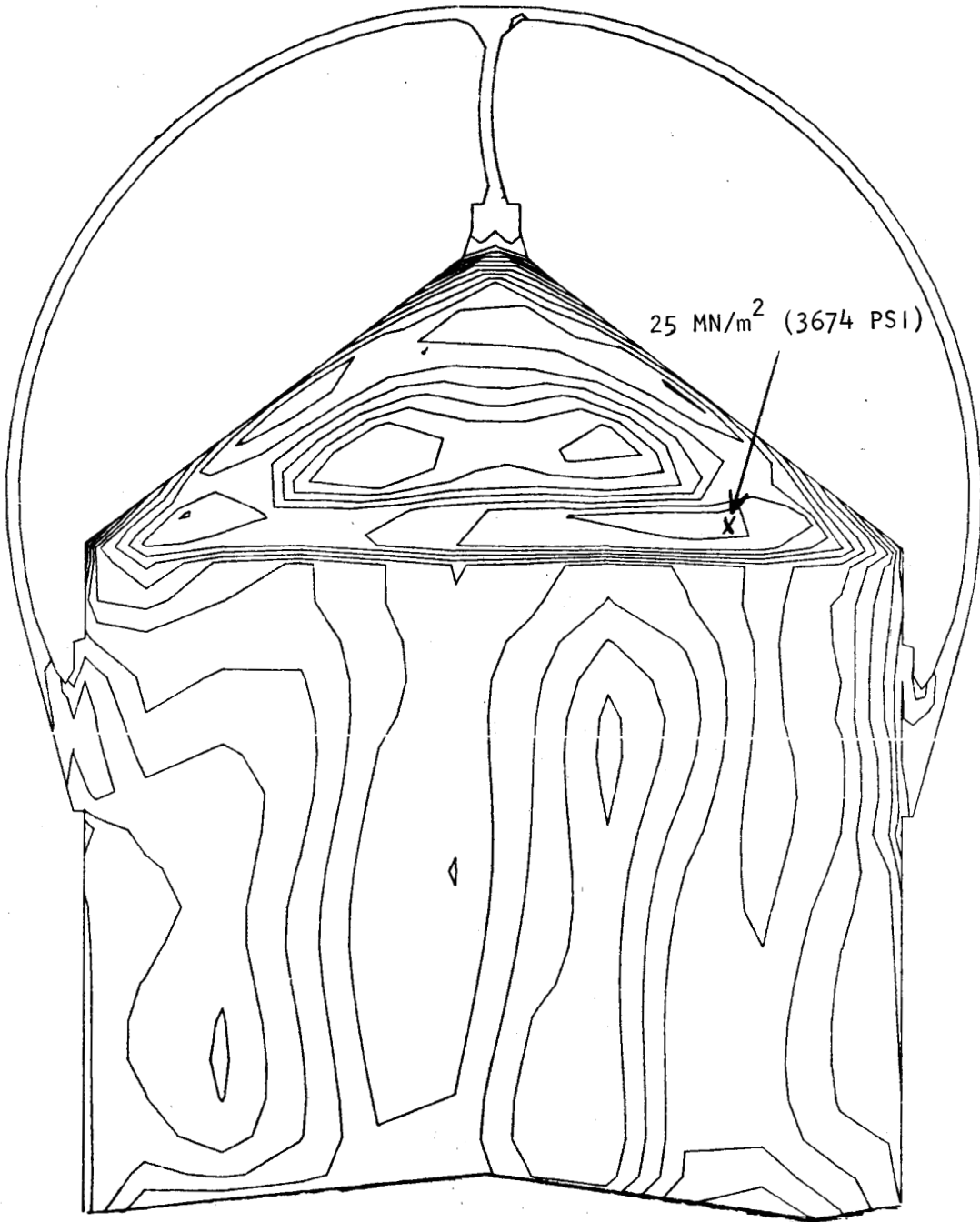


Figure 51.--2-D Von Mises Stress Map at Steady State.

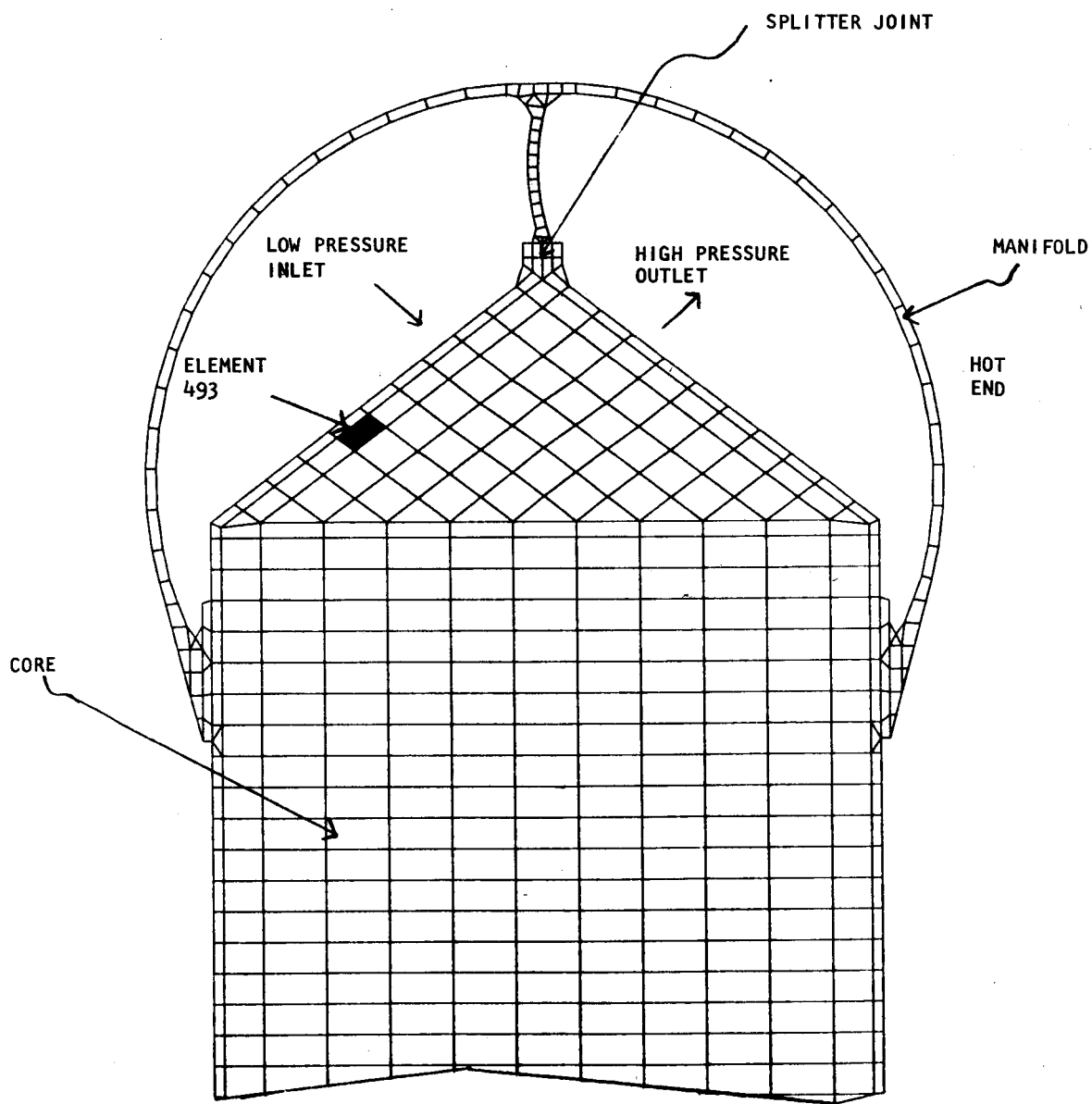
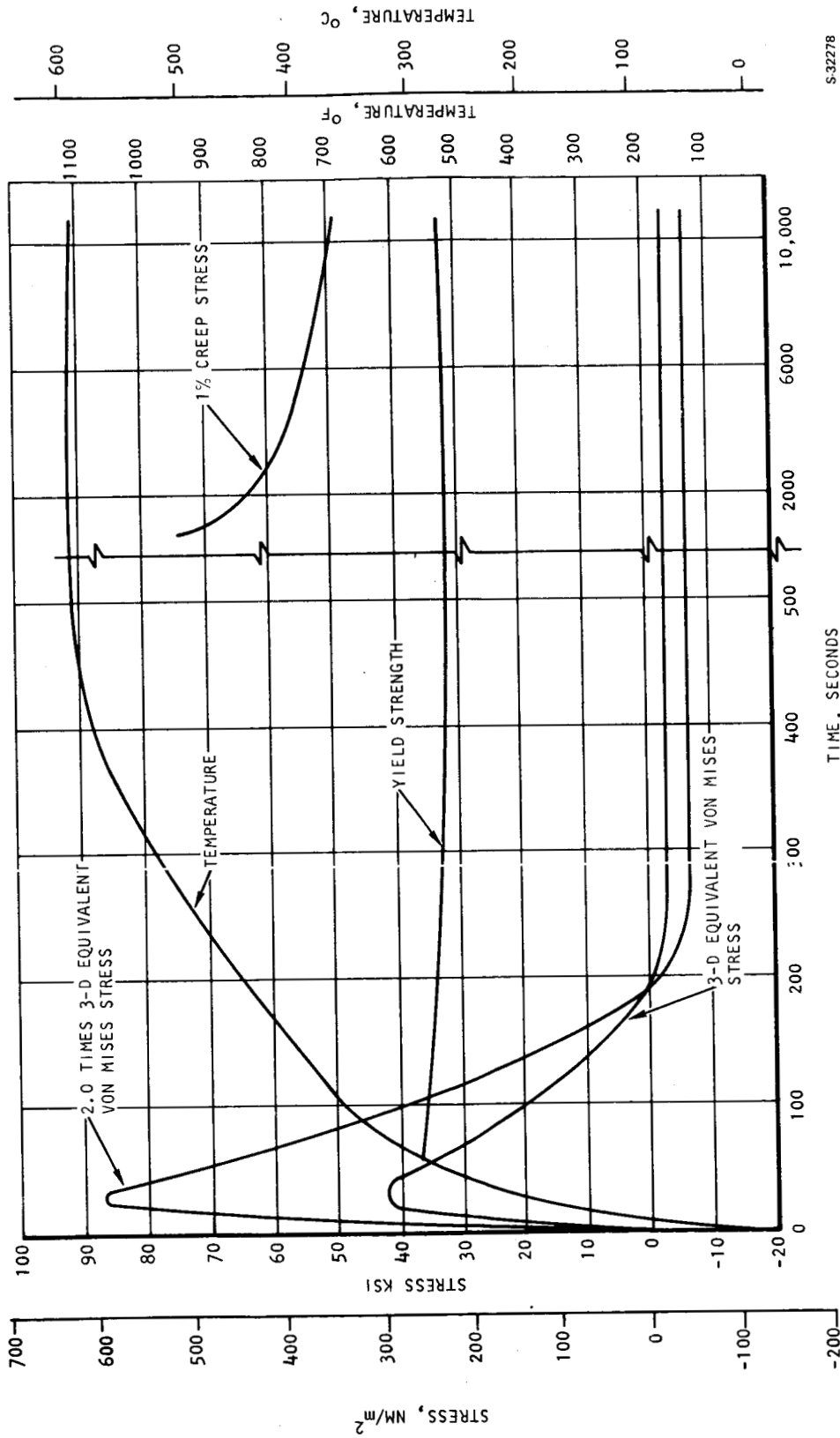


Figure 52.--Location of Most Highly Stressed Element.



S-32278

Figure 53.--Variation of Von Mises Stress, Temperature, Yield Strength, and 1 Percent Creep Stresses with Time for Element 493.

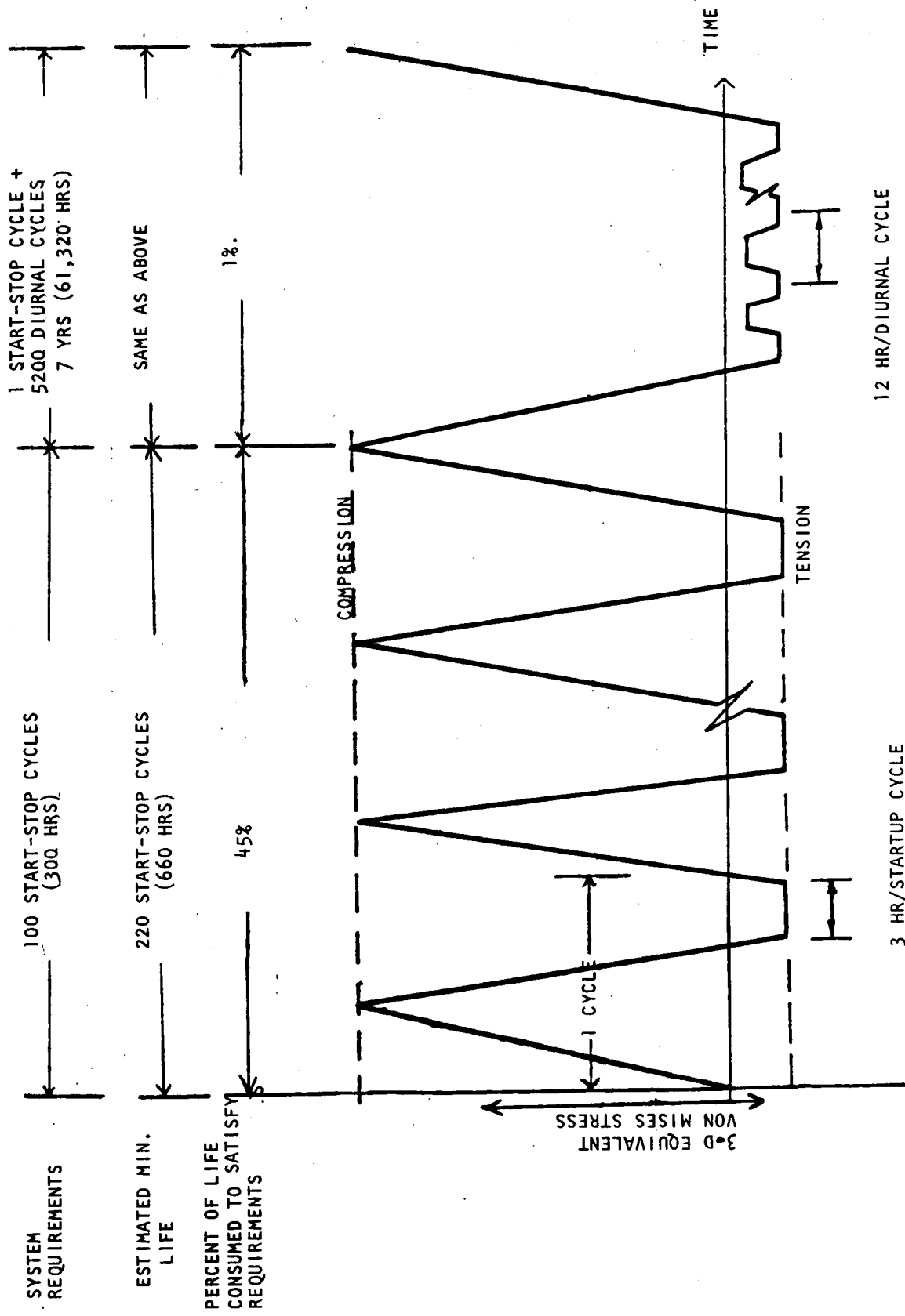
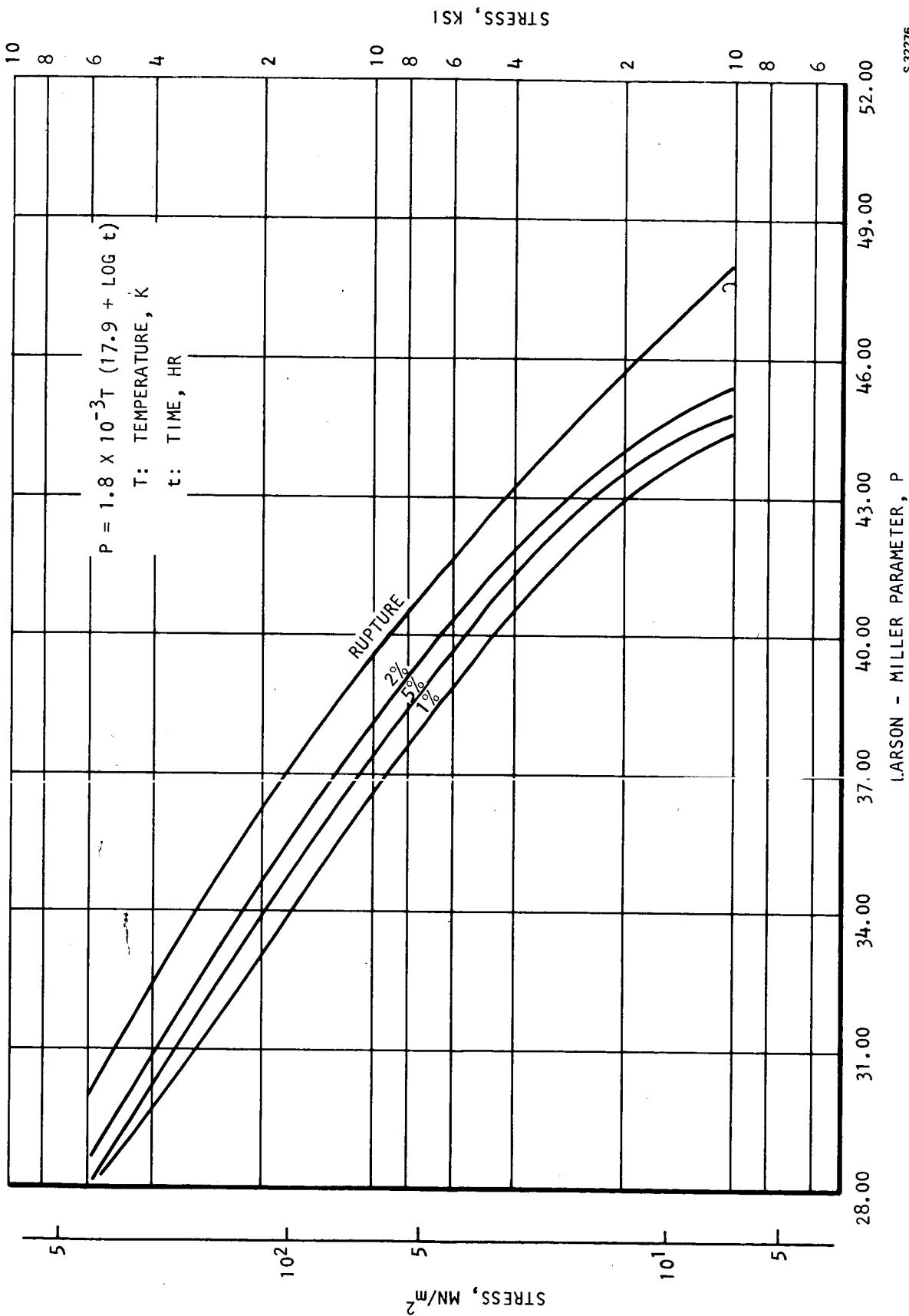


Figure 54.--Life Fraction Analysis.



S-32276

Figure 55.--Hastelloy X -3 Sigma Larson-Miller Curves for 1, 2, 5 Percent Creep and Rupture.

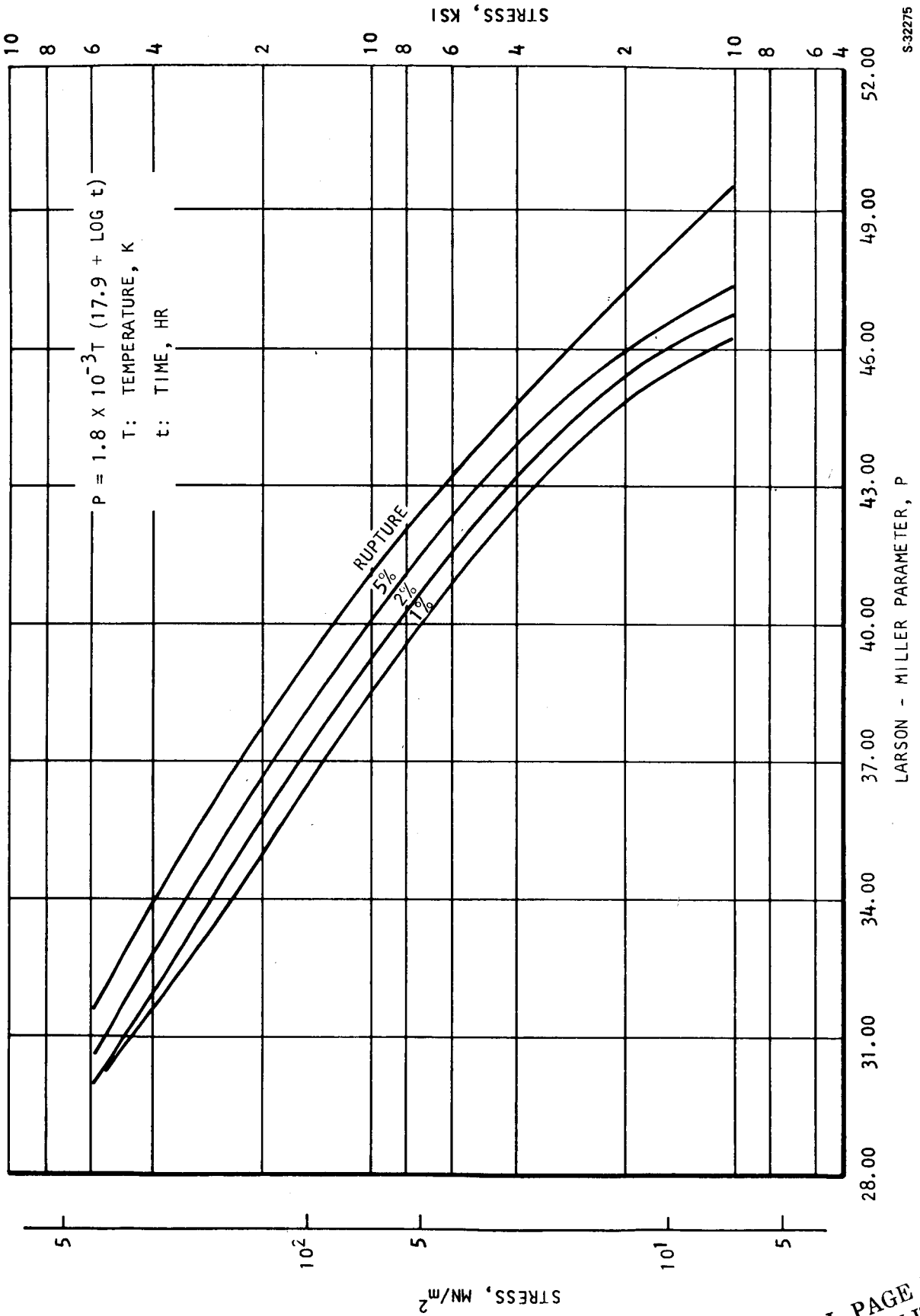


Figure 56. Hastelloy X Nominal Curves for 1, 2, 5 Percent Creep and Rupture

ORIGINAL PAGE IS
OF POOR QUALITY

The conclusions reached as a result of this study are as follows:

1. The structural design data base for Hastelloy X is adequate. Continuing efforts by NASA and DOE will provide the long-term (20,000 hr) creep-rupture properties that are needed to confirm design values.
2. Available data on the creep-rupture properties of braze joints, e.g., Hastelloy X/Palnio 7 filler alloy, are very limited. Long-term data should be obtained to confirm the MBR design values.
3. The specified temperature effectiveness, $E_C = 0.975$, places the heat exchanger design in an especially sensitive area for thermodynamic design. Small changes in flow distribution or manufacturing tolerances have a large impact on performance. Reduction in required effectiveness at these levels is always desirable. It makes design, manufacture, and testing less critical and can produce significant weight reductions.
4. Structural tests including vibration and shock are required to fully qualify the design. A long-term (>5,000 hr) creep-rupture test on a full-size unit or a representative submodule is desirable to increase the design confidence level. This test should be run in conjunction with the basic braze joint tests noted above.
5. An ultrasonic C-scan non-destructive test (NDT) was found to be effective in detecting voids in the seal plate-to-core braze joint; however, this technique could not be used on the manifold attachment flange-to-seal plate braze joint due to the asymmetric flange shape. Instead, representative parts, which were subsequently sectioned for metallurgical analysis, were used to verify the effectiveness of the processing variables, i.e., braze alloy thickness, surface flatness and finish, and the time at temperature. Development of an appropriate NDT to verify full alloy coverage in the flange joint is desirable.
6. Gold-base braze filler alloys are expensive, but because of their desirable attributes, they are still the primary recommendation for this application. As noted above, the long-term strength must be confirmed. Based on the results of the Brayton Cycle Heat Exchanger Technology Program (Reference 12) and the submodule test described in the appendix, a nickel-base alloy, Nicrobraz 30, is a possible alternate for the core matrix braze operation. Again, no long-term creep-rupture data are available for Nicrobraz 30. Isothermal solidification brazing, a recent development described in Reference 20, holds promise for producing braze joints with creep-rupture properties that approach those of the parent metal. High bonding processes or elaborate tooling are not required. The basic process, therefore, appears to be applicable to the MBR and consideration should be given to its development for the MBR.

7. Based on the most recent projection of the flight system startup cycle, the low-cycle fatigue life of the recuperation is predicted to be a minimum of 220 cycles. This is an excess of the BIPS requirement of 100 startup cycles.

APPENDIX

LOW-COST, HIGH-TEMPERATURE BRAZE ALLOY DEVELOPMENT

Palniro 1, a gold-base braze alloy, is used to braze the MBR plate-fin matrix because of its excellent flow characteristics, minimum penetration and alloying with the parent metal, high strength, and high ductility. Palniro 1 is an excellent braze alloy in all respects except for its high cost, which is prohibitive for terrestrial applications. As part of the Brayton-Cycle Heat Exchanger Technology program (Reference 12), an effort was conducted to find an alloy of reasonable cost that could meet or exceed the performance of Palniro 1. The primary factors considered in this evaluation were ductility, erosiveness, oxidation resistance, weldability, creep strength, and low-cycle fatigue resistance. The evaluation was confined to existing alloys.

Special attention was given to ductility. Braze joint cracking, which was observed during tests of Brayton-cycle recuperators, was believed to be a low-cycle fatigue failure caused in part by the low ductility of the Nicrobraz 130 (AMS 4778) braze alloy. This alloy is widely used on steel heat exchangers at AiResearch and has proven to be satisfactory in most applications. It was believed, however, that its use at temperatures above 920°K (1200°F) in a plate-fin heat exchanger was beyond the material capability. Palniro 1 was specified for all succeeding applications because of its high ductility and strength at 1000°K (1350°F).

Twenty-two alloys were screened; the final selections were a combination alloy, 75 percent Nicrobraz 210 and 25 percent Nicrobraz 30, and straight Nicrobraz 30. At the MBR design point conditions, 10 years and 1000°K, the creep-rupture properties of the combination alloy used in a single-passage plate-fin were superior to those of either Nicrobraz 30 or Palniro 1. The results, taken from Reference 12, are presented in fig. 57. The higher creep strength of the nickel base alloys is mostly attributed to the larger fillets obtained--a direct result of using a larger quantity of alloy per unit area.

Continued development of the 210/30 combination alloy was performed as part of the MBR program. A submodule core assembly, half the stack height and half the gas flow length of the full-size unit, was stacked and brazed using the 210/30 combination alloy. The module was identical with those used in the Reference 12 technology program. Photographs of the core assembly in the stacking fixture are shown in fig. 58.

The header bar sides of the core were machined in preparation for the seal plate braze operation. The braze alloy was found to be ductile and no machining problems were encountered; however, development was halted at this point because of other results, discussed below.

A full-size core assembly using spare parts from the HXDA program (Reference 5) was brazed as a check on the performance of the 210/30 combination alloy. On application of the proof pressure, separation occurred

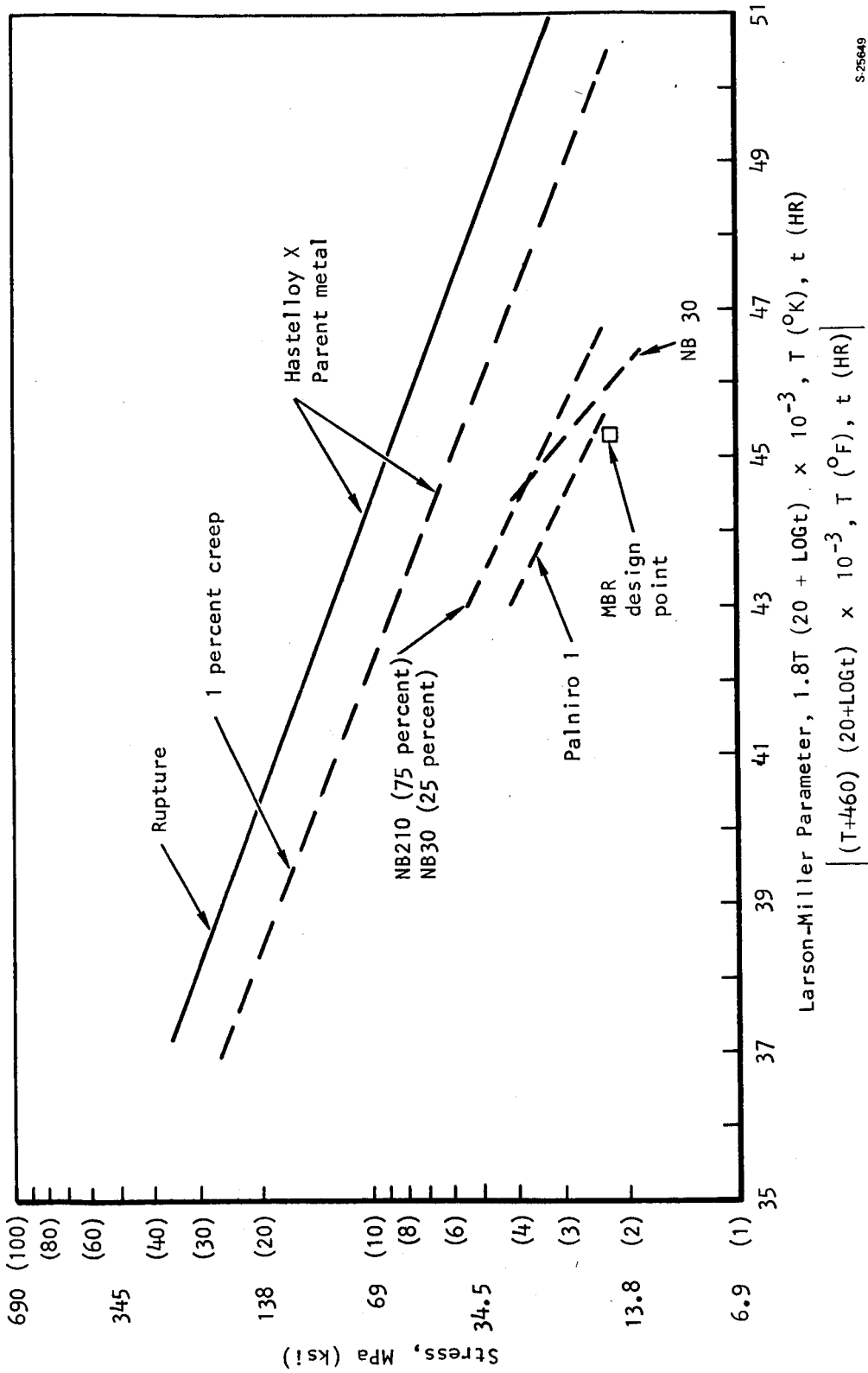
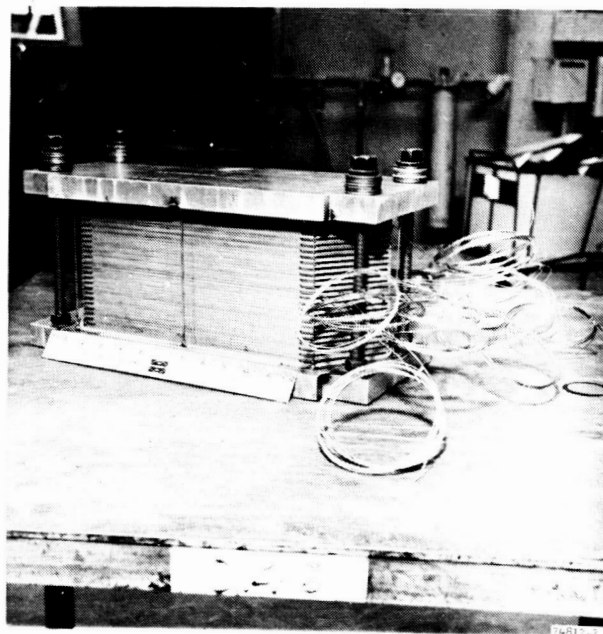
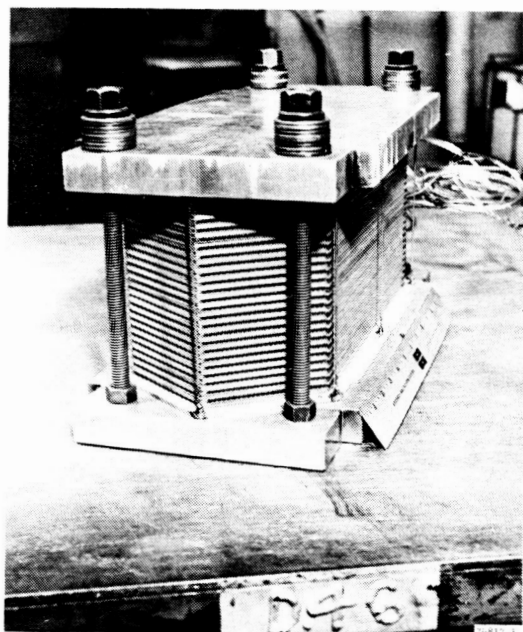


Figure 57.---Plate-Fin Creep-Rupture Behavior (from Reference 12).

ORIGINAL PAGE IS
OF POOR QUALITY



F-27047

Figure 58.--MBR Submodule in Stacking Fixture--210/30 Combination
Braze Alloy

at the plate-to-fin braze joint. Metallurgical evaluation indicated that the alloy had melted only at the joints between tube-plates and header bars. Photomicrographs of representative sections of the core gave the appearance that there was inadequate melting and flow of braze alloy, even though the unit was above 1700°F for a total of 5.5 hours in the vacuum braze furnace.

It was determined that the 210/30 combination alloy exhibits a wide solidus-liquidus range and during a long cycle, more than 3.5 hours above 1250°K (1800°F), the Microbraz 210 components do not fully melt. The net result is that the braze joints are too weak to be considered for the MBR application. All small-scale test specimens used in the initial development program were brazed using a cycle that subjected the parts to a total time of 1.5 hours above 1250°K (1800°F) to simulate a typical full-size heat exchanger cycle. For a cycle of this duration, the combination alloy is believed to be effective.

A long-duration cycle, at least 3 hours above 1250°K (1800°F), was predicted for the full-size MBR. This is close to the critical time, and hence the recommendation to stop any further submodule development. Although the submodule braze is probably acceptable, adequate braze alloy melting and flow could not be assured for the full-size MBR.

No adverse effects have been observed using Microbraz 30 in a long-duration braze cycle. The alloy should be effective for a Brayton-cycle recuperator application.

Further tests are required to evaluate its low-cycle fatigue behavior.

REFERENCES

12

1. Anderson, A.F.: Recuperator Development Program, Solar Brayton Cycle System, AiResearch Manufacturing Company Report HT-66-0207, March 19, 1968.
2. Morse, C.J., Richard, C.E., and Demogenes, C.: Task 1 Summary Report--Brayton Heat Exchanger Unit Development Program, AiResearch Manufacturing Company Report HT67-2275(3), Oct. 18, 1967.
3. Morse, C.J., Richard, C.E., and Duncan, J.D.: Final Design Report--Brayton Heat Exchanger Unit Development Program, NASA CR-120816, AiResearch 71-7450, May 29, 1971.
4. Richard, C.E., Morse, C.J., and Duncan, J.D.: Design Study--Alternate Brayton Heat Exchanger Unit, AiResearch Manufacturing Company Report 69-5194, July 2, 1969.
5. Duncan, J.D., Gibson, J.C., Graves, R.F., Morse, C.J., and Richard, C.E.: Final Design Report--Brayton Heat Exchanger Unit Development Program (Alternate Design), NASA CR-121269, AiResearch 73-9461, August 2, 1973.
6. Kerwin, P.T.: Analysis of a 35- to 150-Kilowatt Brayton Power-Conversion Module for Use with an Advanced Nuclear Reactor, NASA TN D-6525, Sept. 1971.
7. Coombs, M.G., Morse, C.J., and Richard, C.E.: Conceptual Design Study of a Nuclear Brayton Cycle Heat Exchanger and Duct Assembly (HXDA), NASA CR-72783, AiResearch 70-6691, December 4, 1970.
8. Coombs, M.G., Gibson, J.C., and Richard, C.E.: Pressure Containment Tests in Support of the Nuclear Brayton-Cycle Heat Exchanger and Duct Assembly (HXDA), NASA CR-72815, AiResearch 70-7044, Jan. 4, 1971.
9. Coombs, M.G., Morse, C.J., and Richard, C.E.: Preliminary Design Study of a Nuclear Brayton Cycle Heat Exchanger and Duct Assembly (HXDA), NASA CR-72816, AiResearch 70-7045, Jan. 4, 1971.
10. Kerwin, P.T.: Design Point Characteristics of a 15- to 80-kW(e) Nuclear-Reactor Brayton-Cycle Power System, NASA TM X-67811, Aug. 1971 (presented at the 1971 Intersociety Energy Conversion Engineering Conference, Boston, Mass., Aug 3-6, 1971).
11. Coombs, M.G., Morse, C.J., Graves, R.F., Killackey, J.J., and Gibson, J.C.: Topical Report--Brayton-Cycle Heat Exchanger and Duct Assembly (HXDA), Preliminary Design and Technology Tests, NASA CR-121011, AiResearch 72-8622, Oct. 15, 1972.

C-2

12. Killackey, J.J., Coombs, M.G., Graves, R.F., and Morse, C.J.: Final Report--Brayton-Cycle Heat Exchanger Technology Program", NASA CR-135158, AIResearch 75-12055, August 1976.
13. Perlmutter, M.: Inlet and Exit-Header Shapes for Uniform Flow Through a Resistance Parallel to the Main Stream, Trans. ASME, J. of Basic Engineering, Vol. 82, pp 361-370, September 1961.
14. London, A.L., Klopfer, G., and Wolf, S.: Oblique Flow Headers for Heat Exchangers--The Ideal Geometries and The Evaluation of Losses, TR 63, Dept. of Mech. Engr, Stanford University, Aug 1966.
15. Technical Staff: Failure Mode, Effect, and Criticality Analysis--Mini-Brayton Recuperator, AIResearch Manufacturing Company Report 75-11418, April 18, 1975.
16. Killackey, J., Mosinskis, G., and Preston, R.: Performance Test Plan Mini-Brayton Recuperator 190930-1-1, AIResearch Manufacturing Company Report 76-12948, July 9, 1976.
17. Preston, R.: Acceptance Test Procedure for Mini-Brayton Recuperator, PN 190930-1-1, AIResearch Mfg. Co. Report 76-13202, October 12, 1976.
18. Technical Staff: Transient Analysis Isotope Brayton Flight System, AIResearch Manufacturing Company of Arizona Report 75-311279, May 19, 1975.
19. Technical Staff: Topical Report - Thermal Transient Analysis of the Brayton Isotope Power System (BIPS) Recuperator, AIResearch Mfg. Co. of Calif. Report 76-13483, Oct. 1977.
20. Duvall, D.S., Owczarski, W.A., and Paulonis, D.F.: A New Method for Joining Heat Resistant Alloys, Welding Journal, April 1974, pp. 203-214.
21. Technical Staff: Superalloy Brayton Isotope Power System (BIPS-S) Design Report, AIResearch Mfg. Co. of Arizona Report 31-2626, July 1977.

ORIGINAL PAGE IS
OF POOR QUALITY

REPORT DISTRIBUTION LIST
BRAYTON HEAT EXCHANGER TECHNOLOGY PROGRAM
CONTRACT NAS3-15347
APRIL 1977

Copies

1. NASA Lewis Research Center 21000 Brookpark Road Cleveland, OH 44135 Attention: (See List Below)	
G. M. Ault (MS 3-5)	1
R. E. English (MS 3-15)	1
R. A. Rudey (MS 500-202)	1
L. I. Shure (MS 500-202)	1
R. P. Migra (MS 500-202)	1
W. D. Klopp (MS 105-1)	1
J. A. Heller (MS 500-202)	1
P. T. Bizon (MS 49-1)	1
J. H. Dunn (MS 500-202)	1
P. T. Kerwin (MS 500-210)	14
T. J. Moore (MS 105-1)	1
R. H. Titran (MS 105-1)	1
L. W. Schopen (MS 500-305)	1
Technology Utilization (MS 3-19)	1
Report Control (MS 5-5)	1
Reliability and Quality Assurance (MS 500-211)	1
Library (MS 60-3)	2
2. National Aeronautics and Space Administration Washington, DC 20546 Attention: (See List Below)	
J. Lazar (Code RPE)	1
J. P. Mullin (Code RPP)	1
L. Holcomb (Code RPI)	1
3. NASA Scientific & Technical Information Facility P. O. Box 8757 Balt/Wash International Airport, MD 21241 Attention: Accessioning Department	30
4. NASA - Marshall Space Flight Center Marshall Space Flight Center, AL 35812 Attention: Library	1

REPORT DISTRIBUTION LIST (Continued)

	<u>Copies</u>
5. NASA-Flight Research Center P. O. Box 273 Edwards, CA 93523 Attention: Library	1
6. NASA-Ames Research Center Moffitt Field, CA 94035 Attention: Library	1
7. NASA-Goddard Space Flight Center Greenbelt, MD 20771 Attention: Library	1
8. NASA-Langley Research Center Langley Station Hampton, VA 23365 Attention: Library	1
9. Jet Propulsion Laboratory 4800 Oak Grove Drive Pasadena, CA 91103 Attention: Library	1
10. NASA-Manned Spacecraft Center Houston, TX 77058 Attention: (See List Below)	
Library	1
A. Redding	1
11. ERDA Div. of Nuclear Research Washington, DC 20545 Attention: (See List Below)	
J. H. Lombardo (MS G-434)	1
D. Kenney (MS 82-2200)	1
R. Brouns (MS G-434)	1
12. Air Force Systems Command Aeronautical Systems Division Wright-Patterson Air Force Base OH 45438 Attention: Library	1

REPORT DISTRIBUTION LIST (Continued)

	<u>Copies</u>
13. Bureau of Naval Weapons Dept. of the Navy Washington, DC 20025 Attention: Code RAPP	1
14. Institute for Defense Analyses 400 Army-Navy Drive Arlington, VA 22202 Attention: Library	1
15. Massachusetts Institute of Technology Cambridge, MA 02139 Attention: Library	1
16. Battelle Memorial Institute 505 King Avenue Columbus, OH 43201 Attention: Library	1
17. Power Information Center University of Pennsylvania 3401 Market Street, Room 2107 Philadelphia, PA 19104	1
18. Aerospace Corporation 2350 E. El Segundo Blvd. El Segundo, CA 90045 Attention: H. T. Sampson	1
19. Continental Aviation & Engineering Corporation 12700 Kercheval Avenue Detroit, MI 48215 Attention: Library	1
20. The Boeing Company Aero-Space Division Box 3707 Seattle, WA 98124 Attention: Library	1
21. Curtiss-Wright Corporation Wright Aero Division Main and Passaic Streets Woodridge, NJ 07075 Attention: Library	1

REPORT DISTRIBUTION LIST. (Continued)

	<u>Copies</u>
22. Garrett Corporation AiResearch Manufacturing Company 402 South 36 Street Phoenix, AZ 85034 Attention: (See List Below)	
J. McCormick	1
H. Longee	1
23. Garrett Corporation AiResearch Manufacturing Company 9851 Sepulveda Blvd. Los Angeles, CA 90009 Attention: O. A. Buchmann	1
24. General Electric Company Missile & Space Vehicle Dept. 3198 Chestnut Street Philadelphia, PA 19104 Attention: (See List Below)	
Library	1
D. Wein	1
25. General Electric Company Lynn, MA 01905 Attn: Library	1
26. General Electric Company Mechanical Technology Laboratory R & D Center Schenectady, NY 12301 Attention: Library	1
27. General Motors Corporation Indianapolis, IN 46206 Attention: Library	1
28. Franklin Institute Research Labs. Benjamin Franklin Parkway at 20th Street Philadelphia, PA 19103 Attention: Library	1
29. General Electric Company Missile and Space Division Cincinnati, OH 45215 Attention: W. Zimmerman	1

REPORT DISTRIBUTION LIST (Continued)

	<u>Copies</u>
30. Lear Siegler, Inc. 3171 S. Bundy Drive Santa Monica, CA 90406 Attention: Library	1
31. Lockheed Missiles & Space Company P. O. Box 504 Sunnyvale, CA 90488 Attention: Library	1
32. McDonnell-Douglas Corporation Lambert Field St. Louis, MO 63166 Attention: Library	1
33. North American Rockwell Corporation Space Division 12214 Lakewood Blvd. Downey, CA 90241 Attention: Library	1
34. Northern Research & Engineering Co. 219 Vassar Street Cambridge, MA 02139 Attention: Library	1
35. Mechanical Technology Inc. 968 Albany-Shaker Road Latham, NY 12110 Attention: Library	1
36. Solar Division of International Harvester 2200 Pacific Highway San Diego, CA 92112 Attention: Library	1
37. Sunstrand Energy Systems 4747 Harrison Avenue Rockford, IL 61101 Attention: E. C. Kruger	2
38. TRW Systems Division One Space Park Redondo Beach, CA 90278 Attention: Library	1

REPORT DISTRIBUTION LIST (Continued)

Copies

- | | | |
|-----|---|---|
| 39. | Union Carbide Corp.
Linde Division
P. O. Box 44
Tonawanda, NY 14152
Attention: Library | 1 |
| 40. | Westinghouse Electric Corporation
Astronuclear Laboratory
P. O. Box 10864
Pittsburgh, PA 15236
Attention: Library | 1 |
| 41. | Williams Research
Walled Lake, MI 48088
Attention: Library | 1 |
| 42. | Naval Ship Engineering Center
Hyattsville, MD 20782
Attention: Frank Welling | 1 |
| 43. | Naval Research Laboratory
Code 6623
Washington, DC 20375
Attention: R. L. Statler | 1 |